

2015

Single-molecule Biomechanics of von Willebrand Factor A-domains

Yan Xu

Lehigh University

Follow this and additional works at: <http://preserve.lehigh.edu/etd>



Part of the [Mechanical Engineering Commons](#)

Recommended Citation

Xu, Yan, "Single-molecule Biomechanics of von Willebrand Factor A-domains" (2015). *Theses and Dissertations*. 2889.
<http://preserve.lehigh.edu/etd/2889>

This Dissertation is brought to you for free and open access by Lehigh Preserve. It has been accepted for inclusion in Theses and Dissertations by an authorized administrator of Lehigh Preserve. For more information, please contact preserve@lehigh.edu.

**Single-molecule Biomechanics of von Willebrand Factor
A-domains**

by

Yan Xu

A Dissertation

Presented to the Graduate and Research Committee

of Lehigh University

in Candidacy for the Degree of

Doctor of Philosophy

in

Mechanical Engineering

Lehigh University

May 2015

Copyright 2015 © by Yan Xu

All rights reserved.

Approved and recommended for acceptance as a dissertation in partial fulfillment of the requirements for the degree of Doctor of Philosophy

Name: Yan Xu

Dissertation Title: Single-molecule Biomechanics of von Willebrand Factor A-domains

Defense Date

Dr. Xiaohui (Frank) Zhang, Dissertation Director, Chair

Approved Date

Committee Members:

Dr. Alparslan Oztekin

Dr. Xuanhong Cheng

Dr. Edmund Webb III

Dr. Chao Zhou

ACKNOWLEDGEMENTS

PhD Advisor

Dr. Xiaohui (Frank) Zhang: for the solid support, inspiring guidance, generous help and heartwarming encouragement, also for being an amazing mentor, an outstanding scientist and an endearing friend.

Doctoral Committee

Dr. Alparslan Oztekin: for joyful discussions, brilliant ideas and input to my work, the enthusiasm in research and for the awesome Christmas party every year.

Dr. Xuanhong Cheng: for coaching me in microfluidic devices, showing me what a capable researcher should be and countless help to me.

Dr. Edmund Webb III: for passionate discussions, critical questions and humorous but inspiring commands.

Dr. Chao Zhou: for teaching me in biophotonics, allowing me to run some experiments with his facilities, also for the tremendous help in my job searching.

Collaborators and Lab mates

Dr. Thomas A. J. McKinnon, Dr. Renhao Li, Dr. Yizhen Wang, Dr. Bu Wang, Dr. Ming-Tzo Wei, Dr. Wenli Ouyang, Dr. Rachael Barton, Logan MacDonald, Fengqiang Li, Matthew Dragovich, Chenyu Wu, Wei Zhang, Yan Guo, Wei Wei, Haoling Ma, Chelsea

Coffey, Ohmny Romero, Krista Schutt, Jing Liu, Yu Song, Caroline Multari, and Chao Zhao for kindly sharing materials, devices and expertise.

Family and Friends

Quanxi Xu and Chunrong Ma: my dearest parents who have trusted and supported me all this time, giving me everything they have and missing me wherever I am.

Shuo Zhang, Dr. Amit Belwalkar, Dr. Yartin S Karpe, Thomas Meiseid, Marie A. Bartos, Brian Flynn, Dr. Xiao Liu, Dr. Yi Hu, Dr. Qian Wu, Dr. Zhen Peng, Dr. Guan Sun, Dr. Xu Li, Dr. Shanshan Liu, Dr. Chao Xu, Dr. Yang Yu, Bo Lin, Tianyi Luo, Ran Huang, Bo Han, Kanlun Li, Zhou Yang, Yuanyuan Wang and Yi Chen, for being so nice and helpful to me, also for sharing both the happiness and sadness of life with me.

George Lyons Sensei, Patti Lyons Sensei and all the Bucks County Aikido members, for not only training my techniques and strength in AIKIDO, but also taking care of me like family.

TABLE OF CONTENTS

ACKNOWLEDGEMENTS	IV
TABLE OF CONTENTS	VI
LIST OF FIGURES	X
LIST OF TABLES	XIII
ABSTRACT.....	1
CHAPTER 1	3
INTRODUCTION	3
1. MOTIVATION- VON WILLEBRAND DISEASE (VWD)	3
2. ABOUT VON WILLEBRAND FACTOR (VWF).....	4
2.1. Biosynthesis of VWF	4
2.2. Domain structure and function.....	5
2.3. Hemostasis and thrombosis.....	7
3. FACILITIES AND DEVICES.....	10
3.1. Atomic Force Microscope (AFM).....	10
3.2. Miniature Optical Tweezers	15
3.3. Microfluidic Device	17
CHAPTER 2	20

BIOMECHANICAL CHARACTERIZATION OF VWF-COLLAGEN

INTERACTION	20
1. INTRODUCTION	20
2. MATERIALS AND METHODOLOGY.....	22
2.1. Samples and Materials	22
2.2. Setup the Atomic Force Microscope (AFM).....	23
2.3. Coating the Probes	25
3. RESULTS AND DISCUSSION	32
3.1. Experimentally Measure the Rupture Force and loading Rate for Dynamic Force Spectrum.....	32
3.2. Adhesion Percentage and Control Group.....	36
3.3. Identify The Most Probable Rupture Force Under Each Pulling Speed.	38
3.4. Fitting Data with The Bell- Evans Model	40
3.5. Utilize AFM Unbinding Assay to Define The Force Spectrum for Mutant VWF Multimers	47
4. CONCLUSION	54
CHAPTER 3	57

IDENTIFICATION OF A JUXTAMEMBRANE MECHANOSENSITIVE DOMAIN IN THE PLATELET MECHANOSENSOR GLYCOPROTEIN IB-IX

COMPLEX	57
1. INTRODUCTION	57
2. MATERIALS AND METHODOLOGY.....	60
2.1. Biotinylated GPIb-IX complex	60

2.2. VWF A1 Domain	61
2.3. Antibodies	61
2.4. Botrocetin	61
2.5. DNA Handles	61
2.6. Beads for Optical-tweezers	62
2.7 Setup for the Pulling Assay on The Optical-Tweezers Platform	63
3. RESULTS AND DISCUSSION	65
3.1. Optical-tweezers Unfolding Assay on VWF A1 Domain-GPIb-IX.....	65
3.2. Locate the Mechanosensitive Domain (MSD) within GPIb-IX Complex	66
3.3. Measure the Enhancement of Botrocetin on VWF A1 Domain-GPIb-IX Complex Interaction.....	70
4. CONCLUSION	72
CHAPTER 4.....	74
BIOMECHANICAL PROPERTIES OF VON WILLEBRAND FACTOR (VWF) MULTIMER.....	74
1. INTRODUCTION	74
2. MATERIALS AND METHODOLOGY	75
2.1. VWF multimer	75
2.2. Microfluidic Flow Chamber.....	75
3. RESULTS AND DISCUSSIONS.....	77
3.1. Unfolding the VWF Multimer with Atomic Force Microscope (AFM)	77
3.2. Characterization of the Interaction between VWF and Collagen under Shear Flow.....	78

3.3. Characterization of the Domain-Domain Interactions within the VWF Multimer	81
4. CONCLUSION	86
CONCLUDING REMARKS AND OUTLOOK	88
BIBLIOGRAPHY	91
VITA	99

LIST OF FIGURES

FIGURE 1. STRUCTURE OF VWF TUBULES AND THE WPB MEMBRANE.	5
FIGURE 2. FIVE STRUCTURAL DOMAINS OF VON WILLEBRAND FACTOR (VWF)	6
FIGURE 3. A. SCHEMATIC OF THE HOMEBUILT AFM. B. TYPICAL AFM PULLING CURVES USING TITIN I27.	10
FIGURE 4. A. AFM CANTILEVERS. B. SCHEMATIC OF AN AFM CANTILEVER TIP. (REPRINTED FROM BRUKER WEBSITE).....	11
FIGURE 5. A. OPTICAL TWEEZERS. B. FLUIDIC SETUP OF MINIATURE OPTICAL TWEEZERS. C. OPTICAL LAYOUT OF MINIATURE OPTICAL TWEEZERS (REPRINTED FROM HTTP://TWEEZERSLAB.UNIPR.IT/CGI-BIN/MT/HOME.PL).....	16
FIGURE 6. SCHEMATIC OF THE HOMEBUILT MICROFLUIDIC DEVICE. B. PICTURE OF THE WAFER USED TO MAKE PDMS MICROFLUIDIC DEVICES. C. DEVICE ASSEMBLED ON GLASS SLIDE WITH INLET AND OUTLET PUNCHED.....	17
FIGURE 7. SCHEMATIC OF THE HOMEBUILT AFM WITH IMPLEMENTATION OF THERMO CONTROL COMPONENT.	25
FIGURE 8. OXIDATION AND GAS PHASE APTES SILANIZATION OF SILICAON NITRIDE TIPS. 26	
FIGURE 9. REACTION OF NHS-AMINO GROUP THAT CONVERTS ACETAL INTO ALDEHYDE.. 28	
FIGURE 10. SCHEMATIC OF THE UNBINDING ASSAY SETUP..	30
FIGURE 11. TYPICAL PULLING CURVES PLOTTED BY IGOR SOFTWARE	35
FIGURE 12. CONTROL EXPERIMENT GROUP.	37
FIGURE 13. HISTOGRAMS OF THE RUPTURE FORCE FOR VWF MONOMER-COLLAGEN UNBINDING	38

FIGURE 14. HISTOGRAMS OF THE RUPTURE FORCE FOR VWF A3 DOMAIN-COLLAGEN UNBINDING.....	39
FIGURE 15. DYNAMIC FORCE SPECTRUM OF VWF MONOMER-COLLAGEN AND VWF A3 DOMAIN-COLLAGEN WITH FITTED BELL MODEL PARAMETERS.....	43
FIGURE 16. COMPARISON OF BOND LIFETIME AS A FUNCTION OF THE FORCE OF A3-COLLAGEN INTERACTIONS, A1-GPIB α INTERACTIONS AND A2 UNFOLDING.	45
FIGURE 17. RIBBON DIAGRAM OF THE VWF WITH MUTANT A3 DOMAIN..	47
FIGURE 18. DYNAMIC FORCE SPECTRUM OF WT VWF-COLLAGEN INTERACTIONS, INCLUDING WT VWF MULTIMER, VWF MONOMER AND VWF A3 DOMAIN.	49
FIGURE 19. DYNAMIC FORCE SPECTRUM OF NEM TREATED VWF-COLLAGEN INTERACTION, COMPARING WITH WT VWF MULTIMER.	51
FIGURE 20. DYNAMIC FORCE SPECTRUM OF S1731T VWF MUTATION (GREEN) AND W1745C VWF MUTATION (ORANGE), COMPARING WITH WT VWF MULTIMER (BLUE).	52
FIGURE 21. TYPE I COLLAGEN WITH VWF: AG ELISA. ERROR BARS REPRESENT MEAN \pm SD OF 3 SEPARATE EXPERIMENTS PERFORMED IN DUPLICATE [22].	53
FIGURE 22. DYNAMIC FORCE SPECTRUM OF ALL THE SAMPLE PAIRS: WT MULTIMER VS. COLLAGEN (BLUE), A3 DOMAIN VS. COLLAGEN (RED), WT MONOMER VS. COLLAGEN (BLACK), NEW TREATED VWF VS. COLLAGEN (PINK), S1731T VWF MUTATION VS. COLLAGEN (GREEN) AND W1745C VWF MUTATION VS. COLLAGEN (ORANGE).	55
FIGURE 23. RIBBON STRUCTURES OF THE VWF-GPIB-IX COMPLEX BINDING [78].	58
FIGURE 24. DIAGRAM OF THE OPTICAL-TWEEZERS SETUP [76].	64
FIGURE 25. TYPICAL UNFOLDING CURVE OF VWF A1 DOMAIN-GPIB-IX [76].	65

FIGURE 26. UNFOLDING CURVES OF GPIB-IX WITH WM23 AND 5G6 ANTIBODIES.....	67
FIGURE 27. AVERAGE UNFOLDING EXTENSION OF GPIB-IX PULLED BY WM23 AND 5G6.	68
FIGURE 28. SCHEMATIC OF A PROPOSED MODEL SHOWING THE MECHANOSENSITIVE MECHANISM OF GPIB-IX [76].	69
FIGURE 29. HISTOGRAMS OF THE RUPTURE FORCE WHEN UNBINDING VWF MONOMER FROM GPIB-IX WITH AND WITHOUT BOTROCETIN.....	70
FIGURE 30. LIFETIME (S) VERSUS RUPTURE FORCE (pN) OF VWF MONOMER-GPIB-IX WITHOUT (TOP) AND WITH (BOTTOM) BOTROCETIN.	71
FIGURE 31. UNFOLDING THE PLASMA AFM MULTIMER. A. AFM FORCE-EXTENSION CURVE OF VWF MULTIMER. B. AFM FORCE-EXTENSION CURVE OF VWF MONOMER.....	77
FIGURE 32. MICROFLUIDIC SYSTEM TO ACHIEVE CONTROLLABLE FLOW FIELD.	79
FIGURE 33. SCHEMATIC OF DOMAIN-DOMAIN INTERACTIONS.	81
FIGURE 34. SCHEMATIC OF THE ANTIBODY-BASED PULLING ASSAY.	82
FIGURE 35. PULLING VWF MONOMER WITH THE ANTIBODY-BASED PULLING ASSAY.	85

LIST OF TABLES

TABLE 1. CLASSIFICATION AND SUMMARY OF VON VILLEBRAND DISEASE (VWD).....	4
TABLE 2. SPECIFICATION OF AFM CANTILEVER (BRUKER).....	12
TABLE 3. SPECIFICATION OF AFM CANTILEVER TIPS (BRUKER).....	12
TABLE 4. SPECIFICATION OF THE VWF SAMPLES.....	22
TABLE 5. PRESET PARAMETERS OF THE AFM.....	33
TABLE 6. SUMMARY OF THE BELL MODEL PARAMETERS FOR EACH SAMPLE IN THE UNBINDING ASSAY.....	56
TABLE 7. COMPARISON OF THE DUDKO MODEL FITTED PARAMETERS BEFORE AND AFTER ADDING BOTROCETIN	72

ABSTRACT

von Willebrand Factor (VWF) is a polymeric plasma glycoprotein which is very important for the hemostasis of bleeding blood vessels. When blood vessels are injured, the hydrodynamic force in the bloodstream experiences a sharp increase and the stability of the flow field is disturbed simultaneously. However, von Willebrand factor (VWF), by bridging over platelets and exposed collagen, forms hemostatic plugs to stop bleeding. Responding to the high shear rate in the blood stream, the multimeric VWF wisely alters its conformation from the original compact-like coil to a thread-like shape and exposes as many functional domains as possible, to secure increased binding strength with collagen and higher capturing efficiency with platelets. During the entire process of hemostasis and thrombosis, the A-domains, including A1, A2 and A3, behave as the most influential function group within VWF.

A single-molecule study is an experiment that investigates the properties of individual molecules. It has been increasingly utilized into biological studies since late 1980s. The main reasons that single-molecule study can be implemented into biological applications are as follows: first, it is a very direct method that performs precise measurement on the most fundamental parameters (e.g. force, strength, stiffness) of the biological sample; second, the single-molecule study is conducted in real time, hence it enables simultaneous observation that perfectly fulfills demands to record certain biological phenomena (e.g. morphology, stimulation, conformational change); third, it can achieve outstanding resolution and sensitivity, which make single-molecule studies

an ideal method to characterize both the structural and functional properties for biomolecules such as cells and tissue both intermolecularly and intramolecularly.

Within this dissertation, two single-molecule devices: atomic force microscope and optical tweezers are employed to study the A-domains of von Willebrand factor (VWF). First, the interaction between VWF and collagen has been comprehensively characterized in domain, monomer and multimer phases. Meanwhile, a quantitative comparison has been given to identify the functional defects of different mutations of von Willebrand Disease (VWD). Second, the adhesiveness between VWF and glycoprotein1 (GP1) receptor on the platelet membrane has been studied carefully to unveil the mechanism of hemostasis and thrombosis. Similarly, the mutant VWF with defects in platelet binding has been examined. Third, based on the first two experiments, another set of experiments has been done on multimeric VWF protein. A new assay method by using two different VWF antibodies to measure intra-molecular interactions within the VWF multimer on the platform of optical tweezers was developed.

Throughout the entire study, the A1, A2 and A3 domains within VWF are discussed comprehensively from both functional and structural perspectives. Meanwhile, the data from wild type samples are always compared with the ones from mutations. Therefore, the structural defects are connected with the functional ineffectiveness. Finally, based on the result of this dissertation, several diagnostic solutions are proposed.

CHAPTER 1

Introduction

1. Motivation- von Willebrand Disease (VWD)

von Willebrand Factor (VWF) has been a subject of research interest since last century, because it is the root cause of von Willebrand Disease (VWD). VWD (found in 1926; named after Erik Adolf von Willebrand) is the most common hereditary coagulation abnormality reported in humans. Statistically, one in 100 individuals has a functional defects or no/low expression of the von Willebrand factor (VWF), but the majority of them have relatively mild symptoms. Therefore, the prevalence of VWD with clinical significance is about one per 10,000 [1]. The more severe VWD patients are proportionally more likely to be female. Additionally, those with O blood type are more likely to suffer from severe and apparent symptoms. Obvious symptoms are usually in the form of easy bruising, nosebleeds, bleeding gums, heavy menstrual periods, and blood loss during childbirth. Based on clinical observation and pathology studies, there are three general types of hereditary von Willebrand Disease: VWD Type 1, VWD Type 2, and VWD Type 3. Within each type, there are various subtypes [2-4]. The most common types of VWD are classified and summarized as in **Table 1** below. While the development of new diagnostic techniques has promoted the discovery of more new subtypes, a therapeutic solution to cure VWD has not been fully established. Nowadays, the main treatment for severe VWD patients is still blood infusion.

Table 1. Classification and Summary of von Willebrand Disease (VWD).

Type	Description	VWF	Prevalence	
1	Bleeding following surgery, noticeable easy bruising, or menorrhagia	Heterozygous for the defective gene, decreased production	70%-80%	
2	2A	Ristocetin co-factor activity is low and reduced or absent large VWF multimers	Qualitatively defective, decreased platelet binding and multimerization	10%-15%
	2B	Thrombocytopenia	Abnormally enhanced platelet binding	≈5%
	2M	High molecular weight large VWF multimers	Decreased platelet binding and normal multimerization	Rare
	2N	Quantitatively decreased coagulation factor VIII	Deficiency of coagulation factor VIII binding	Rare
3	Extremely low Factor VIII level	Complete absence of VWF production	Rare	

2. About von Willebrand Factor (VWF)

2.1. Biosynthesis of VWF

von Willebrand Factor (VWF) is a polymeric plasma glycoprotein critical for hemostasis of bleeding. von Willebrand Factor has a very unique structure, which enables it to assemble during biosynthesis into helical tubules and then be stored for rapid exocytic release in Weibel-Palade bodies (WPB) [5]. During the biosynthesis process, the VWF glycoprotein is first synthesized as pre-propeptide [5, 6]. Following the removal of the signal sequence, the pre-propeptide is transferred into the endoplasmic reticulum (ER) [7]. Afterwards, the N-linked glycans are introduced into the ER and help construct the inter-monomer disulphide bonds in the C-terminal cystine-knot (CK) domain.

Consequently, VWF monomers are assembled into dimers in the endoplasmic reticulum by crosslinking of cysteine residues. Finally, the molecules are translocated to Golgi, where the propeptide is modified by O-linked glycans to form the multimeric structure [6]. The multimers are condensed and stored in Weibel-Palade Bodies (WPB) in the shape of helical tubules [8]. As shown in **Figure 1a**, a so called paracrystal structure has been reported based on the Cryo-EM study on Weibel-Palade Bodies[8].

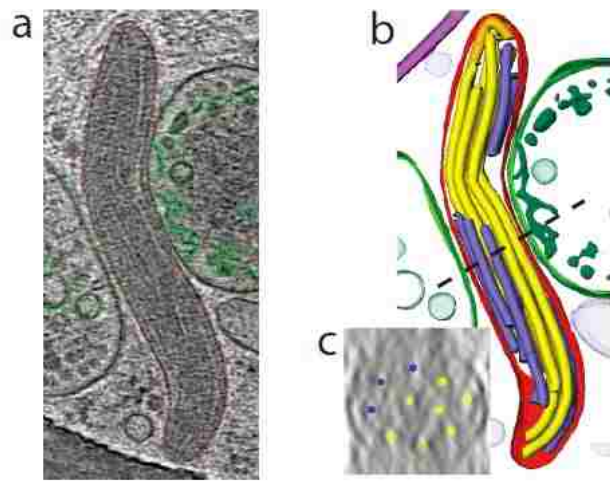


Figure 1. Structure of VWF tubules and the WPB membrane. **a.** Cryo-EM section of a tomogram showing segmentation contours for membranes (red: WPB membrane). **b.** Model of VWF tubules and WPB membrane. The yellow tubules represents full-length of the granule, orange shows the bending part and shorter ones are marked in blue. **c.** 250 Å projected tomogram cross-section at dashed black line in **b** [8].

2.2. Domain structure and function

VWF precursor (pro-VWF) has a molecular weight of about 350 kDa. It is synthesized with a signal peptide and five structural domains arranged in the order of D1-D2-D'-D3-A1-A2-A3-D4-B1-B2-B3-C1-C2-CK (**Figure 2**) [5]. When the vessel is injured, the D1 and D2 domains are trimmed off. Disulfide bonds are formed in D'-D3

domain to form multimers. Another very important property of D'-D3 domain is the binding affinity with Factor VIII (FVIII), an essential coagulation factor in blood [9]. FVIII circulates in the blood stream after being produced in the liver, and binds onto the D'-D3 domain of von Willebrand Factor under a normal condition. As soon as the vessel is injured, FVIII is immediately activated and unbinds from D'-D3 domain of VWF to initiate blood clotting. On the other end of the mature VWF monomer, the C domain binds with activate platelet integrin $\alpha_{Ib}\beta_3$ [10]. This interaction initiates the interposition of VWF multimer and platelet, which prepares for the strengthened binding between the platelet glycoprotein Ib (GPIb) and the VWF A1 domain in the later step of hemostatic plug formation [11].

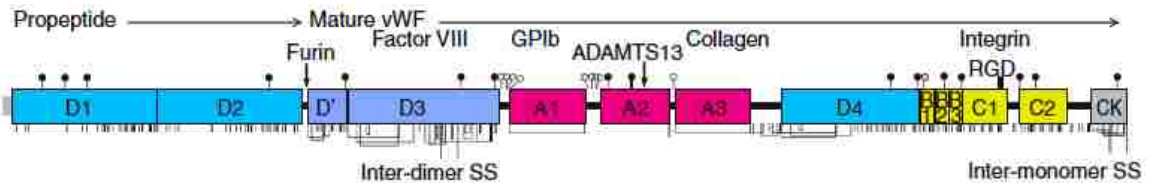


Figure 2. Five structural domains of von Willebrand Factor (VWF) [5].

This dissertation will focus on studying the A-domains of VWF. The A1 domain is known to bind with a membrane glycoprotein Ib (GPIb) on platelets. At the same time, researchers suspect that the A1 domain also binds with collagen fibers to initialize the immobilization of VWF [12]. The A2 domain contains no disulfide bonds, so that it can be unfolded when subjected to pulling force. As unveiled by Zhang, et al. in [13], the A2 domain demonstrates outstanding elasticity that responds to the hydrodynamic force

simultaneously. More interestingly, the A2 domain acts as a safety factor, which cleaves itself while exceed platelets attach on during the blood clotting process [5, 13, 14]. The studies by Zhang and Springer show a self-truncation mechanism during the formation of hemostatic plugs. The metalloprotease ADAMTS13 cleaves the Tyr¹⁶⁰⁵-Met¹⁶⁰⁶ bond [13, 15] when the A2 domain is stretched. The A3 domain works as an anchor to fix the VWF onto exposed collagen (types I, III, and VI) of sub- endothelial matrix when the vessel is injured, so it is extremely essential [16] to determine the efficiency of the hemostatic plug formation.

2.3. Hemostasis and thrombosis

In human body, the blood is circulating in the healthy vessels. The red blood cells predominate in the axial stream, due to the hydrodynamic force gradient, while biconvex disc-shaped platelets are margined to move along the vessel wall. Thus, platelets are at an optimal position to closely monitor the integrity of the endothelial cells of the vessel wall. Normal endothelial cells expose a non-adhesive surface to blood flow. When the vessel wall is injured and the endothelial cells are damaged, the sub-endothelial matrix that contains rich collagen fibers is exposed to blood and initiates the binding of platelets to form a hemostatic plug. Platelet binding is initiated via a collagen receptor, integrin $\alpha 2\beta 1$ (GPIa-IIa) on the membrane. Afterwards, the binding is strengthened via the GPVI receptor.

Adhesion of platelets to the exposed sub-endothelium is influenced dramatically by shear rates [17]. When the shear rate reaches a very high level, e.g. in small arteries,

initial binding of platelets to collagen by $\alpha 2\beta 1$ and GPVI doesn't generate sufficient adhesion. In this scenario, von Willebrand Factor released from Weibel-Palade bodies (WPB) starts to play an essential role. It immobilizes on collagen fibers and bridges with the GPIb-IX-V receptor on the platelet membrane. In the second stage of platelet adhesion, platelets aggregate and undergo dramatic metamorphosis by extruding multiple filopodia to increase their surface contact area on the sub-endothelial matrix.

VWF binding on collagen is mainly triggered by its conformational change. S. W. Schneider in [17] concludes that there is a threshold shear rate that determines the start of the dominant conformational stretch. As soon as the shear rate of the flow field increases beyond this threshold value, VWF multimers undergo large conformational changes to expose as many functional domains as possible to the bleeding site. In terms of elongation of VWF under high shear flow, the cutting edge studies show that the coiled-globular shaped molecule can elongate to ten micrometers or more [5, 14, 15]. The VWF multimeric structure is initially stored in Weibel-Palade bodies (WPB) before the start of hemostasis. Moreover, as reported in [13, 18], within 2 hours after release from WPB into the circulation, ultra-long VWF multimer is cleaved by ADAMTS13 (a disintegrin and metalloprotease with a thrombospondin type 1 motif, member 13) into smaller fragments with a wide range of size distributions. This process is repeated rapidly during the hemostasis process. Consequently, the length regulation of VWF is much more reasonable if it can be measured in post-secretion process [5].

As reported in [13, 18], within 2 hours after release from WPB into the circulation, ultra-long VWF multimer is cleaved by ADAMTS13 (a disintegrin and metalloprotease

with a thrombospondin type 1 motif, member 13) into smaller fragments with a wide range of size distributions. This process is repeated rapidly during the hemostasis process. While the VWF multimers are undergoing elongation, more binding sites are exposed to platelets. Thus the unfolding of VWF enables its maximum hemostatic function, i.e. immobilizes as many platelets as possible in a very short period of time. Moreover, stretched VWF multimers contact collagen in the sub-endothelial matrix at multiple binding sites to maintain firm platelet immobilization. The adhered vWF multimers eventually form a network to quickly capture platelets from the bleeding stream. Some researchers have determined the key role of multimeric VWF self-association or polymerization [19-21] in the formation of platelet plugs in hemostasis. Lots of studies have been conducted to understand the biochemistry of VWF- collagen adhesion. But a very limited number have looked at the adhesion strength (VWF-collagen and VWF-platelet). Therefore, characterizing the mechanical property of this ultra-long protein, especially the A-domains is an important task to understand the molecular mechanism of blood clotting especially under high shear flow during vessel injury.

Finally, the pathological VWF mutations from different types of VWD patients are of extraordinary importance to establish the function of different domains. Many mutant VWF proteins have been identified. For instance, a British team led by Dr. Thomas A. J. McKinnon has successfully matched different VWF pathology with defects in the A3 domain[22] and the A2 domain [23]. Another group in Mayo Clinic reported an A1 mutant VWF [24], which has what symptom?

3. Facilities and Devices

3.1. Atomic Force Microscope (AFM)

Atomic force microscopy (AFM) is one type of scanning probe microscopy (SPM) with spatial resolution on the order of a fraction of a nanometer and force resolution down to single pico-Newton [25]. Nowadays, it is commonly implemented to measure biophysical properties biomolecules and bioparticles.

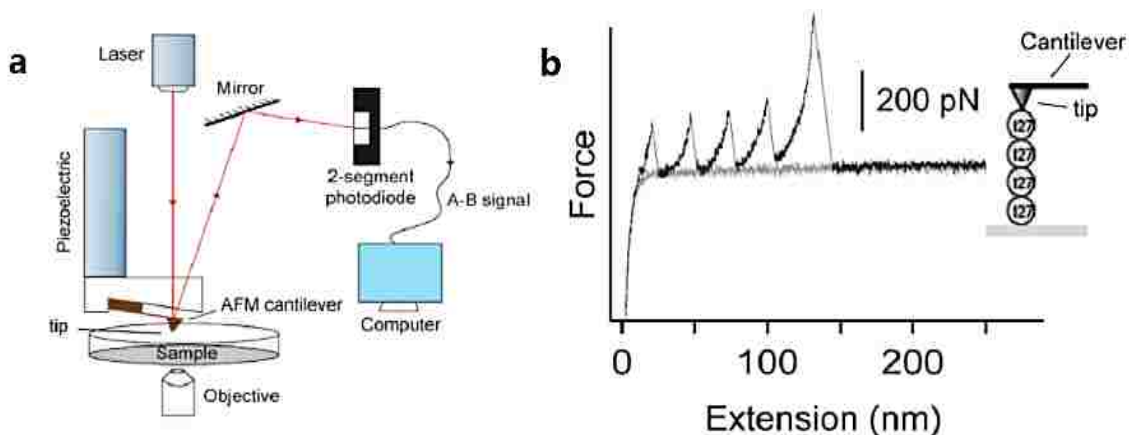


Figure 3. **a.** Schematic of the homebuilt AFM. **b.** Typical AFM pulling curves using Titin I27.

A schematic diagram of the home-built atomic force microscope (AFM) used in this dissertation is shown in **Figure 3a**. The most important parts in this setup include a piezoelectric actuator, cantilever and photodiode detector. The piezoelectric effect is understood as the linear interaction between the mechanical and the electrical state in piezoelectric ceramic materials with no inversion symmetry [26]. In the home-built AFM, the piezoelectric ceramics exhibits a reverse piezoelectric effect: generation of a

mechanical strain from an applied electrical field. By controlling the voltage applied on the piezoelectric ceramic, a displacement of the probe can be achieved precisely. The setup used here has a displacement range of 15 micrometer and probe moving speed of 0.4 micrometer/s to 40 micrometer/s.

As shown in **Figure 3b**, the pyramid-shaped tip repeatedly approaches, contacts and retracts from the substrate. Since the size of the tip is very small (**Table 2** and **3**), interaction between a single receptor–ligand pair [27] is achievable. A typical AFM force scanning curve i.e. voltage vs. piezoelectric actuator’s displacement is shown in **Figure 3b** using four Titin I27. When the AFM cantilever tip contacts the Titin I27 immobilized on a gold-coated substrate, specific interactions occurs between Tintin I27 and the xxx functionalized tip. As the piezoelectric actuator retracts, the pulling force applied on the sample increases linearly due to the bending of cantilever.

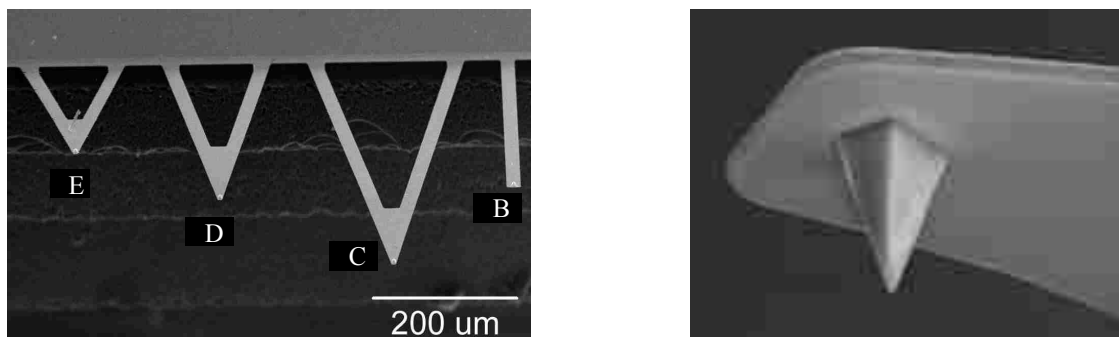


Figure 4. **a.** AFM cantilevers. **b.** Schematic of an AFM cantilever tip. (Reprinted from Bruker website).

Table 2. Specification of AFM cantilever (Bruker).

Shape	Resonant Freq. (kHz)			Spring Const. (N/m)			Length (μm)			Width (μm)		
	Nom.	Min	Max.	Nom.	Min.	Max.	Nom.	Min.	Max.	Nom.	Min	Max.
A Triangular	22	15	30	0.07	0.025	0.14	175	170	180	22	17	27
B Rectangular	15	10	20	0.02	0.005	0.04	210	205	215	20	15	25
C Triangular	7	4	10	0.01	0.005	0.02	310	305	315	20	15	25
D Triangular	15	10	20	0.03	0.01	0.06	225	220	230	20	15	25
E Triangular	38	26	50	0.1	0.05	0.2	140	135	145	18	13	23
F Triangular	125	90	160	0.6	0.3	1.2	85	80	90	18	13	23

Table 3. Specification of AFM cantilever tips (Bruker).

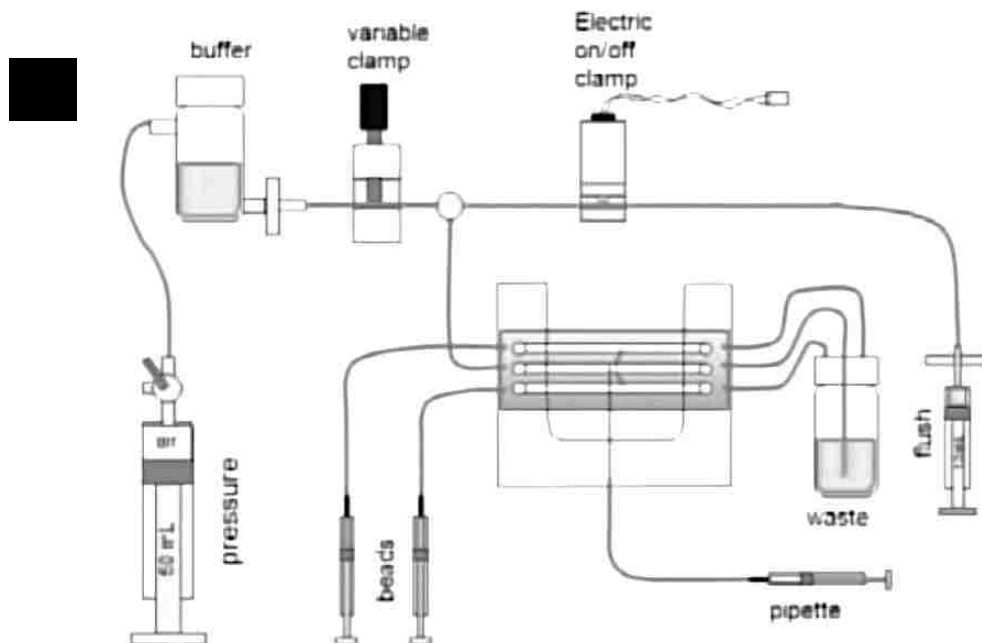
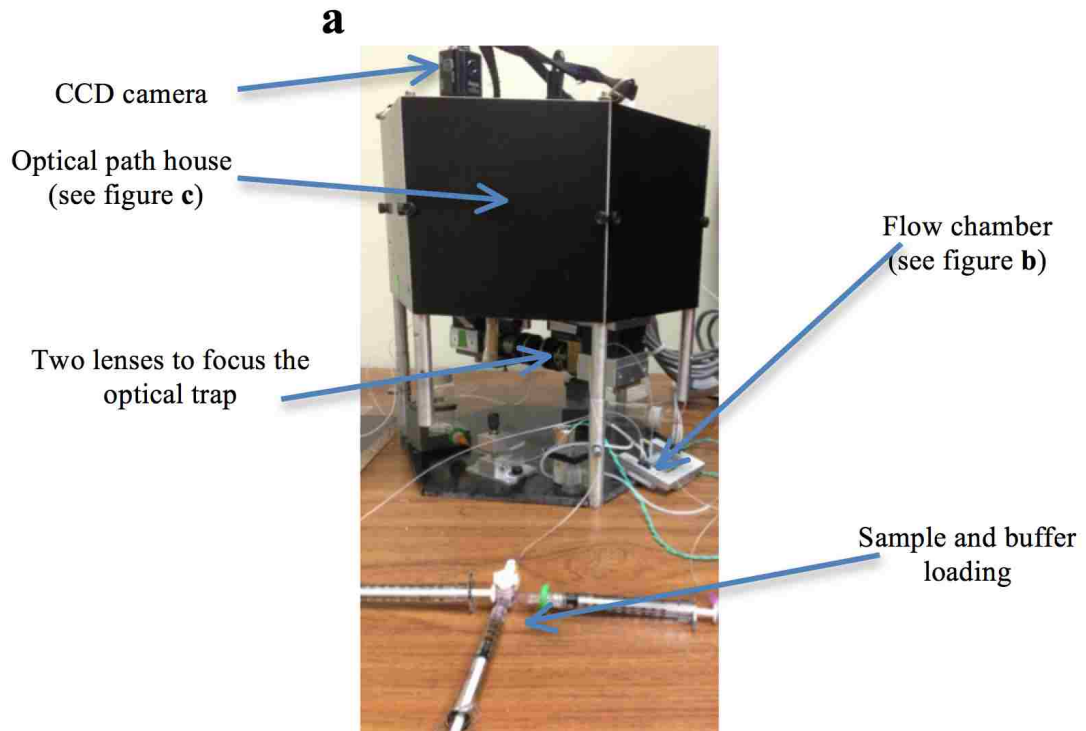
Geometry	Rotated (Symmetric)
Tip Height (h)	2.5 ~ 8.0 μm
Front Angle (FA)	15 \pm 2.5 $^\circ$
Back Angle (BA)	25 \pm 2.5 $^\circ$
Side Angle (SA)	17.5 \pm 2.5 $^\circ$
Tip Radius (Nom)	20 nm
Tip Radius (Max)	60 nm
Tip SetBack (TSB)(Nom)	4 μm
Tip Set Back (TSB)(RNG)	0 ~ 7 μm

The cantilevers used in this work are made of Silicon Nitride by the Bruker Company. By assembling a cantilever at the bottom of the piezoelectric actuator, it conducts the linear movement of the piezoelectric ceramic to the tips at its very front end. A photograph of three cantilevers is shown in **Figure 4a**, and one tip in **Figure 4b**. Detailed specification is summarized in **Table 2** and **3**. The cantilever can be moved with a sub-nanometer resolution in z-direction, which is conventionally perpendicular to the sample plane. During the controllable displacement of the cantilever, the tip repeats contact-retraction cycle on the objective samples on the stage. Consequently, the electrical signals are linearly converted to the displacement of the cantilever tips (passed down from the piezoelectric actuator). In this way, the indenting or pulling force is applied simultaneously. By following the displacement of piezoelectric actuator, the cantilever tip is driven to move in the resolution of sub-nanometer. Based on this mechanical setup, an optical system that includes a light source and a segmented photodiode detector, makes the data collection straightforward but accurate. The customized setup is specifically designed to conduct single molecule spectroscopy in biological samples. In the force-scanning mode [28, 29], a laser (wavelength = 655nm) is focused on the back of the cantilever tip. Due to the reflective gold coating, the laser is deflected and collected by a photodiode sensor via a controllable mirror. The optical signal is then transformed into electric current. The difference of the signal detected from the upper and lower quadrant of the photo detector monitors the deflection of the cantilever tip. Following Hooke's Law for small displacements, the interaction force between the tip and the sample is then determined from this signal after a proper calibration of the spring constant of the cantilever. Taking the properties of the biological

sample into consideration, the contact-retraction loading cycle has to be set within physiological range. The tip of the cantilever can be functionalized with silane, polymer, protein ligands, etc. to establish specificity. For example, polylysine coated cantilever tip can capture cells or protein through electrostatic interaction, which can be further used to measure the interactions between cells or between biomolecules and cells. In this dissertation, proteins are covalently coupled to AFM cantilever tip to study the VWF-ligand interactions.

The mechanical strength of ligand-receptor binding cannot be directly extrapolated from the binding affinities measured by conventional biochemical techniques. In fact, the force resistance can only be measured by specific force measuring techniques [30], such as atomic force microscopy (AFM) [31], bio-membrane force probe [32], or transient tether measurements using flow chamber [33]. Among these, single molecule techniques such as optical tweezers and AFM are more informative because they define the molecular components of the reactions. In this dissertation, AFM is the main technique used to measure mechanical strength.

3.2. Miniature Optical Tweezers



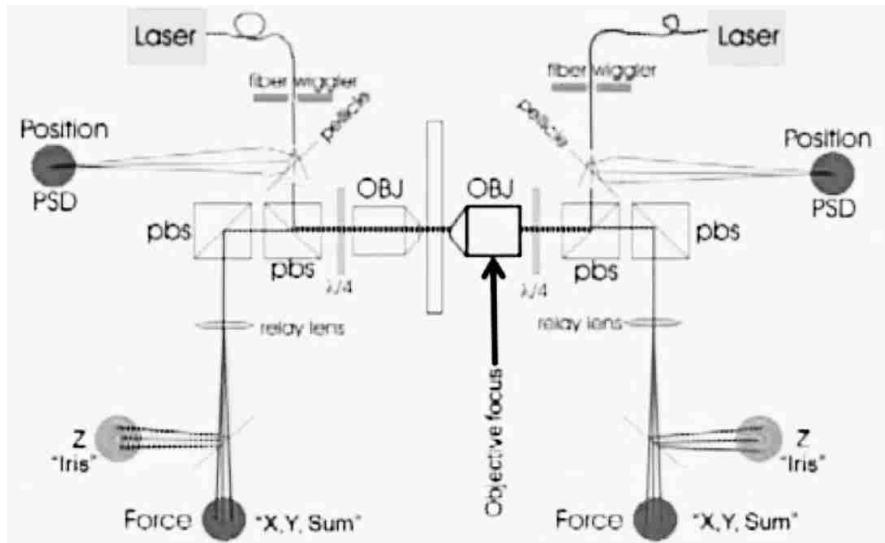


Figure 5. **a.** Optical tweezers. **b.** Fluidic setup of miniature optical tweezers. **c.** Optical layout of miniature optical tweezers (Reprinted from <http://tweezerslab.unipr.it/cgi-bin/mt/home.pl>).

Devices for optically trapping small particles are better known as "optical traps" or "optical tweezers". Those optical tweezers apply one or more laser beams refracted by a microscopic object to trap, levitate and move the object. [34]. By focusing a laser beam through a microscope objective lens down to a very small spot (focal region), particles with high indices of refraction, such as glass, plastic, or oil droplets, are optically attracted to and permanently trapped at the beam's focal region (**Figure 5b** and **c**). From the perspective of biological applications, optical traps can achieve minute forces in sub-piconewton (10^{-12}) range. The miniature optical tweezers used in this dissertation, shown in **Figure 5a**, have two advantages over most other units: instead of calculating force based on spring constants and displacements, the miniature optical tweezers directly

measures force without complicated calibration steps. Moreover, this device has a small size and is portable, compared to classic ones that require to be assembled on big optical tables. Additionally, the small size allows better isolation from surrounding noises and reduces optical interference. The main limitation of the miniature optical tweezers is that the force cannot exceed 100 piconewton (pN). Thus, for single molecular experiments that require relatively high loading, AFM is more applicable. On the other hand, the miniature optical tweezers are more accurate for small force measurements, e.g. the intramolecular and the intermolecular interaction between VWF and GPIbIX, which will be covered in later parts of this dissertation.

3.3. Microfluidic Device

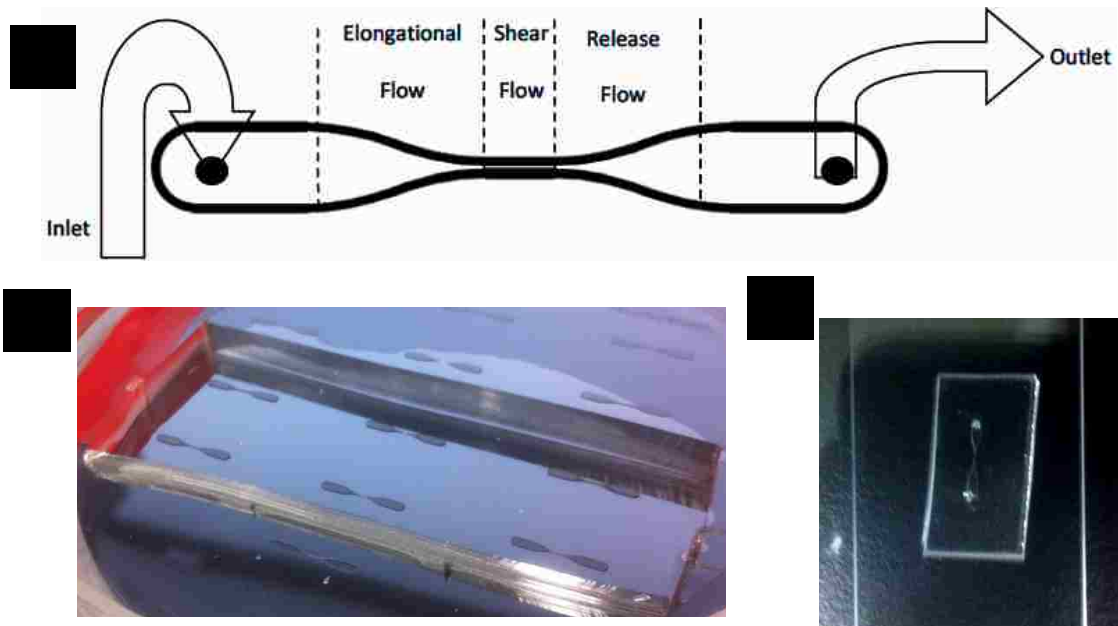


Figure 6. Schematic of the homebuilt microfluidic device. **b.** Picture of the wafer used to make PDMS microfluidic devices. **c.** Device assembled on glass slide with inlet and outlet punched.

Microfluidics are powerful research tools with a broad range of applications. Since their first demonstration in the 1950s, microfluidics has been applied in many disciplines, including physics, chemistry, biology, medical devices and medicine [35-38]. Microfluidic devices with characteristic dimensions on the micron scale can manipulate small volume of fluids with controllable flow fields. The main advantages can be summarized as follows: low reagent and sample volumes are needed, outstanding capability in parallel experiments, ability to mimic the physiology of the environment and pathological input, easy to isolate interesting factors of the objective procedure, ability to control local experimental parameters accurately and it has an extremely low cost.

Figure 6 shows the design of a microfluidic channel used in this work to achieve controllable hydrodynamic fields. The device has a spindle-like shape so molecules in the flow experience elongation, high shear and release in the three segments. This design simulates the elongational flow field occurs during bleeding. As a result, conformational changes of biopolymers and wall-effect interactions under laminar flow fields can be studied. The micro-channel is made of polydimethylsiloxane (PDMS) and bound with thin glass coverslips via an oxygen plasma treatment [39]. PDMS is optically clear, and, in general, inert, non-toxic, and non-flammable. This work focused on the high shear flow region in the middle, which provides a driving force for the conformational change. To achieve steady and continuous high shear rate flow in the channel, a Harvard syringe pump is utilized. Then flow rate of the pump setting can be figured out by simple calculation as following:

$$H = \bar{V} \cdot A = \frac{2A^2}{P} \cdot \dot{\gamma} \quad (1)$$

Where \bar{V} denotes the average velocity of flow, A denotes area of the cross-section, P denotes the wetted perimeter, and $\dot{\gamma}$ denotes the aimed shear rate. The internal surface of the channel is coated with functional layers depending on the flowing particles.

CHAPTER 2

Biomechanical Characterization of VWF-collagen Interaction

1. Introduction

It has already been mentioned in the earlier chapter that to stop the bleeding from an injured blood vessel, a process known as coagulation forms the hemostatic plug to immediately stop bleeding at the damaged vessel wall. During this process, platelets that are circulating in the blood stream have been used as the main material of the plug. More importantly, the von Willebrand Factor (VWF) plays the most essential role by functioning as an injury locator, shear flow sensor [17] and platelet anchor [16]. The hemostatic plug formation starts with adhesion of blood platelets to perivascular connective tissue exposed at the damaged vascular wall through integrin-collagen interactions [40]. This rapid response is just an initial immobilization of platelets to locate the injured site and start the activation process. However, the bond in between is far from enough to resist the high shear flow induced by the damaged vessel. von Willebrand Factor (VWF) is a natural solution for the human body, acting as the hero that firmly anchors onto the exposed collagen fiber with its A3 domain, and strengthens the immobilization of a platelet with its A1 domain [41, 42].

Existing studies have shown that VWF is able to bind with collagen types III, IV, and I in the binding to the sub-endothelial matrix [43, 44]. The A3 domain (residues 923–1109) of VWF serves as the main binding site of collagen [45]. However, some research groups have shown that the A1 domain binds types I and III collagen, though contrasting

evidence has been reported by other groups. [46, 47]. Therefore, does the A1 or A3 domain of VWF bind with collagen solo, or do both of them bind together during the hemostasis process? This has been a long-lasting question in the field and will be further discussed in this chapter. From a larger scale, researchers have also conducted experiments in multimeric VWF to study the binding affinity to the collagen surface. A group led by Schneider has reported their result from a shear-induced stretching assay by using collagen coated microfluidic devices [17]. They further showed the formation of VWF network observed under flow conditions.

In a parallel manner, several remarkable theoretical studies have been done regarding the VWF-collagen interaction. In biochemistry, this type of interaction belongs to the reversible ligand-receptor-type bonds [48], which are very common in biological systems [49]. The typical way to deal with this kind of problem is utilizing the Bell model, which is a physical chemistry theory that claims the difference in activation energy between two reactions of the same family is proportional to the difference of their enthalpy of reaction [50-52]. As to simulating the VWF-collagen interaction, the Bell model has desirable capabilities that parameterize the energy landscape in a simplistic manner by clearly define each of the interacting entities as bound or unbound, and has included an energy term due to the externally applied force [51, 52]. Based on this theory, a so-called force spectroscopy methodology has been employed to quantify the biochemical bond over the past decade or so [53-55]. Narrowing down to the VWF-collagen bond, the height of the energy barrier tells the transition rate between the association and disassociation state, e.g. greater height further impedes the bond and obstructs both the forward and backward transition while a smaller height shows a swift



binding-unbinding transition [48, 53]. At the same time, the width of the energy barrier between the two states describes by what degree the interaction can be influenced by external force, which will be discussed in later sections [50, 52].

2. Materials and Methodology

2.1. Samples and Materials

Within this chapter, an experiment is conducted to characterize the bond between different VWF and collagen. For the VWF here, the samples include: VWF monomer, VWF A3 domain, wild type VWF multimer, NEM- treated VWF multimer [23], W1745C mutant VWF multimer and S1783A mutant VWF multimer [22]. The detailed specification of the sample is summarized in **Table 4**.

Table 4. Specification of the VWF samples.

Sample	Production	MW (kDa)	Structure	Description	Concentration (µg/ml)
VWF Monomer	CHO Stable Cells, Recombinant.	260	Dimeric	From Sino Biological Inc.	200
VWF A3 Domain	HEK293T cell, Recombinant	25	Domain	Made in our lab	1k
WT VWF Multimer	HEK293T cell, Recombinant		Multimeric	From Dr. TA. McKinnon	200
NEM VWF Multimer	HEK293T cell, Recombinant		Multimeric	From Dr. TA. McKinnon	1k

Sample	Production	MW (kDa)	Structure	Description	Concentration (µg/ml)
S1731T	HEK293T cell, recombinant	████████	Multimeric	Made in our lab	1k
W1745C	HEK293T cell, Recombinant	████████	Multimeric	Made in our lab	1k

For the collagen substrate on the sample stage, the human placenta type I collagen from Sigma Aldrich has been used for the entire study. The product is reconditioned in water with acetic acid added to pH 3.0 to obtain a stock solution with the final concentration of 2mg/ml. The selected experimental buffer is Phosphate-buffered saline (PBS). The AFM cantilever is Bruker Nano's MLCT-UT cantilever, and the glass slide to coat VWF is the common microscopy glass slide, 75 x 25 x 1 mm. It was cut into very small pieces before the coating step. Also, the amine-functionalized glass slide from NANOCS, 75 x 25 x 1 mm, is employed in the experiment too. Since this product has the amino group coated on the surface already, the coating process is partially simplified.

2.2. Setup the Atomic Force Microscope (AFM)

The atomic force microscope (AFM) is employed as the experimental platform of this study. The reasons are as follows: first, the measurement is localized on the bond between single molecules; second, based on the flow experiment in [17], the desired force to disassociate VWF from collagen can be higher than 100 piconewton (pN), which

is the upper limit of optical tweezers' measurement range; third, to make the force loading rate of unbinding comparable with the fluid dynamic loading in the flow experiment, the pulling has to be maintained at a relatively high speed and the AFM performs well within this speed range.

Additionally, the energetic property of the VWF-collagen binding is another question expected to be answered. Consequently, the experiment should also be able to run at different temperatures. By taking this into the design of the unbinding assay, a temperature control component has been implemented in the homebuilt AFM device. As shown in **Figure 7**, the temperature control device used in this assay consisted of two Omega Engineering KHLV-0502 Kapton (polyimide film) insulated flexible heaters wired in parallel to a Volteq Hy3005D DC power supply and an Omega engineering HSTC series hermetically sealed, tip insulated, j-type thermocouple wired to a NI DAQ 6215 which records the temperature data for the experiments. The two flexible heaters are adhered to a highly thermally resistant plastic microscope stage. Placed on top of the stage is the 35mm culture dish of which the flexible heaters are situated such that they are adjacent to two of the sides the dish. The thermocouple is allowed to touch the bottom of the dish and monitor its temperature. Note that the area of interest was considered to be small enough that there is not a significant temperature variation across its surface.

Furthermore, from the initial tests, the temperature across the surface can be shown by the thermocouple to at a relatively steady state during the experiment. The temperature is adjusted by varying the voltage from the power supply and waiting for a steady state to be reached on the bottom of the dish. Last, by taking the physiology factor into account,

the temperature should be limited within a certain range. Since this thermo device is not capable to decrease the temperature, the low end is at room temperature while the maximum is lower than 40° C for the most cases. As shown in the schematic in **Figure 7**, the homebuilt AMF with the temperature control component is setup to run the unbinding assay on VWF-collagen interaction.

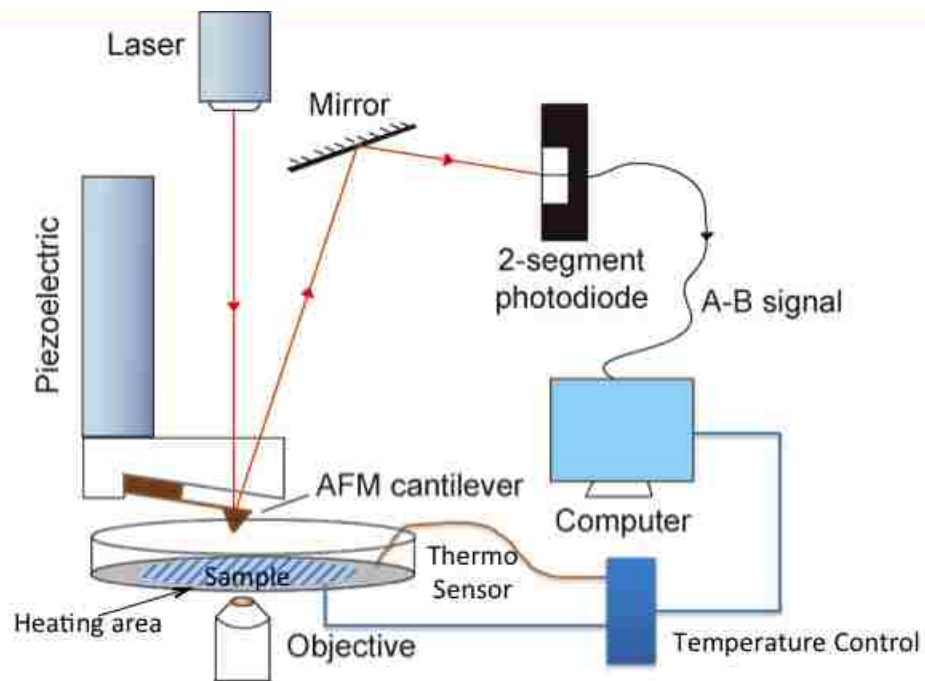


Figure 7. Schematic of the homebuilt AFM with implementation of thermo control component.

2.3. Coating the Probes

Within this chapter, the most essential task is to measure the binding affinity between VWF and collagen. Thus it is essential that the single molecule measurement has

been localized on the binding sites of the two samples. To better achieve the single molecule condition, the most important preparation step is coating the objective proteins onto the probes. To implement the probe functionalization into the AFM, the two objective substrates are immobilized on the AFM cantilever tip and underneath the sample stage. Within this chapter, both sides are using the same coating methodology. In summary, there are three layers coated chronologically: (3-Aminopropyl)triethoxysilane (APTES), Acetal-PEG27-NHS and aiming ligand/protein/cell.

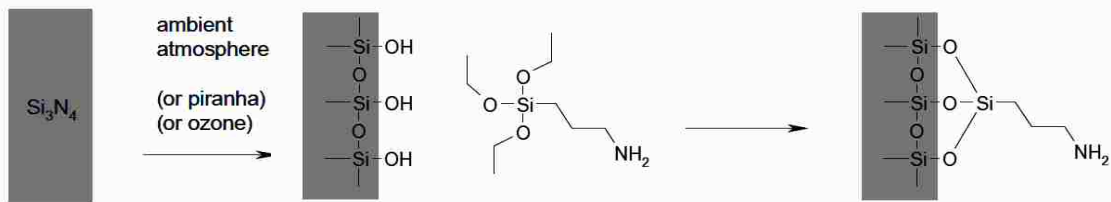


Figure 8. Oxidation and gas phase APTES silanization of silicaon nitride tips

First, for the (3-Aminopropyl)triethoxysilane (APTES) coating layer, the so-called Gas Phase coating method (<http://www.jku.at/biophysics/content>) has been used to guarantee the quality of the amino-functionalization. AFM tips are mainly composed of silicon nitride (or silicon). They can be oxidized spontaneously in the ambient atmosphere, such that a thin layer of silicon dioxide is formed on the surface of the cantilever tips. The oxidation layer contains Si-OH group, which can be used for further chemical functionalization (see **Figure 8**). In the past, the rapid liquid phase amino-silanization protocols were followed for this step. For this method, the APTES silane was simply buffered with polar solvents for example the Ethanol. Although the curing time of

the liquid-phase methods are as short as 15-20min, they are still inapplicable because long, sticky polymers are easily formed, which render AFM tips extremely sticky [56]. As to the application into the VWF- collagen unbinding experiment, a lot of nonspecific adhesion had been observed due to the inhomogeneous amino-silanization layer. Comparatively, the gas-phase amino-silanization allows depositing monomeric APTES molecules to form a homogeneous coating layer while avoiding the formation of large, sticky clusters [56, 57]. **Figure 8** shows the entire conjugation process of the APTES silanization. The amino-functionalization steps are ordered from left to right.

The detailed protocol of using gas-phase amino-silanization to coat the AFM cantilever and glass slide is as the following (the original protocol is from <http://www.jku.at/biophysics/content>):

1. Wash cantilevers (glass slides, cut in small piece) in chloroform for 5 min \times 3 times.
This step should be done in clean glass containers. Dry the cantilevers (glass slides) with nitrogen gas, continue with the next step.
2. Flush desiccator chamber (5 L) with argon gas (through the narrow opening in the lid) for 5 min.
3. Place two Eppendorf reaction vial lids in the desiccator, fill one with 30 μ L fresh APTES and another one with 10 μ L triethylamine under argon.
4. Place the dried cantilevers (glass slides) in the desiccator close to the two reagents from step 4. Seal the desiccator, incubate for 2 h.

5. Open the lid of the desiccator, remove the trays with APTES and triethylamine, flush desiccator with fresh argon for 5 min to remove the rest of gas-phase APTES. Incubate the cantilevers (glass slides) in argon for at least 48 hours to reinforce the coating.
6. Preferably, the amino-functionalized cantilevers (glass slides) can be stored under argon in a dust box for one week.

Second, the second coating layer with the PEG linker (Acetal-PEG-NHS, from <http://www.jku.at/biophysics/content>) should be put on the amino-functionalized cantilevers (glass slides) as soon as possible. Although the APTES coating is supposed to be functional for one week, based on the practical experience, the best effect can be achieved if the PEG cross-linker is coated on right after the amino-functionalization. As shown in **Figure 9**, the PEG has two different arms on each end: NHS group and acetal group. When the PEG cross-linker contacts with the AFM cantilever tip in the solvents, the NHS group binds with amino group immediately. Furthermore, the acetal group can be converted into aldehyde group by immersing the entire cantilever (or glass slide, cut into small pieces) in 1% citric acid for 10 min. After that, the last step is the coupling of the protein and quenching the free aldehyde group [58].

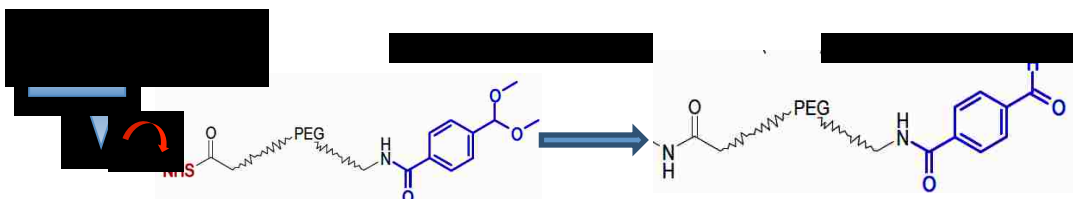


Figure 9. Reaction of NHS-amino group that converts acetal into aldehyde.

The detailed procedure to cross-link the amino-functionalized cantilevers (glass slides) with objective protein is conducted by following the protocol below (the original protocol is from <http://www.jku.at/biophysics/content>):

1. Dissolve 1 mg of Acetal-PEG-NHS cross-linker in 0.5 ml chloroform, transfer the solution into the reaction chamber by using the scaled Hamilton glass syringe, add 30 μ L trimethylamine, and mix well.
2. Immediately immerse the amino-functionalized cantilevers (or glass slides) in the reaction chamber to react with the PEG, cover the chamber, and incubate for 2 h.
3. Wash with chloroform for 10 min \times 3 times. Dry with nitrogen gas.
4. Up to this step, the acetal PEG coated cantilevers (glass slides) can be stored in desiccator under argon for up to several months.
5. Soak PEG coated cantilevers (glass slides) in 1 % citric acid (in water) for 10min.
6. Wash in water for 5 min \times 3 times, then dry with nitrogen gas. After this step, the acetal has been converted to aldehyde that needs to link with objective protein immediately.
7. Freshly prepare a 1 M solution of sodium cyanoborohydride (Sigma Aldrich). The recipe is: 13mg NaCNBH₃ + 20 μ L 100mM NaOH + 180 μ L DI water.
8. Immerse the cantilevers (or glass slides) into 100 μ L protein (e.g., VWF, VWF A3, Mutant VWF or collagen) solution with the concentration of 1-2 μ M. With PBS, the VWF and collagen stock samples are diluted by 20 and 7 folds, respectively.

9. Add 2 μL of the 1 M sodium cyanoborohydride solution, pipette up and down carefully, seal with Parafilm, and incubate under room temperature for 1 h.
10. Pipette 5 μL of ethanolamine (1 M, pH 8.0) to the coating solution (while the cantilevers and glass slides are still soaking in it), pipette up and down to mix well, seal with Parafilm and then incubate for 10 min.
11. Wash in PBS or any other experimental buffer of choice for 5 min \times 3 time.

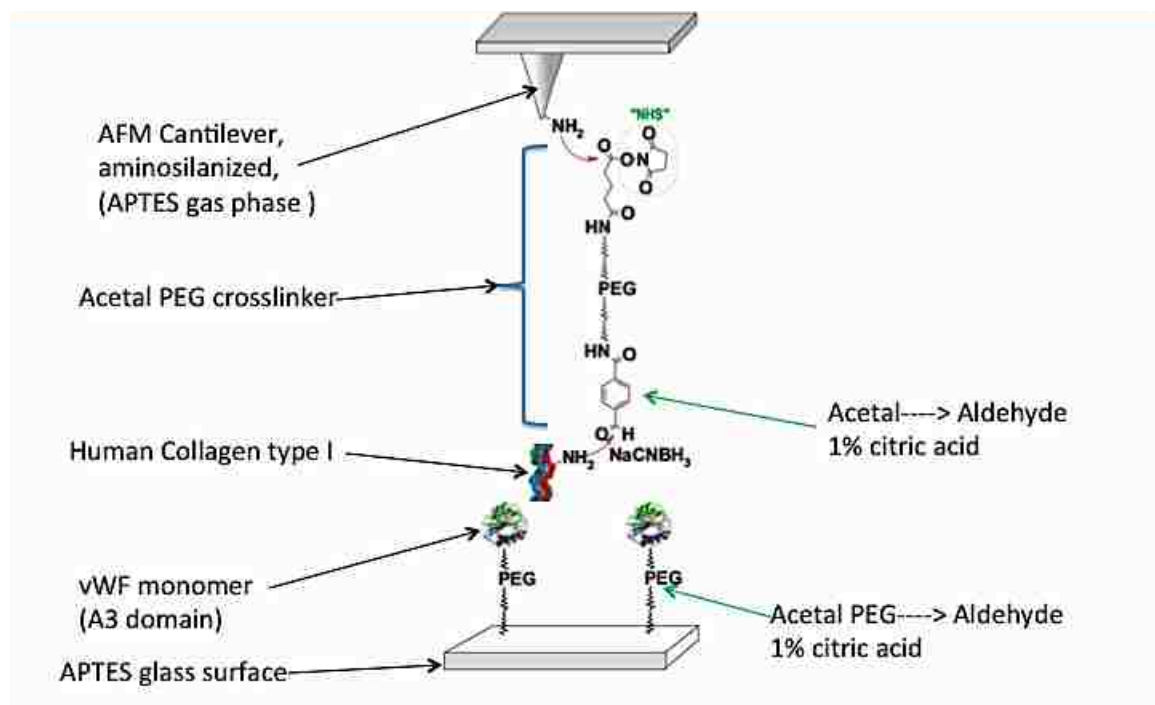


Figure 10. Schematic of the unbinding assay setup. The VWF-collagen unbinding assay is setup on AFM platform [59]. From the top to the bottom: AFM cantilever is mounted with the crystal holder that will perpendicularly drive the cantilever tip, the cantilever tip is coated with APTES in gas phase, acetal PEG crosslinker is conjugated to link the NHS with amino group, collagen is coated on the PEG layer after the acetal group is converted into aldehyde by 1% citric acid, VWF is coated with the same PEG on the functionalized glass piece, the VWF coated glass piece is placed in non-treated culture dish with PBS.

Third, before the start of experiment, the functionalized cantilever is freshly mounted on the cantilever holder of the AFM. On the other side, the coated glass piece is placed in a non-treated petri dish, which was fixed on the sample stage perpendicularly under the cantilever. The entire setup of the VWF-collagen unbinding assay is illustrated as in **Figure 10** above.

There is one challenge throughout the experiment: how to guarantee that a measurement is conducted between single molecules. There is a criterion that has been used a lot for single molecule study. Based on one statistic calculation, when the percentage of specific adhesion is roughly about 30%, people believe the assays are under single molecule situation. This particular detail will be discussed later, but the method of preparing the experiment to achieve single molecule measurement should be solved during the setup stage of the experiments. The easy but effective way to do it is adjusting the sample density on both the probe and substrate. After several preliminary trials regarding the ratio of the coating density, the optimal concentration for collagen and VWF has been determined, which are listed in the previous protocol above.

3. Results and Discussion

3.1. Experimentally Measure the Rupture Force and loading Rate for Dynamic Force Spectrum

The first measurement was conducted on the VWF monomer-collagen and the VWF A3 domain-collagen. Although it has been reported that the A3 domain is the major binding site for collagen [60], some other researches claim that A1 domain binds with collagen as well [46, 47]. The adhesive interaction between VWF and collagen maintains the immobilization of VWF that further assist platelets to rapidly attach to the injured vessel wall in the blood flow stream. As mentioned before, VWF experiences significant hydrodynamic forces in circulation within the human body when hemorrhage occurs in the vessels. Therefore, it is very important to understand the mechanisms that enable adhesion bonds to resist the shear forces in the vasculature.

As introduced earlier, by applying the piezoelectric actuator, the AFM cantilever conducts controllable “touch” between VWF and collagen. The entire movement contains two parts: approaching and retraction. The cantilever moves perpendicularly at a preset speed, and then approaches the collagen substrate on the sample stage. When the two proteins contact each other, the piezoelectric actuator continues applying indentation until the force reaches the preset threshold value that prevents the cantilever from penetrating the substrate. Also, the “dwell time” (i.e., contact time) is set initially by the software to make sure VWF and collagen fully interact with each other. The preset parameters for trails are listed in **Table 5** below. The experiments were conducted between VWF monomer and collagen, VWF A3 domain and collagen. The scanning range determines

the perpendicular distance that the cantilever moves without touching anything. For instance, if the VWF coated slide is 10 μm from the original point of the cantilever, the piezoelectric will move 10 μm down until it touches with the slide. The indentation force will then increase until the threshold. At this moment, the approaching ends and the retraction starts after the dwell time passes. The time between scans is the gap period that separates each scan allowing the sample to relax enough for the next cycle.

Table 5. Preset parameters of the AFM

Preset Parameter	Values for Different Trails
Samples	VWF monomer/VWF A3 vs. Collagen
Pulling speed ($\mu\text{m/s}$)	0.75, 1.50, 3.13, 6.27, 9.40
Scanning range (μm)	0~15
Indentation Threshold (mV)	< 200
Dwell time (s)	0, 1/6, 1/3, 1/2
Time between scans (s)	2

For each force scanning cycle, the Igor software records one pulling curve, which is plotted with all the data points collected during the entire scanning process. In **Figure 11**, some typical pulling curves are shown. For each force-scanning curve, the X-axis is the displacement of the cantilever in μm , and the Y-axis is the different signal (A-B), which is proportional to the force being applied on the sample. The positive voltage shows the

force loading is pulling, conversely, the negative voltage means indenting. By matching the resultant curve with the approaching-retraction cycle of the force-scanning mode of AFM, **Figure 11** describes the process as follows: First, the collagen coated cantilever starts moving down to approach the VWF coated glass slide on the bottom. This stage is illustrated by the blue (lower) curve in the direction marked by the blue arrow. Second, after the cantilever touches the collagen substrate, the tip is bent immediately and its deflection signal increases negatively. The sudden drop of the blue curve near the y-axis shows this stage. Third, after the controllable indentation is kept for the dwell time, the collagen coated cantilever starts retraction from the contacting stage. The recovery part of the red curve that overlaps with the blue drop records the retraction. At this point, if there is any adhesion between the samples, the retraction curve will track a positive peak as shown in the left ones of **Figure 11**. Finally, along with the retraction of the cantilever, the pulling force keeps increasing so that the bond between the samples ruptures when the adhesive affinity breaks. The bended cantilever tip then springs back after released. By showing on the plot, the retraction curve (red) falls back to the zero line. One of the most essential parameters that determine the dynamic force spectrum of a biochemical bond is the rupture force of the retraction during each force scan. Those adhesion peaks not only show the magnitude of the pulling force at the moment when the specific bond breaks but they also reflect the force loading rate with the value of the local slope. One of the adhesion peaks is zoomed in and shown in **Figure 11**. As marked in the figure, the adhesion peak in the pulling curve slants up to achieve the maximum pulling force, and then ruptures and drops back to the standard line. After calibration (measure the spring constant and the voltage-force ratio of the cantilever tip), the Y-direction height of the

peak can be converted to the magnitude of the rupture force, and the fitted slope will be used to calculate the individual force loading rate. The raw data is then collected by recording the y-direction height and the local slope for each adhesion peak.

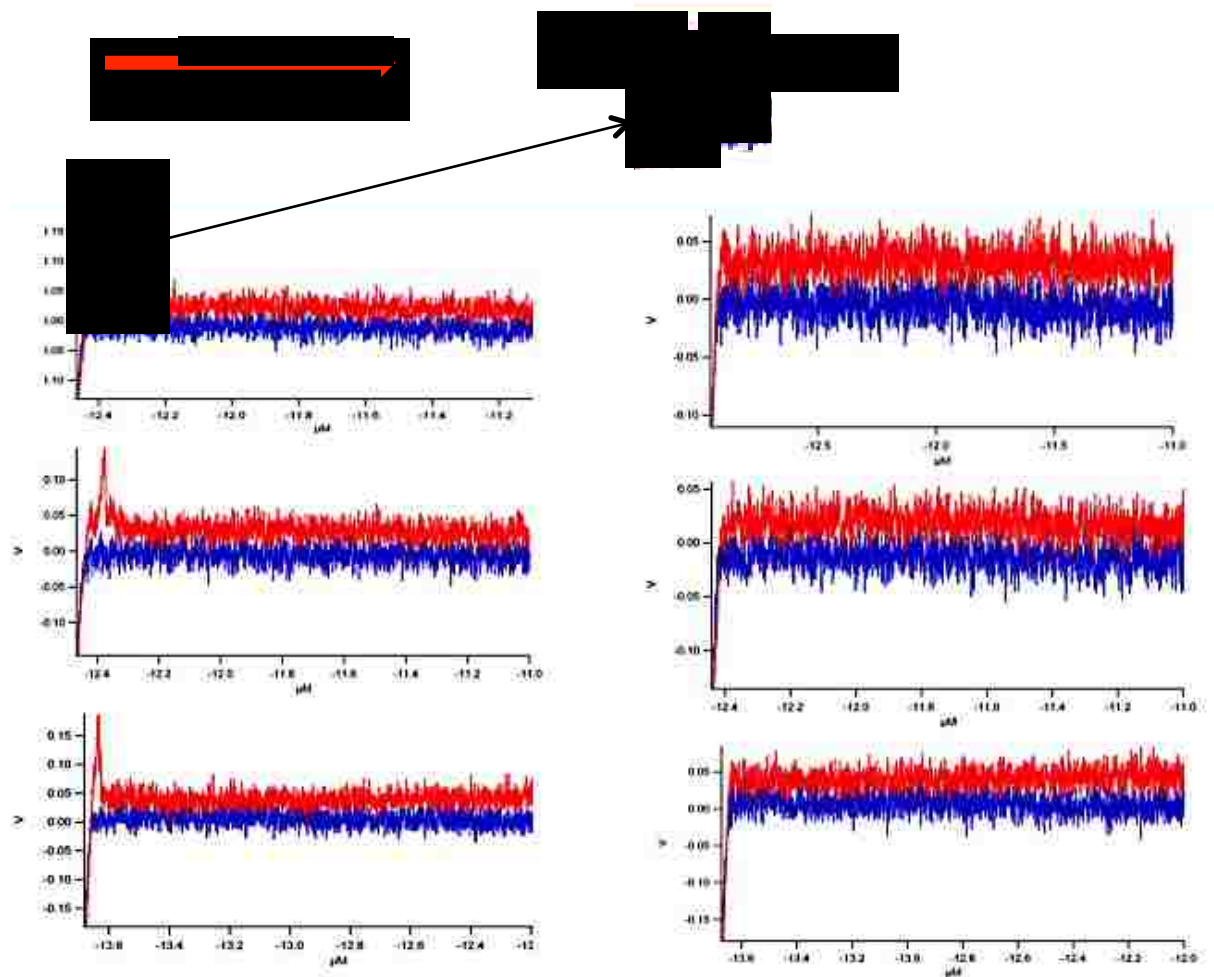


Figure 11. Typical Pulling curves plotted by Igor software (Blue: approaching, Red: retraction). Left: force scans with adhesion between samples. Right: force scans without adhesion between samples.

3.2. Adhesion Percentage and Control Group

Up until this step, it has not been clear whether the interactions measured by this experiment stem from the specific binding between VWF and collagen. There are two possibilities of non-specific interactions: first, the acetal PEG may not be fully converted into aldehyde, but will it bind with the substrate underneath? Second, by using the ethanolamine (1 M, pH 8.0) to quench the free aldehyde group in the very last step of the coating, all the aldehyde-amino binding sites are blocked for sure, but will the ethanolamine quenched aldehyde still interact with the substrate on the other side of the assay? To exclude these two possibilities, control experiments have to be carefully conducted. As shown in **Figure 12**, from left to right, bar one to five represent the adhesion percentage of each experimental control group, six and seven represents the two adhesion percentage of the experiments of VWF monomer-collagen and A3 domain-collagen. Before mounted on AFM, every pair was quenched by ethanolamine to eliminate free aldehyde sites. The three control experiments are: (1) Control-PEG vs. VWF, (2) Control-Collagen vs. PEG, (3) Control-PEG vs. PEG. After that, from bar 4, each one presents the adhesion percentage of different sample pair: (4) Collagen vs. VWF monomer, (5) Collagen vs. VWF A3 domain, (6) Collagen vs. WT VWF multimer, (7) Collagen vs. NEW treated VWF multimer, (8) Collagen vs. S1731T mutation, (9) Collagen vs. VWF A1 domain and (10) Collagen vs. W1745C mutation. The result clearly shows condition six and seven are of a higher percentage of adhesion and it roughly agrees with the single molecule criterion. The specification of the VWF-collagen unbinding assay is confirmed. More importantly, the experiment on Collagen vs. VWF A1 domain here serves as an essential evidence to prove that the A1 domain is not

a binding site of collagen Type I. As reported in existing literature [61-63], VWF A1 domain binds with collagen Type IV. However, there is still no result on the adhesion between collagen type I and VWF A1 domain. This point is actually very beneficial to our study. Since the interference of A1-collagen interaction can be excluded throughout the entire experimental trial, the study was then focused on the collagen-A3 binding.

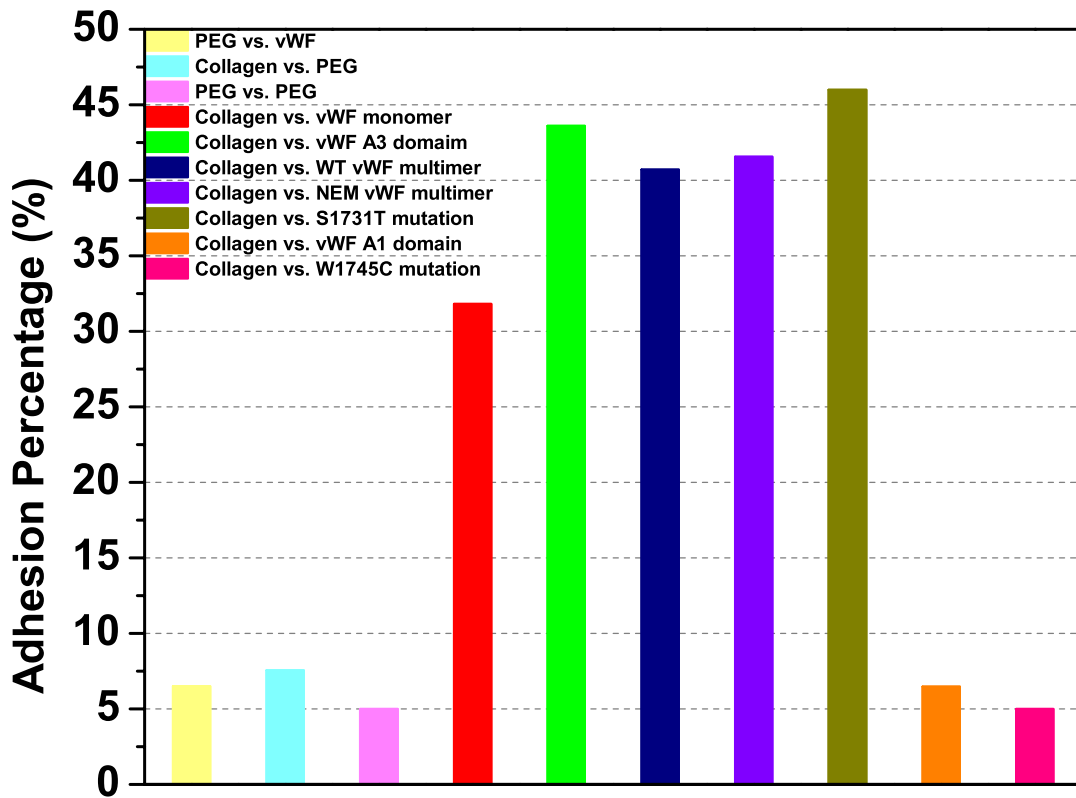


Figure 12. Control experiment group. Every one is quenched with ethanolamine. Adhesion percentage: (1) Control-PEG vs. VWF, (2) Control-Collagen vs. PEG, (3) Control-PEG vs. PEG, (4) Collagen vs. VWF monomer, (5) Collagen vs, VWF A3 domain, (6) Collagen vs. WT VWF multimer, (7) Collagen vs. NEW treated VWF multimer, (8) Collagen vs. S1731T mutation, (9) Collagen vs. VWF A1 domain and (10) Collagen vs. W1745C mutation.

3.3. Identify The Most Probable Rupture Force Under Each Pulling Speed.

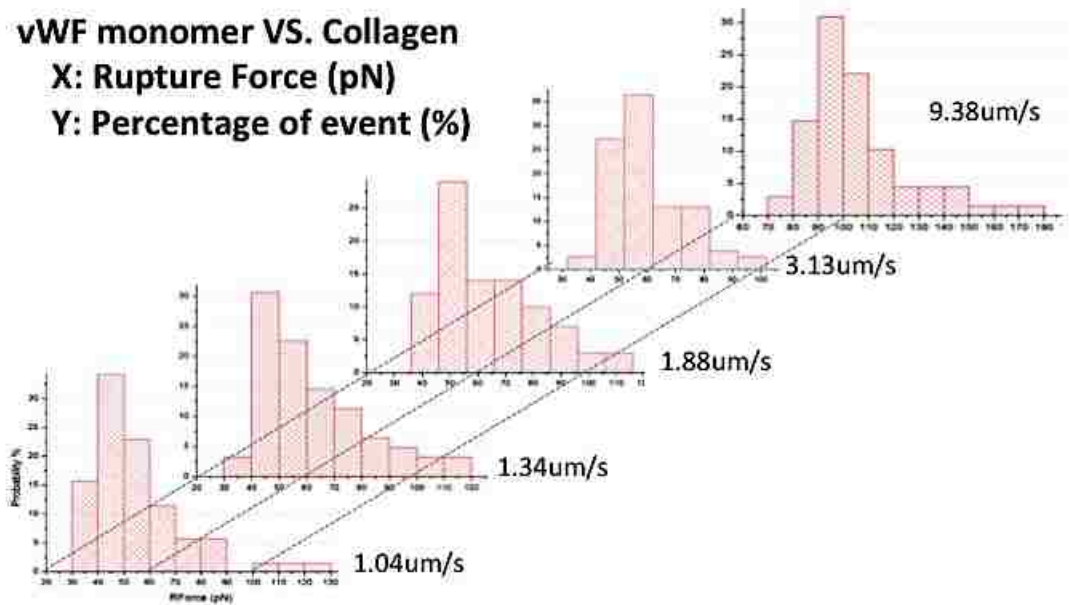


Figure 13. Histograms of the rupture force for VWF monomer-collagen unbinding. X-axis is the magnitude of rupture force with unit of pN. Y-axis is the probability of event under certain rupture force range. Five pulling speeds distribute from 1.04 $\mu\text{m/s}$ to 9.38 $\mu\text{m/s}$.

Equivalently, for each sample pair, the unbinding assay is run at different pulling speeds as a trail. While different loading rates are applied, the rupture force varies dependently. Particularly, the experiment on VWF monomer – collagen has been done at five pulling speeds (can be easily convert to loading rate by multiplying spring constant). Recall the Bell- Evans model for plotting the dynamic force spectrum, the very first step is to post-process the raw data to find out the most probable rupture force under each pulling speed. To do that, a statistical analysis is employed here on the raw data. The

histograms (probability) of the rupture force at different pulling speeds are shown in **Figure 13**.

The same measurement scenarios have also been conducted on VWF A3 domain-collagen interaction, which is shown in **Figure 14**. For this sample pair, the experiment has been run under four different pulling speeds that are comparable with VWF monomer-collagen unbinding assay.

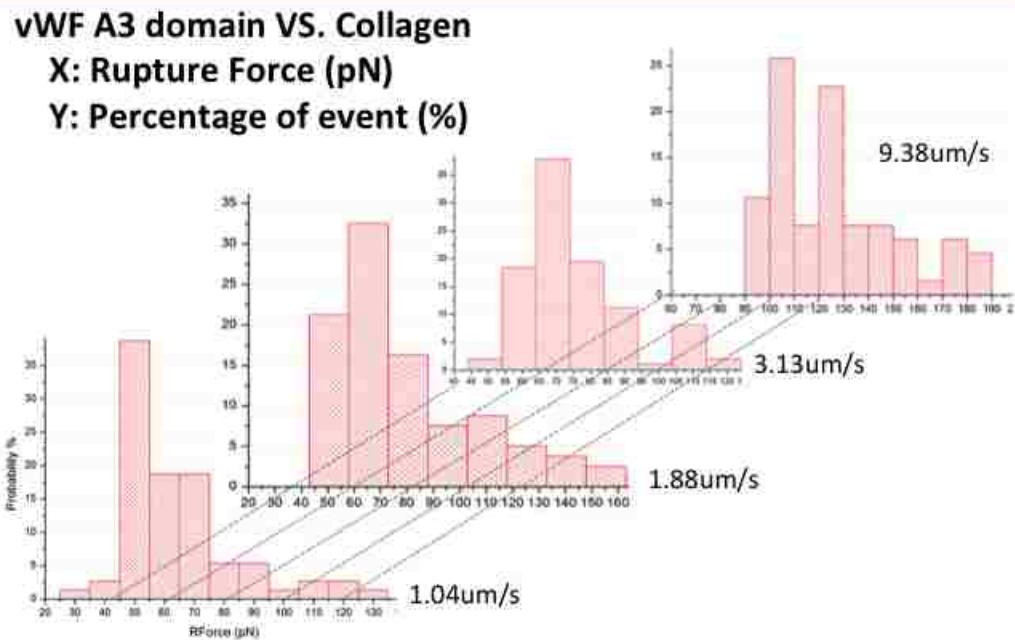


Figure 14. Histograms of the rupture force for VWF A3 domain-collagen unbinding. X-axis is the magnitude of rupture force with unit of pN. Y-axis is the probability of event under certain rupture force range. Four pulling speeds distribute from 1.04 $\mu\text{m/s}$ to 9.38 $\mu\text{m/s}$.

From the histograms in **Figure 13** and **14**, it is very clear that the most probable rupture force is increasing along with the pulling speed. Each pulling speed ($\mu\text{m/s}$) is then

converted to the force loading rate (pN/s) by multiplying it with the calibrated spring constant of the AFM cantilever tip. After that, the dynamic force spectrum was plotted as the most probable rupture force versus the force loading rate. The data fitting process will be discussed in the next section.

3.4. Fitting Data with The Bell- Evans Model

The dynamic force spectrum is specifically developed to analyze the properties of adhesive bond in biochemistry, chemistry and physics fields. Biochemistry scientists have been working on those kinds of theoretical models for several decades. In 1978, Bell proposed his work and later modified by Evans and other researchers [50, 52]. The Bell model is built by utilizing the transition state theory. As shown in equation (2) below, the formula describes how the influence of an external force can exponentially change the rate of bond dissociation:

$$\text{[Redacted Equation]} \quad (2)$$

Where f is external force in the unit of N, k_0 is the dissociation rate constant obtained in the absence of the applied force, T is absolute temperature in the unit of Kelvin, k_B is Boltzmann's constant: $1.3806488 \times 10^{-23} \text{ m}^2 \text{ kg s}^{-2} \text{ K}^{-1}$ and γ is the energetic barrier distance between the bond state and the transition state along the reaction coordinate. Consequently, the Bell model describes that the dissociation rate of the adhesive bond increases exponentially to an external pulling force. Although there is no precise

theoretical justification for the correctness of exponential relation proposed by Bell, recent experimental studies have shown support and general acceptance of this model [53, 54, 64]. The two parameters k_0 (disassociation rate constant) and Δx (barrier distance) are the two key parameters calculated by Bell model. In chemical theory, they describe the depth and the width of the potential barrier, respectively. Based on this understanding, the energy potential of the protein–ligand bond can be accurately defined by the force spectrum. Furthermore, in biomechanics, the Δx value is even more important than others, because it indicates the force resistance of an adhesive bond. To better explain, if the γ value of the protein–ligand bond is small, the external force will have the minimum influence on the bonds' off rate $k_{off}(f)$ under certain external force f , due to the multiplication of f and Δx is small. Conversely, if the Δx value of the protein–ligand bond is large, then the binding will be very sensitive to external force. Again, the reason is the multiplication $f \cdot \Delta x$ term becomes much larger here, which increases the activation potential respectively. Therefore, the parameter γ has also been referred to as the “mechanical strength” of a receptor–ligand bond. However, the value γ is not directly related to the change of the net free energy, thus it cannot be directly extrapolated from the binding affinities.

Originally, the Bell model is utilized to govern how the bond dissociation is effected by the constant pulling forces. However, with the setup of the AFM, pulling the sample pair with a constant force is hard to achieve experimentally. Under this circumstance, running the unbinding assay in linearly increasing force is more feasible by simply applying a constant pulling speed on the experimental probe. In 1997, Evans and

colleagues then modified Bell model to expand its capability that can handle the case of linearly increasing force. While the pulling force is increasing linearly, the most probable force f^* , can be expressed as a function of the loading rate r_f ($r_f=df/dt$):

$$\text{[Redacted Equation 3]} \tag{3}$$

This developed model is called Bell-Evans model (Equation 3). It shows that the most probable unbinding force f^* (rupture force) has a linear relationship with the natural logarithm of r_f . Experimentally, the most probable unbinding force f^* (rupture force) is obtained from its histogram as elaborated earlier. From the plot of f^* versus $\ln(r_f)$, the Bell model parameters can be obtained from the slope and the y-intercept of the linear fit.

$$\Delta x^\ddagger = \frac{k_B T}{m}$$

$$k_0 = \frac{1}{m} \exp\left(-\frac{b}{m}\right)$$

The plot of f^* vs. $\ln(r_f)$ was then named “Dynamic Force Spectrum” [50]. By fitting with the Bell-Evans model, the dynamic force spectrum of VWF monomer-collagen and VWF A3 domain-collagen with the Bell model parameters are plotted and shown in **Figure 15**. Respectively, these two adhesive bonds are very similar to each other. From the single molecule AFM experiment, the strength of VWF monomer-collagen and VWF A3 domain-collagen bonds has been measured. Also, from the similarity between the two sample pairs on the force spectrum, it can be confirmed that, at least with the recombinant proteins samples tested, the A3 domain within VWF is the dominant binding site of collagen.

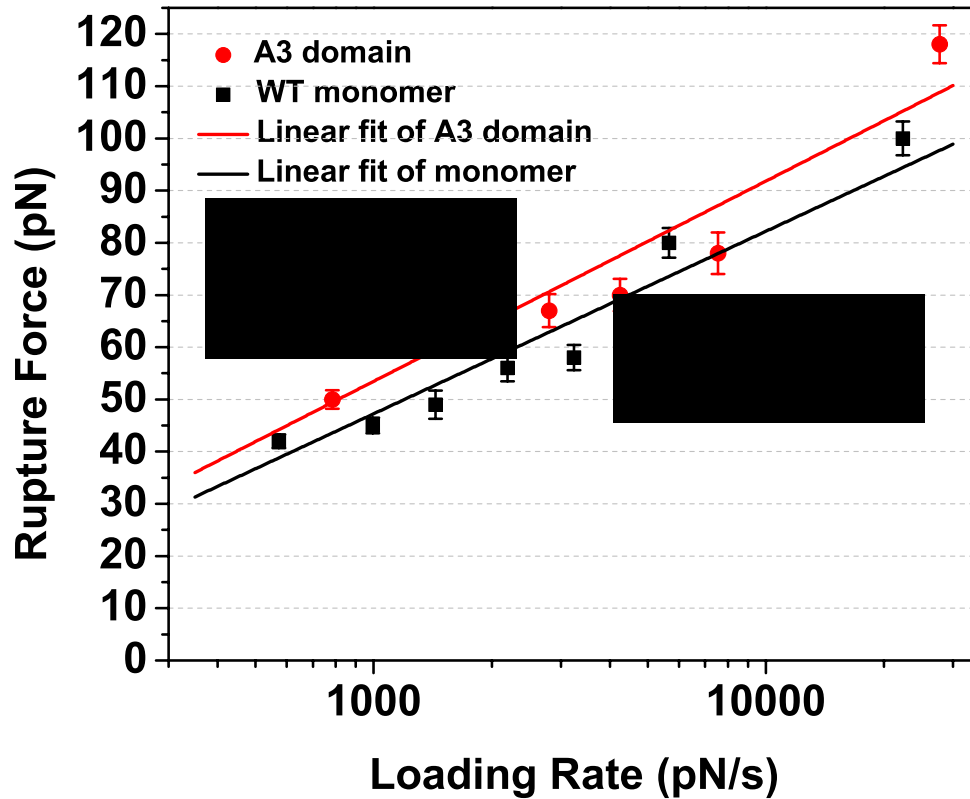


Figure 15. Dynamic force spectrum of VWF monomer-collagen and VWF A3 domain-collagen with fitted Bell model parameters.

In human plasma, VWF exists in a multimeric form, composed of up to 200 monomers. VWF multimers can reach a molecular weight of 2×10^6 Daltons and a length of up to $100 \mu\text{m}$ when stretched [4]. With such enormous length, multimeric VWF carries many binding sites for platelets and collagen and suffers highly significant hydrodynamic forces in the circulating system. When large multimeric VWF circulates in the vasculature, the force applied to stretch the VWF has been estimated to be tens of pico-Newtons. Our data indicate that one to a few A3-collagen bonds would be able to resist the force imposed by the blood flow. This allows the VWF to anchor on the collagen-exposed vessel wall and allows sufficient time for the VWF to elongate on the surface,

which further exposes more A3 to attach VWF. Consistently, in vivo experiments have indicated that efficient VWF binding to collagen is highly dependent on the presence of VWF multimers of high or ultrahigh molecular weight.

VWF binds to collagen at 2 sites: the A3 domain (residues 1683-1874) contains the main site for fibrillar types I and III collagen found within perivascular connective tissue, and the A1 domain (residues 1260-1471) binds non-fibrillar type VI collagen within the subendothelial matrix. However, some research groups have shown that the A1 domain binds types I and III collagen, though contrasting evidence has been reported by other groups. In this study, using an A1 domain that has been shown to bind platelet GPIb-IX, we did not observe any specific A1-collagen binding. It is conceivable, however, that the unbinding force between A1 and collagen was too weak to be detected using our AFM, which has detection limit of 20 pN.

Upon tissue damage, the A3 domain first anchors the VWF onto subendothelial collagen. Subsequently, the A1 domain, via its engagement with GPIb-IX, captures platelets from the flowing blood. When both A3 and A1 bind their ligands, significant tensile forces develop along the bonded chain consisting of GPIb α , A1-A2-A3 and collagen. The mechanical properties of A1-GPIb α and A3-collagen interactions dictate the lifetime of the bonded chain. Fig. 4 shows a comparison of the mechanical properties of the A1-GPIb α and A3-collagen interactions. An examination of the kinetic lifetime profiles revealed that when the force was lower than 20 pN, the A1-GPIb α bond is stronger than the A3-collagen bond. However, for higher forces, the A3-collagen bond is stronger, which is consistent with the notion that VWF is only indispensable under high

shear, which leads to the application of larger forces on the bonded chain. In contrast, in lower shear or static conditions, platelets can adhere to collagen via the integrin receptor $\alpha 2\beta 1$.

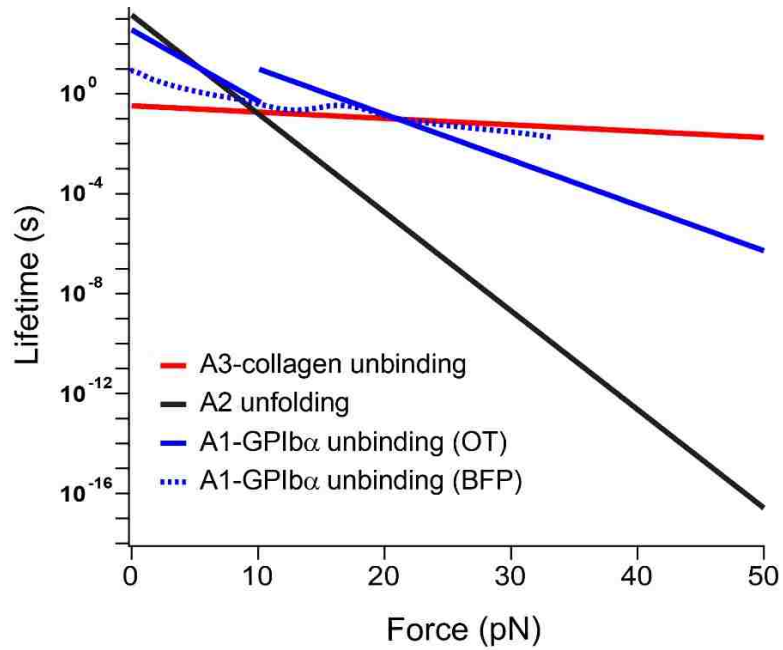


Figure 16. Comparison of bond lifetime as a function of the force of A3-collagen interactions, A1-GPIb α interactions and A2 unfolding. The force-dependent lifetimes (1/dissociation rate) of the complexes were determined by the Bell model parameters, shown in **Figure 15**, or from literature.

The A2 domain, a mechanosensor located between A1 and A3, can be unfolded and cleaved by enzymes to prevent excessive platelet aggregation. The tension developed along the bonded chain may unfold the A2. A comparison of the lifetimes of the A3-collagen interaction and A2 unfolding (**Figure 16**) revealed that the A2 lifetime is longer than the A3-collagen interaction when the force is less than 10 pN. Therefore, for pulling forces less than 10 pN, A2 remains folded. However, when the force is greater than 10

pN, the lifetime of the A3-collagen interaction becomes longer than the folded A2, suggesting that A2 is unfolded under high forces before the bonded chain detaches. This unfolding may allow A2 cleavage to take place to prevent platelet aggregation.

In general, the unbinding assay on AFM platform is a very successful implementation of mechanical methodology into biological study. Probing the mechanical and energetic properties of the bioaffinity with single-molecule method, not only provides a novel quantitative tool to detect the biological interactions, but also uncover the most essential mechanical properties of the interactions. The goal of this work was to establish a more in depth understanding of the biomechanical properties that defines the binding between the A3 domain of VWF and collagen. Our data indicate that the three WT constructs, A3, VWF monomers and VWF multimers, unbind with type I collagen in a similar fashion. Under loading rates of 800 to 20,000 pN/s, the unbinding forces of all three constructs ranged from 50 to 110 pN. The range of loading rates was picked based on the fact that earlier work has demonstrated this to be physiologically relevant to in vivo conditions [17, 65, 66]. Under the assumption that platelets behave as spherical beads with the radius of 1 μm , it can be estimated that at 20 dyn/cm^2 , a typical shear stress found in the microvasculature, the calculated drag force exerted on a single platelet is 64 pN. Therefore, the range of unbinding forces matches the force that VWF potentially receives from a platelet, indicating that one or a few A3-collagen bonds would be able to resist the force imposed by a platelet in blood flow.

3.5. Utilize AFM Unbinding Assay to Define The Force Spectrum for Mutant VWF Multimers

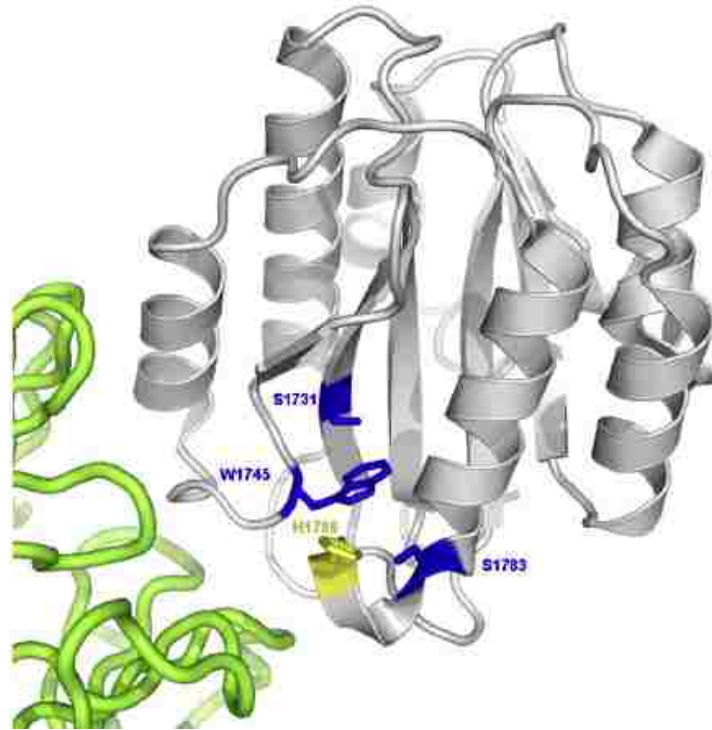


Figure 17. Ribbon diagram of the VWF with mutant A3 domain. The putative collagen-binding surface is toward the lower left of the A3 domain in this view. The 3 naturally mutated residues are shown as blue sticks. H1786 is shown as a yellow stick [22].

As reported in [16, 45], A3 domain binds the fibrillar collagen type I and III, both found in perivascular connective tissue (sub-endothelial matrix). Generally, there are various loss-of-function mutations in the A3 domain, which weaken the VWF-collagen binding. In a recent report published in Blood [22], researchers have studied three mutations: W1745C, S1783A and S1731T which were found in patients with VWD symptoms. By utilizing ELISA type collagen binding assay, W1745C and S1783A were

found to largely abolish VWF-collagen binding, and S1731T weaken binding by roughly 50 percent. Moreover, the group tested another artificial mutation called H1786A, which completely eliminates collagen binding. The locations of the mentioned mutations in A3 domain are marked in **Figure 17**. Therefore, to obtain a comprehensive understanding on the mechanism of the VWF-collagen interaction, also to connect this study with the pathologic deficiency from clinical observation, the AFM unbinding assay has been run on various loss-of-function mutations in the A3 domain. In this way, the molecular determinants that dictate the mechanical strength of A3-collagen complex will be identified as well.

The experimental procedure was very similar as in the experiments discussed earlier in this chapter. After the AFM unbinding assay measurement, the result of different sample pairs was again fitted with Bell-Evans model to obtain the dynamic force spectrum and further predict the potential barrier parameters. By comparing their Bell model parameters, we can finally determine how these mutations alter the force resistance of the A3-collagen affinity within the molecule. Furthermore, we compare the resultant force spectrum (mutants) with previously reported VWF-collagen data from biochemistry assays to help understand the abolishment and establish close connection between the in vitro experiments and clinical observations.

We began with the wild type VWF multimer. Again, the AFM cantilever and the glass slide were amino-functionalized with the gas phase APTES, and then coupled with acetal PEG. Lastly, the cantilever is coated with collagen and the glass piece with WT VWF. After mounting the samples into AFM, the unbinding assay is conducted in five

pulling speed that are the same as we did for VWF monomer and A3 domain. The force spectrum of WT VWF is shown in **Figure 18** together with VWF monomer and A3 domain.

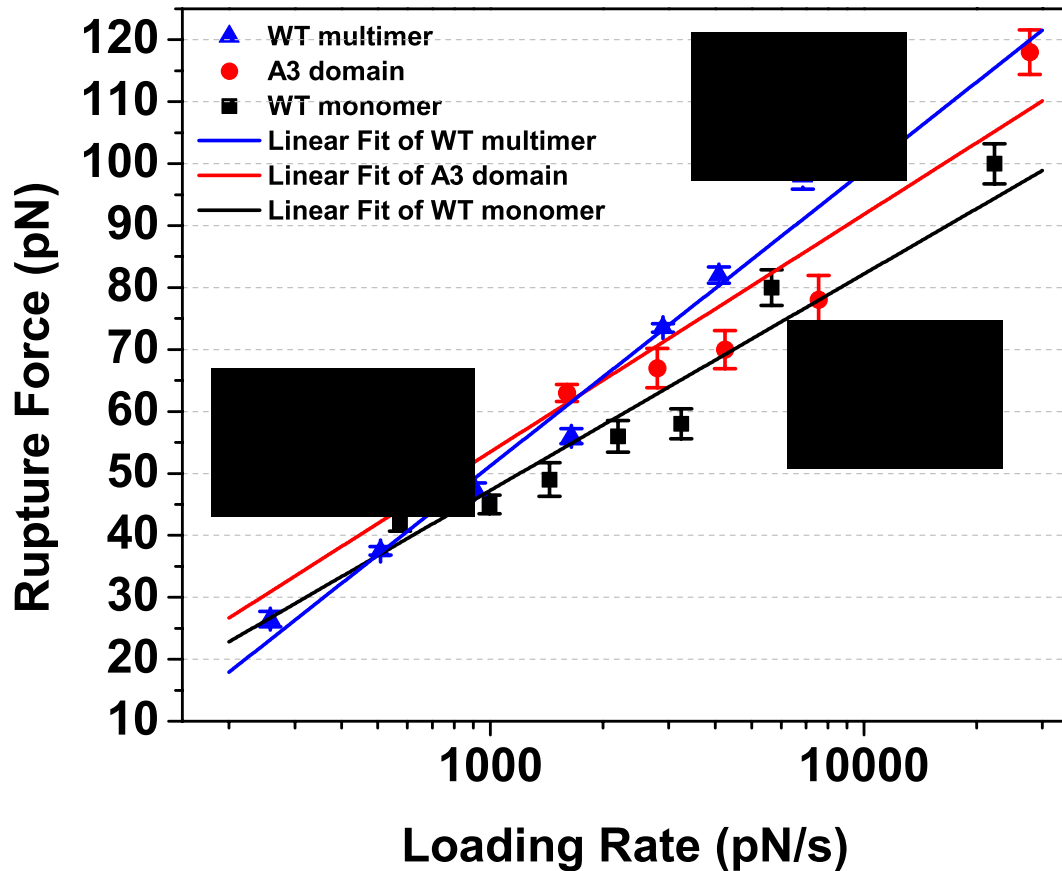


Figure 18. Dynamic force spectrum of WT VWF-collagen interactions, including WT VWF multimer, VWF monomer and VWF A3 domain.

As shown in the plot of **Figure 18**, the blue line (WT VWF multimer) is almost overlapped with the red line (A3 domain) and black line (WT VWF monomer). Also, the resultant k_0 and ΔX are very similar for each case. Therefore, when we pull the WT VWF multimer, the A3 domains on it are still undergoing the unbinding assay with collagen.

The result further proves the A3 domain is the dominant binding site within VWF. We have zoomed out from single domain scale to the multimeric scale of VWF. Moreover, this experiment serves as a linkage of the entire trail, because the mutant VWF samples that will be examined later are multimers. Based on the result of WT VWF multimer, the binding affinity between mutations and collagen will be characterized quantitatively. Another important but obscure issue is VWF's free thiols. Thiol (sulfhydryl) groups on two cysteine residues may form disulfide bonds. Disulfides are in general very important in supporting protein folding, stability and function. The VWF molecule is very rich in cysteines. 8% of matured VWF's 2050 amino acids are cysteines, compared with only 2% cysteines normally existed in human proteins. It has been suggested that mature VWF contains about 80 pairs of disulfide bonds. However, recent studies show that after secretion, the disulfides within VWF can be broken by a few potential mechanisms, such as the presence of reducing agent or enzymes in the circulation or culture media, the exposure of VWF to high shear stress, and the lack of N-linked glycans. Disulfide reduction leads to free thiols present on VWF. How these free thiols affect VWF's structure and function is not well understood.

In this study, multimeric VWF was first mildly reduced by physiologically relevant, submicromolar concentration of reducing agents. The reduced VWF was then treated with N-ethylmaleimide (NEM) to prevent the formation of disulfides among the free thiols. The NEM treated VWF (NEM-VWF), was coupled to glass surface for AFM unbinding assay. As shown in **Figure 19**, DFS revealed that NEM treatment yielded significantly lower unbinding forces between VWF and collagen. Fitting the DFS to the single-barrier Bell-Evans model yielded 3-fold increase of dissociation rate after NEM

treatment. Therefore, the result suggests the presence of free thiols decreases the mechanical strength between VWF and collagen. The underlying mechanism behind this decrease warrants a further exploration.

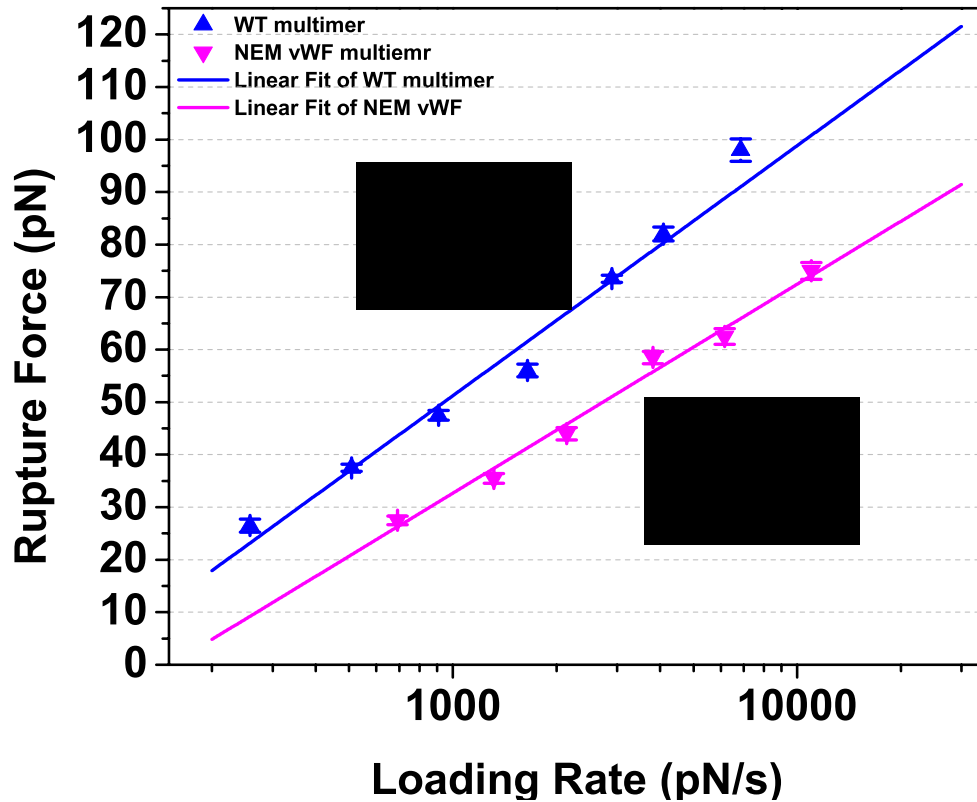


Figure 19. Dynamic force spectrum of NEM treated VWF-collagen interaction, comparing with WT VWF multimer.

At this point, we have obtained the force spectrum of NEM treated VWF multimer. Lastly, the unbinding assay is again conducted on the VWF pathological mutations: S1731T and W1745C. The force spectrum is shown in **Figure 20** with WT VWF multimer as the comparison. It has been reported in [22], the S1731T mutation abolished the A3-collagen binding by about half and W1745C doesn't interact with collagen type I, proved by the ELISA binding assay in **Figure 21**. In the resultant force spectrum of

S1731T mutation, the dissociation rate k_0 is 2-fold greater than that of WT multimer, which agrees with the result of VWF-collagen ELISA binding assay. As to the W1745C mutation, recalling the adhesion percentage in **Figure 12**, it almost has no adhesive affinity with collagen, which agrees with the ELISA result as well.

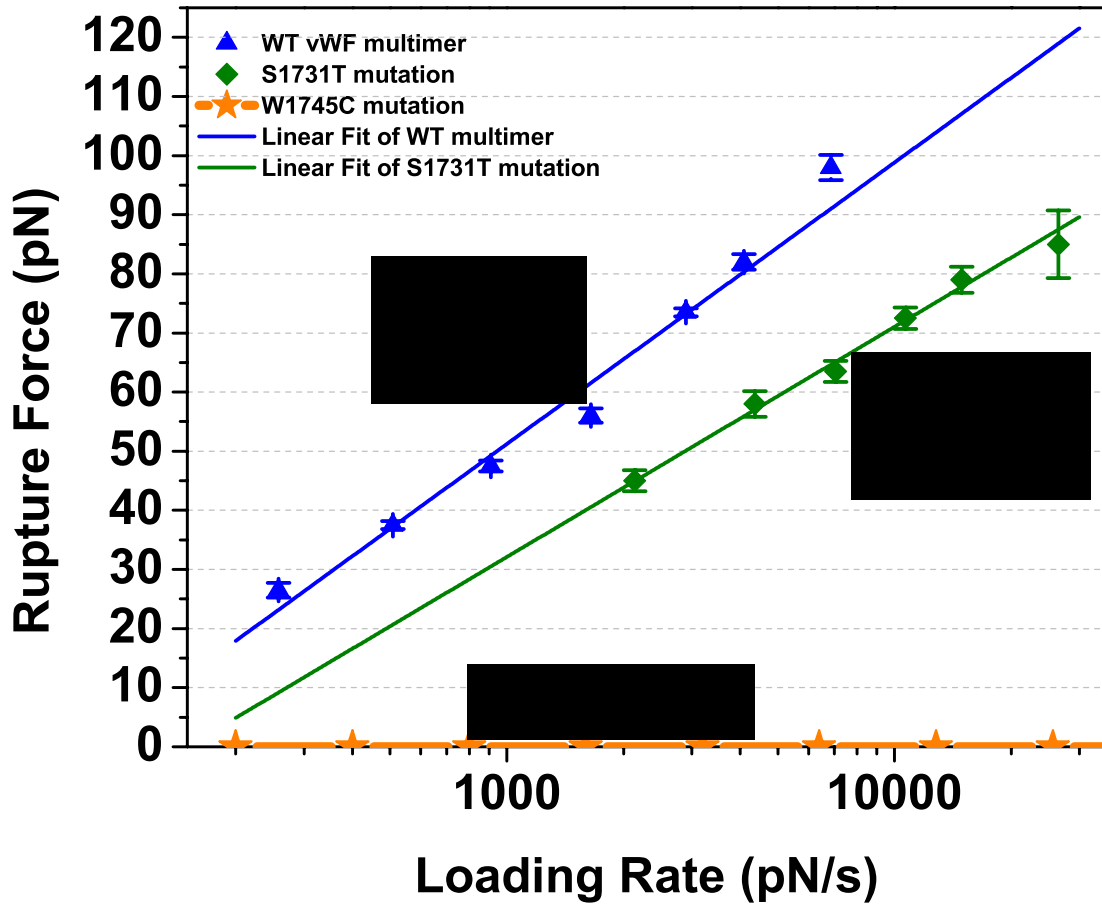


Figure 20. Dynamic force spectrum of S1731T VWF mutation (green) and W1745C VWF mutation (orange), comparing with WT VWF multimer (blue).

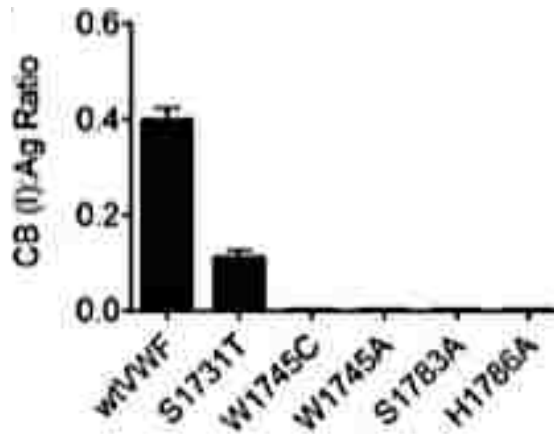


Figure 21. Type I collagen with VWF: Ag ELISA. Error bars represent mean \pm SD of 3 separate experiments performed in duplicate [22].

Functional defects in VWF result in VWD, the most common hereditary bleeding disorder affecting approximately 1% of the population. Type 2M VWD is caused by mutations in A1 or A3 domains that lead to decreased binding of VWF to platelets or collagen. To examine if a change in the overall unbinding force could be correlated to structural mutations found in 2M VWD, unbinding experiments were performed on two VWD A3 domain mutants, S1731T and W1745C. Clinically, S1731T is associated with mild bleeding, and W1745C induces moderate to severe bleeding. Previous ELISA-type collagen binding assays indicated that W1745C VWF does not bind to both type I and III collagen, and S1731T induces only a reduction in binding to type I collagen. In our AFM assay, we did not observe any specific binding between W1745C VWF and collagen. S1731T VWF exhibited specific but significantly decreased unbinding force on collagen. Bell model analysis suggested that S1731T mutation did not change the width of the activation barrier, but suppressed the height of the barrier by 1.1 $k_B T$. Our result is consistent with clinical observations and the previous collagen binding assay. Moreover,

the data demonstrates that after further optimization and validation using human serum samples, the AFM assay could potentially become a very useful tool used to identify future unknown type 2M VWD mutations.

4. Conclusion

In this chapter, unbinding assays on the AFM platform have been carefully conducted. The first experiment was executed to compare the dynamic force spectrum of VWF monomer-collagen with VWF A3 domain-collagen. An overall force spectrum has been plotted to summarize the result of each sample pair as in **Figure 22** and the Bell model parameters are listed in **Table 6**. The result agrees with the initial hypothesis. We have confirmed that: first, A3 domain is the dominant binding site of collagen Type I within VWF; second, the A1 domain doesn't have obvious interactions with collagen; third, the adhesive bond between single VWF A3 domain-collagen is medium (roughly 100 pN level), but still not enough to resist extremely high shear flow during hemostasis process. The conclusions from this chapter also explain why the VWF are always in multimeric structure and the formation of the VWF network in a healthy blood circulating system. Moreover, our data suggest that the VWF-collagen interaction is particularly suitable for mediating platelet-collagen interactions under high shear conditions. VWD A3 mutations alter the mechanical properties of the interaction, resulting in weaker unbinding forces and lower activation barriers. The VWF-collagen interaction also supports A2 unfolding to suppress excessive platelet adhesion. The single molecule experiment on the AFM platform is a reliable and rapid assay methodology to

characterize the bio-interactions between molecules. It supplies biologists a totally new angle to look at the biological system both functionally and structurally. It is noteworthy that the single-barrier Bell-Evans model is the simplest model to interpret our experimental data. The data may also be interpreted by several other models, or by the multiple barrier Bell-Evans model.

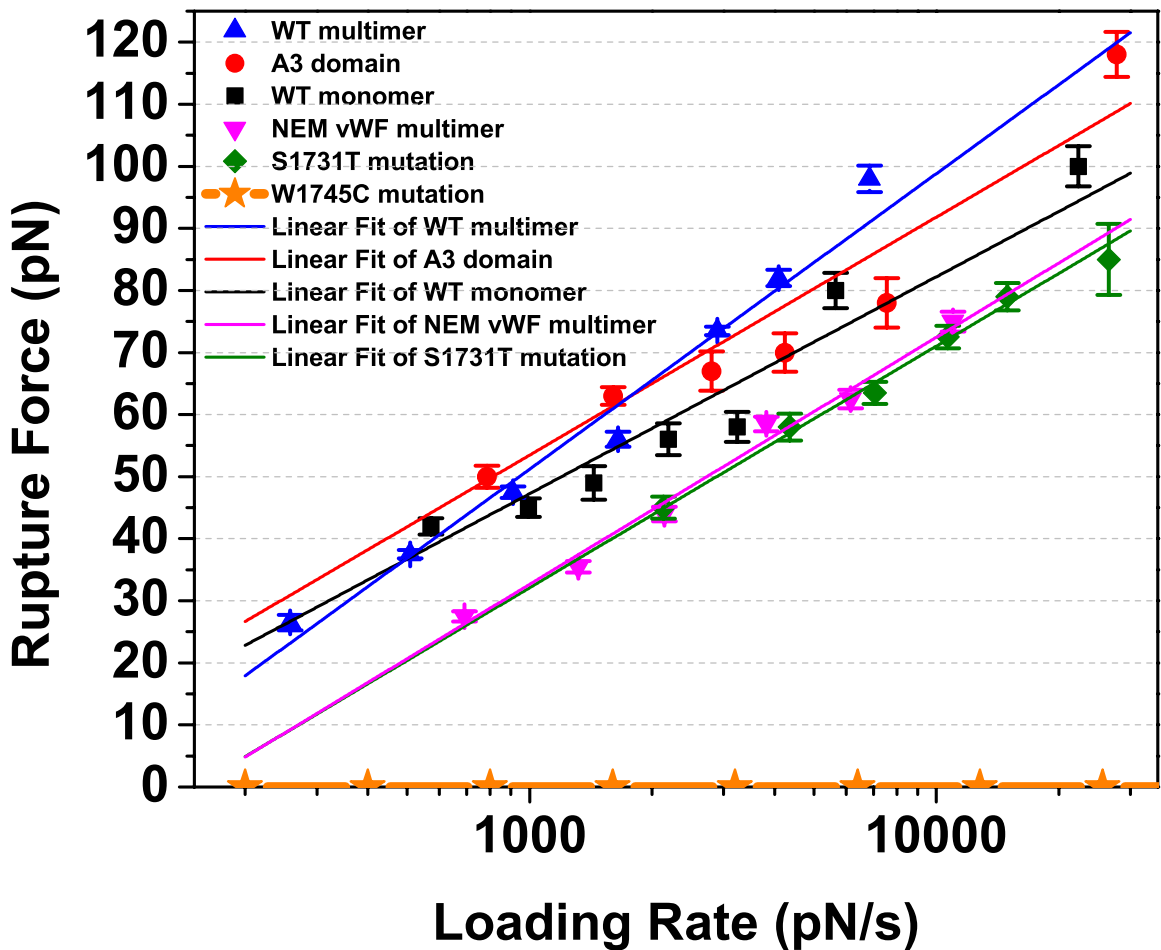


Figure 22. Dynamic force spectrum of all the sample pairs: WT multimer vs. collagen (blue), A3 domain vs. collagen (red), WT monomer vs. collagen (black), NEW treated VWF vs. collagen (pink), S1731T VWF mutation vs. collagen (green) and W1745C VWF mutation vs. collagen (orange).

Table 6. Summary of The Bell Model Parameters for Each Sample in The Unbinding Assay.

Sample	K_0 (s^{-1})	ΔX (nm)
A3	3.016	0.239
Monomer	2.928	0.271
WT multimer	4.06591	0.199035
NEM multimer	8.74785	0.23816
S1731T mutation	8.85773	0.24346

CHAPTER 3

Identification of a Juxtamembrane Mechanosensitive Domain in the Platelet Mechanosensor Glycoprotein Ib-IX Complex

1. Introduction

Physiological hemostasis is an important vascular functionality that enables the blood circulation system to rapidly fix the vessel injury. Throughout the thrombosis process, von Willebrand factor (vWF) and platelets play the most essential roles to mediate healthy hemostasis from pathological thrombosis [68]. Chapter 2 discussed that vWF assists the platelet to localize and immobilize on the damaged part of the vessel wall. On the other hand, the platelet performs aggregation due to the stimulation from vWF. During platelet aggregation, the glycoproteins (GP)Ib-IX and GPIIb-IIIa are the main receptor complexes that process the stimulating signals on the platelet membrane [5, 69, 70]. When vWF is bridging over the collagen and platelet during high shear in the blood stream, it opens up the conformational structure to expose as many functional domains as possible [13, 71, 72]. In the same time, the platelet aggregates to form filopodia, which tremendously increases the contact area of platelet (via a self-association function) [73]. A lot of existing studies have reported that the stimulating signal is transmitted by a subunit of GPIb-IX complex: GPIb α [74-76]. However, how this receptor complex processes the fluid dynamical signal and transforms it into a biological stimulation to mediate platelet functionality remains unknown.

The GPIb-IX complex is structured with GPIb α , GPIb β , and GPIX subunits in a 1:2:1 ratio [77]. Within the complex, the binding site of von Willebrand Factor (vWF) A1 domain, which is a leucine-rich repeat domain, is located in the GPIb α N-terminal. The A1 crystal structures have been determined by [78] and shown below in **Figure 23**. The exact identification of the bond between vWF A1 domain and GPIb IX is still contentious in existing literature [79, 80].

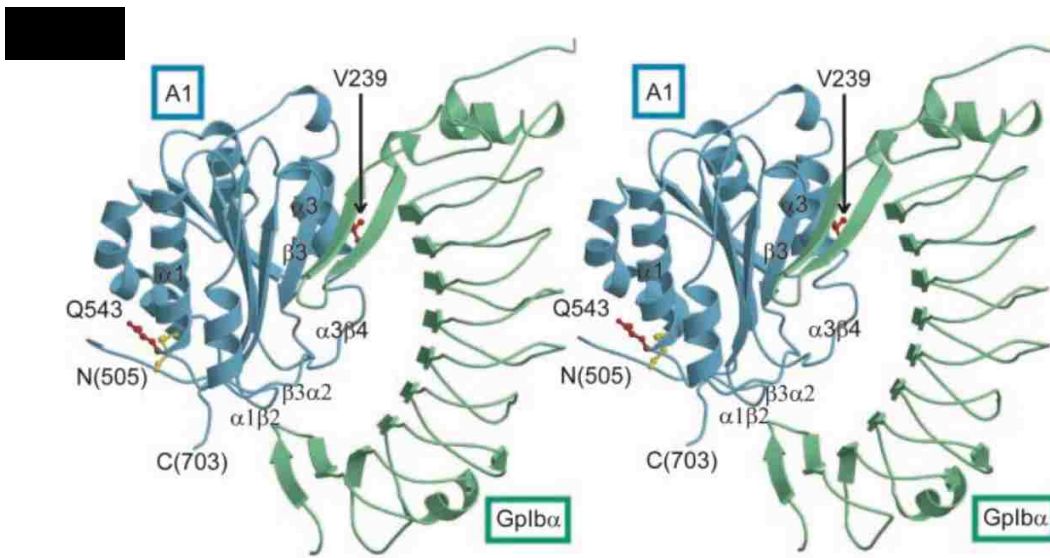


Figure 23. Ribbon structures of the VWF-GPIb-IX complex binding [78].

To identify the mechanosensitive mechanism of the GPIb-IX complex, collaborating with Dr. Renhao Li's group, we employ the optical tweezers pulling assay on VWF A1 domain-GPIb-IX complex [76]. This is the first single-molecule experiment on the full-length recombinant GPIb-IX complex. Specifically, the GPIb-IX complex and recombinant vWF A1 domain (or vWF monomer) are coated on different beads, and then pulled by the optical-tweezers. Since the optical tweezers platform has very good

resolution (sub-picoNewton and nanometer levels), the unfolding of the juxtamembrane stalk region of GPIIb α is expected before the dissociation of vWF A1 domain from the GPIIb-IX complex. Also, the unbinding phenomenon can be measured after the unfolding as well.

Under healthy physiological conditions, the hemostatic plug is not formed in blood circulating system until the vascular damage happens. However the adhesive interaction can be externally changed by botrocetin, a component of Bothrops jararaca venom [81]. It has been reported that the botrocetin promotes the binding affinity between VWF A1 domain and the GPIIb-IX complex on the platelet even when flow field is of relatively low shear. This external enhancement is pathological, because the undesirable interaction causes the loss of effective VWF multimers and a quench of circulating platelets [82, 83]. One hypothesis is the botrocetin first forms a tight binary complex with the VWF A1 domain to enhance its interaction with inactivated GPIIb α [84]. Some other researchers also claim that the botrocetin enhances VWF A1 domain-GPIIb α interaction by inserting an additional binding surface [85]. However, the mechanism of this external enhancement, by which the botrocetin is able to strengthen the binding between VWF and GPIIb-IX complex, is still mysterious in the field.

Building on the platform of optical-tweezers, we are able to physically measure the enhancement from botrocetin throughout the interaction between VWF and GPIIb-IX complex by introducing new fluid environment that contains botrocetin. Under this circumstance, the underlying VWF-GPIIb-IX interaction is immediately placed under the

influence of botrocetin. A comparison then can be easily established to determine the enhancement of bothocetin in a kinetic phase.

2. Materials and Methodology

2.1. Biotinylated GPIb-IX complex

As described in [76], HEK293 Tet-on cells were co-transfected by plasmids pBIG5b-BirA/Ibb/EGFP and pUC19-puro using Lipofectamine 2000 (Invitrogen). The pUC19-puro plasmid was generated by ligating the XhoI fragment of plasmid pTRE2pur (Clontech), which contains the puromycin N-acetyl-transferase expression cassette, into pUC19 vector that had been modified by insertion of an oligonucleotide cassette to contain a single XhoI restriction site in its MCS. Beginning 1 day post-transfection, cells were cultured in Dulbecco's modified Eagle medium supplemented with 10% fetal bovine serum (FBS), 1% penicillin/streptomycin, 5 mg/mL blasticidin, and 2 mg/mL puromycin for 3 weeks. The surviving cells were treated with 3 mg/mL doxycycline for 1 day before being sorted for EGFP fluorescence and surface expression of HA- $\beta\beta$ detected by anti-HA antibody (Sigma-Aldrich/Merck, Darmstadt, Germany). The cells stably expressing BirA/HA-GPIb β /EGFP were further transfected with the pBIG5b-Iba/IX-biotag/mCherry vector, cultured for 3 weeks, and sorted for stable surface expression of GPIb α detected by WM23, and EGFP and mCherry fluorescence. Alternatively, cells stably expressing HA-GPIb β /BirA/EGFP were transiently transfected with pcDNA-Iba-biotag and pcDNA-IX using Lipofectamine 2000. The cells were cultured in the FBS-free

medium containing 3 mg/mL doxycycline and 100 mM D-biotin for 1 day. The cells were harvested and lysed in the lysis buffer (1% Triton X-100, 5 mM CaCl₂, 58 mM sodium borate, 10% protease inhibitor cocktail, 5 mM N-ethylmaleimide, pH 8.0; at approx. 1-2 × 10⁴ cells/mL).

2.2. VWF A1 Domain

Recombinant hexahistidine-tagged VWF A1 domain was made as described in [13], and the VWF monomer was bought from Sino Biotech Inc.

2.3. Antibodies

Antibody WM23 and 5G6 was kindly shared by Dr. Renhao Li. The vWF D domain antibody (mouse monoclonal IgG1, 845 ~ 949) from Santa Cruz Biotechnology was coupled with the vWF monomer. The Fab kit from Pierce was also employed to make Fab version of antibodies.

2.4. Botrocetin

The botrocetin was shared by Dr. Renhao Li with the concentration of 50 µg/ml in 10mM Tris-buffered saline (TBS) buffer, pH 7.4.

2.5. DNA Handles

The DNA handles have been made by following the same protocol in [13]. Two 802-bp DNA handles were generated by PCR with Vent DNA polymerase (New England Biolabs) in 20 mM DTT with pGEMEX 1 plasmid DNA as template (Promega) and the primer 5' thiolmodifier C6-SS- CGA-CGA-TAA-ACG-TAA-GGA-CAT-C and either

5'biotin- or 5'digoxigenin-CAA-AAA-ACC-CCT-CAA-GAC-CC primers (concentration = 1 μ M). Next, handles were activated and coupled to protein through disulfide bonds. The PCR products (10 ml) were then purified by using HiSpeed Plasmid Maxi Kit (Qiagen) according to the manufacturer's protocol with the following modifications. PCR reaction product was diluted 10-fold with QBT buffer (Qiagen) and loaded into pre-equilibrated Qiagen HiSpeed Maxi Tips. Tips were washed with 60 ml of Buffer QC to remove DTT. After that, the DNA (bound in the tips) was eluted with 15 ml of QF buffer and immediately mixed with 0.3 ml 50 mM 2,2'-dithio-dipyridine (DTDP) in DMSO to activate the 5'thiol. Kinetics of release of pyridine-2-thione following activation by DTDP was monitored by absorbance at 343 nm. Derivatized DNA was purified to remove excess DTDP by precipitation with 10.5 ml isopropanol, followed by passing through QIAprecipitator module, with three wash applications of 2 ml 70% ethanol. Derivatized DNA was eluted with 1 mM EDTA in water (pH 8), concentrated 10-fold, and stored at -80°. Typically, the vWF antibody Fab (50 μ L) was treated with 1 mM DTT for 1 hour at room temp. DTT was removed by passing the solution twice through 0.5 ml 7KDa Zeba desalting columns (Pierce). About 5 μ M antibody solution reacted with 10 μ M DTDP-activated DNA handles in 0.2M sodium acetate at pH 5 for 16 hours. Coupled sample (typically 75 μ L) was neutralized by adding 8.3 μ L 1 M Tris pH 8.5, and stored at -80°.

2.6. Beads for Optical-tweezers

Carboxyl-polystyrene 2.0 μ m beads (10 mg, Spherotech, Lake Forest, IL) have been used in all the optical-tweezers experiments.

2.7 Setup for the Pulling Assay on The Optical-Tweezers Platform

2.7.1. Functionalization of the Beads

Similar to the AFM experiments discussed in Chapter 2, the Carboxyl-polystyrene 2.0 μm bead has to be functionalized to establish bioaffinities that can immobilize target samples. The detailed protocol is as follows:

1. Add 10 μl of the Carboxyl-polystyrene 2.0 μm beads into 1.5ml Eppendorf Tube.
2. Centrifuge at 720G for 5 min, discard the supernatant.
3. Dissolve with 0.4 ml PolyLink Coupling Buffer (Polysciences. Inc)
4. Repeat 2-3-2 for 2 times.
5. Add 0.2 ml PolyLink Coupling Buffer to dissolve
6. Freshly prepare 200 mg/ml EDAC solution: 7 mg EDAC+35 μl PolyLink Coupling Buffer.
7. Add 10 μl EDAC solution from 6 to the beads from 5.
8. Shake to mix well for 10min, room temperature.
9. Add protein (Streptavidin/antibody) at about 1mg/ml concentration.
10. Seal with Parafilm and shake to mix for 1 hour, room temperature.
11. Centrifuge 720G for 10min.
12. Wash 5 times with 0.4ml PBST (0.02% Tween 20) for each time.
13. Add 0.2ml PBST (0.02% Tween 20) + 0.2 ml PBS (2mM Sodium Azide)
14. Store in 4°C.

2.7.2. Coat The DNA-Handle Coupled Sample onto The Functionalized Beads

Before the experiment, the functionalized beads are diluted 10-fold and the DNA handle-coupled protein is diluted to about 10 nM concentration and mixed with the beads. Resulting solutions were then mixed well and incubated for 10 min in room temperature. Lastly, the sample was diluted into 1ml with Tris-buffered saline (TBS) and loaded into a syringe.

2.7.3. Optical-tweezers Setup

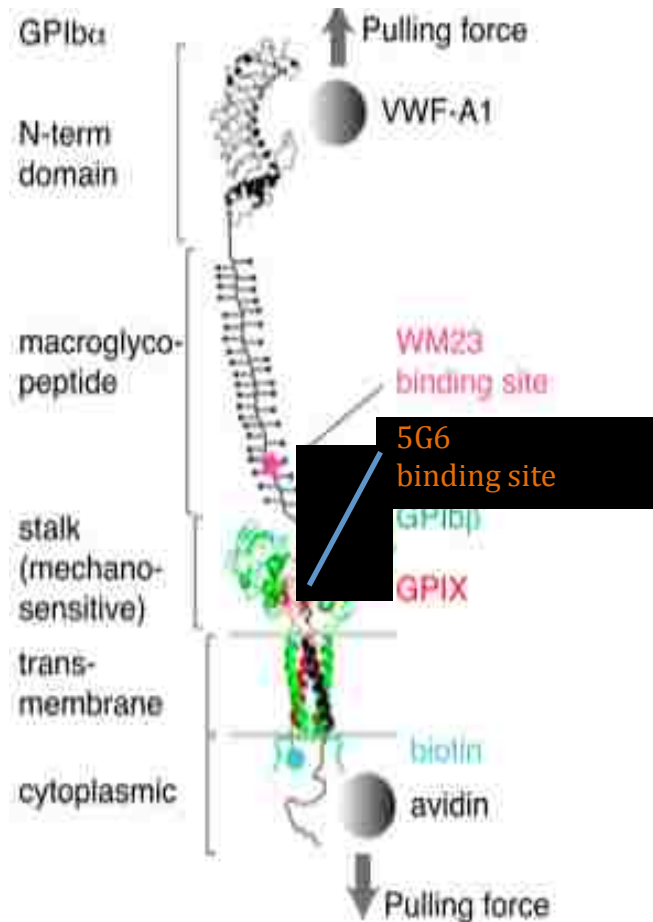


Figure 24. Diagram of the optical-tweezers setup [76].

In the optical-tweezers pulling assay, the laser traps one bead with one of the samples coated on it. Typically, the vWF A1 domain is coupled with Bio-DNA handle and coated on this trapped bead. On the other side, the bead fixed with the micropipette is coated with the biotinylated GPIb-IX complex. As shown above in **Figure 24**, individual domains of GPIb α are marked on the left.

3. Results and Discussion

3.1. Optical-tweezers Unfolding Assay on VWF A1 Domain-GPIb-IX

During the experiment, the optically trapped bead (VWF A1 domain) was driven to repeat the contact-retraction cycle. For each cycle, the VWF A1 Domain was contacted with the GPIb-IX coated bead fixed by the micropipette for about 1 to 5 seconds at a preset contact force (~ 3 pN) and then retracted away in a constant pulling speed. A typical unfolding curve is shown in **Figure 25**.

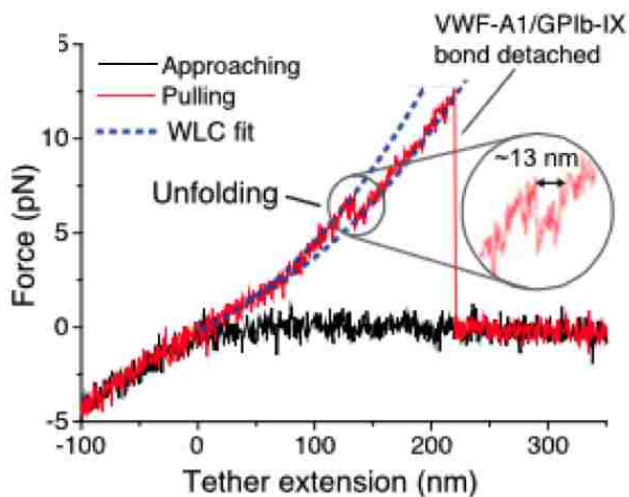


Figure 25. Typical unfolding curve of VWF A1 domain-GPIb-IX [76].

From the plot, the extension length of the tether is about 200nm. Taking the stretching of the DNA handle and the length of the complex into account, the entire extension agrees with the structure of our samples. Furthermore, at the end of the tether, the rupture force (about 10-15pN) is comparable with previously reported results in [86]. Thus the binding strength is relatively weak here, but the result is even more reasonable by considering the physiologic environment in the circulating system. The self-truncation of VWF (by ADAMTS13) has been discussed; coupled with the affinity between VWF and GPIb-IX, they are serving as the safety factor to prevent the vessel from thrombosis. In sum, the implementation of optical-tweezers experiment to measure the binding affinity between VWF A1 Domain and GPIb-IX complex at the single- molecule level is very successful.

3.2. Locate the Mechanosensitive Domain (MSD) within GPIb-IX Complex

Based on the result of the unfolding assay, it has been conformed that there is a domain within the GPIb-IX complex, which can rapidly respond to the external mechanical stimulation and transfer this signal through the entire molecule. Here we named this domain as Mechanosensitive Domain (MSD). After we learned the mechanical properties of MSD from previous unfolding assay, another question is even more important to be studied: where is the mechanosensitive domain located within the GPIb-IX complex? We then narrowed down the scope by running the unfolding assay on different regions of GPIb-IX. Finally, as reported in [76], a so-called stock region exhibits same unfolding properties as we measured from VWF A1-GPIb-IX. To further

confirm the location of MSD is in the stalk region, two antibodies are employed here to locate the MSD.

As shown in **Figure 24**, the WM23 antibody binds on the middle of the macroglycopeptide region. Comparably, another antibody 5G6 binds with some sites inside the stalk region. Hereby, these two different antibodies were coupled with DNA handle and then coated on the avidin bead. We then drove the antibody-coated beads to pull the GPIb-IX complex. If the mechanosensing domain (MSD) that can perform outstanding elasticity to process the mechanical stimulation is in the stalk region, the unfolding spectrum with WM23 and 5G6 antibodies should be different. The unfolding curves are shown in **Figure 26**.

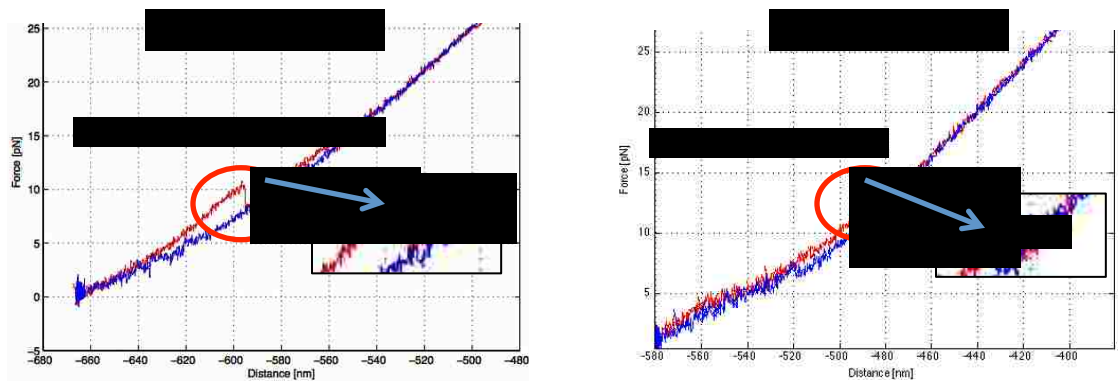


Figure 26. Unfolding curves of GPIb-IX with WM23 and 5G6 antibodies.

Comparing the unfolding curves in **Figure 26**, the unfolding extension is very different from each other, which agrees with our hypothesis. Since the WM23 is bound outside the stalk region, the optical-tweezers were pulling apart the entire stalk region. For 5G6, the optical-tweezers were pulling a part of the stalk region due to the 5G6

antibody bound inside. After analyzing all the data, the average unfolding extensions of WM23 and 5G6 are compared in **Figure 27**. As the bars illustrate, when pulling with WM23 antibody, the GPIb-IX gives about 2-fold unfolding extension compared to the 5G6 antibody. This experimental result gives direct evidence to prove the mechanosensitive domain (MSD) is the stalk region of GPIb-IX complex.

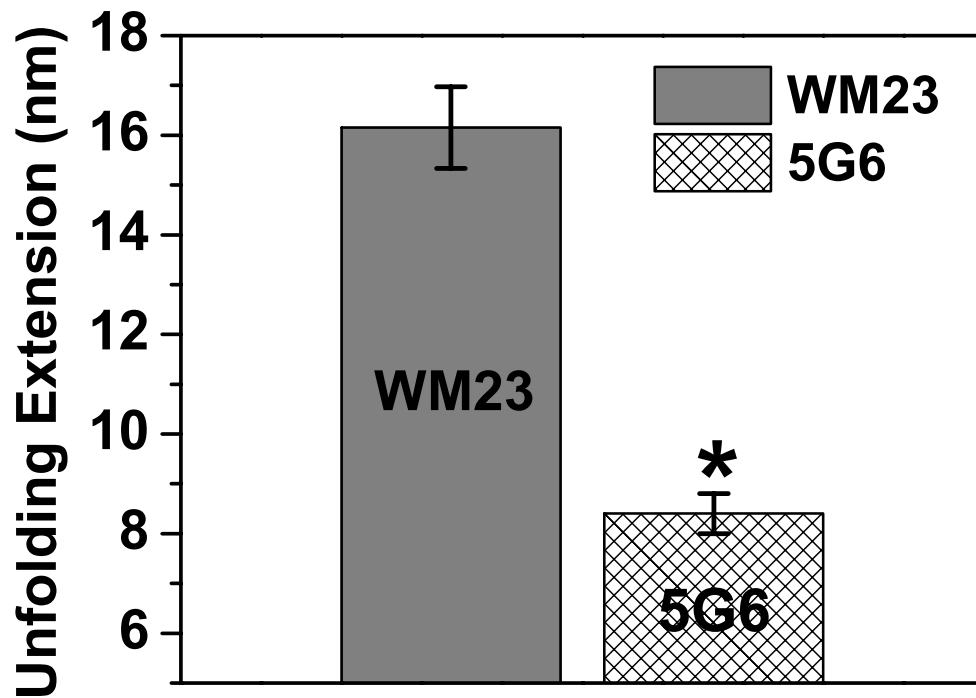


Figure 27. Average unfolding extension of GPIb-IX pulled by WM23 and 5G6.

After the mechanosensitive domain (MSD) has been located, the mechanism of the mechanical signal sensing and processing can be determined. As shown in **Figure 28**, a dynamic model has been proposed to describe the entire signal processing process in GPIb-IX. When the GPIb-IX is inactivated, the MSD in GPIb α is folded (marked in

Figure 28 left). After the platelet anchors on VWF, the external mechanical stimulation from the bleeding stream passes down to the molecule; consequently the MSD unfolds (shown in **Figure 28 right**). The stimulated conformational change in the adjacent extracellular domains of GPIIb and GPIX then sends a signal across the platelet membrane to start the aggregation process of the platelet [76].

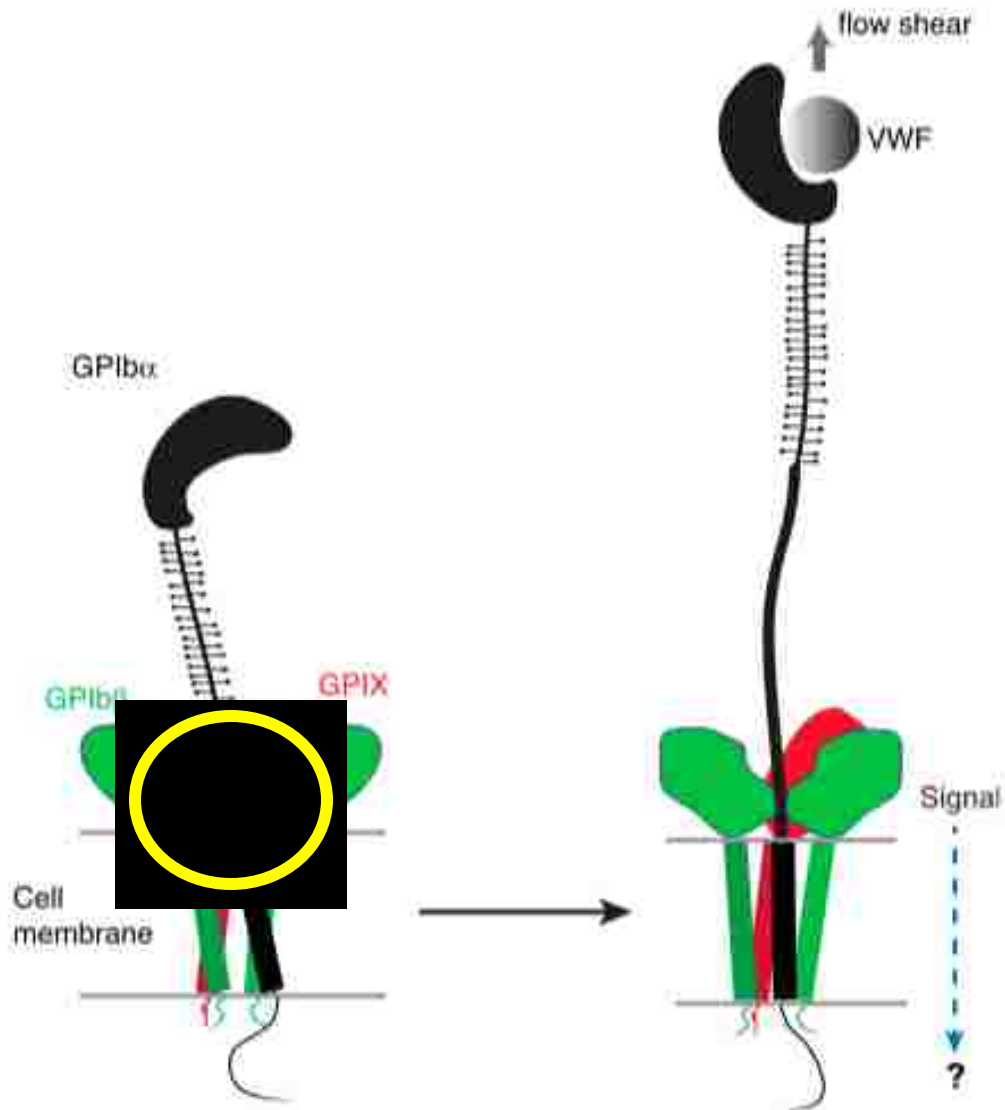


Figure 28. Schematic of a proposed model showing the mechanosensitive mechanism of GPIb-IX [76].

3.3. Measure the Enhancement of Botrocetin on VWF A1 Domain-GPIIb-IX Complex Interaction

By utilizing the optical-tweezers, another similar pulling assay was conducted on VWF monomer-GPIIb-IX complex with the involvement of botrocetin. Particularly, we first coupled the Fab VWF D'D3 antibody (3E2D10, Santa Cruz Biotechnology) with the Bio- DNA handle and then linked it with the avidin bead. Next, the VWF monomer (from Sino Biotech Inc.) was incubated with the antibody-coated beads for 30min. On the other side, the GPIIb-IX complex was coated on avidin beads by following the previous method. During the experiment, the Tris-buffered saline (TBS) buffer was used initially. The unbinding assay was run to record the rupture force between VWF monomer and GPIIb-IX. Afterward, the botrocetin was added into TBS with the concentration of $1\mu\text{g/ml}$. The experimental buffer was then changed to TBS + botrocetin immediately. The exactly same unbinding assay was continued to record the rupture force under botrocetin enhancement. The two data groups were plotted into histogram as shown in **Figure 29**.

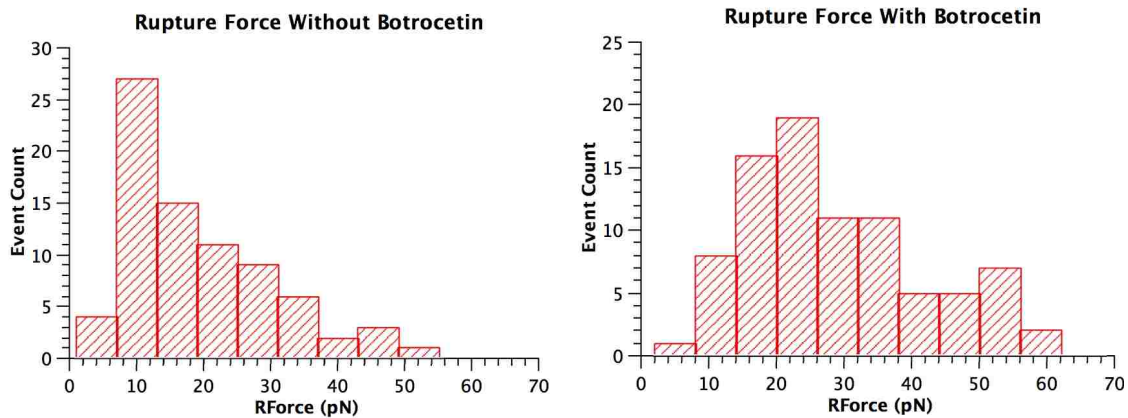


Figure 29. Histograms of the rupture force when unbinding VWF monomer from GPIIb-IX with and without botrocetin.

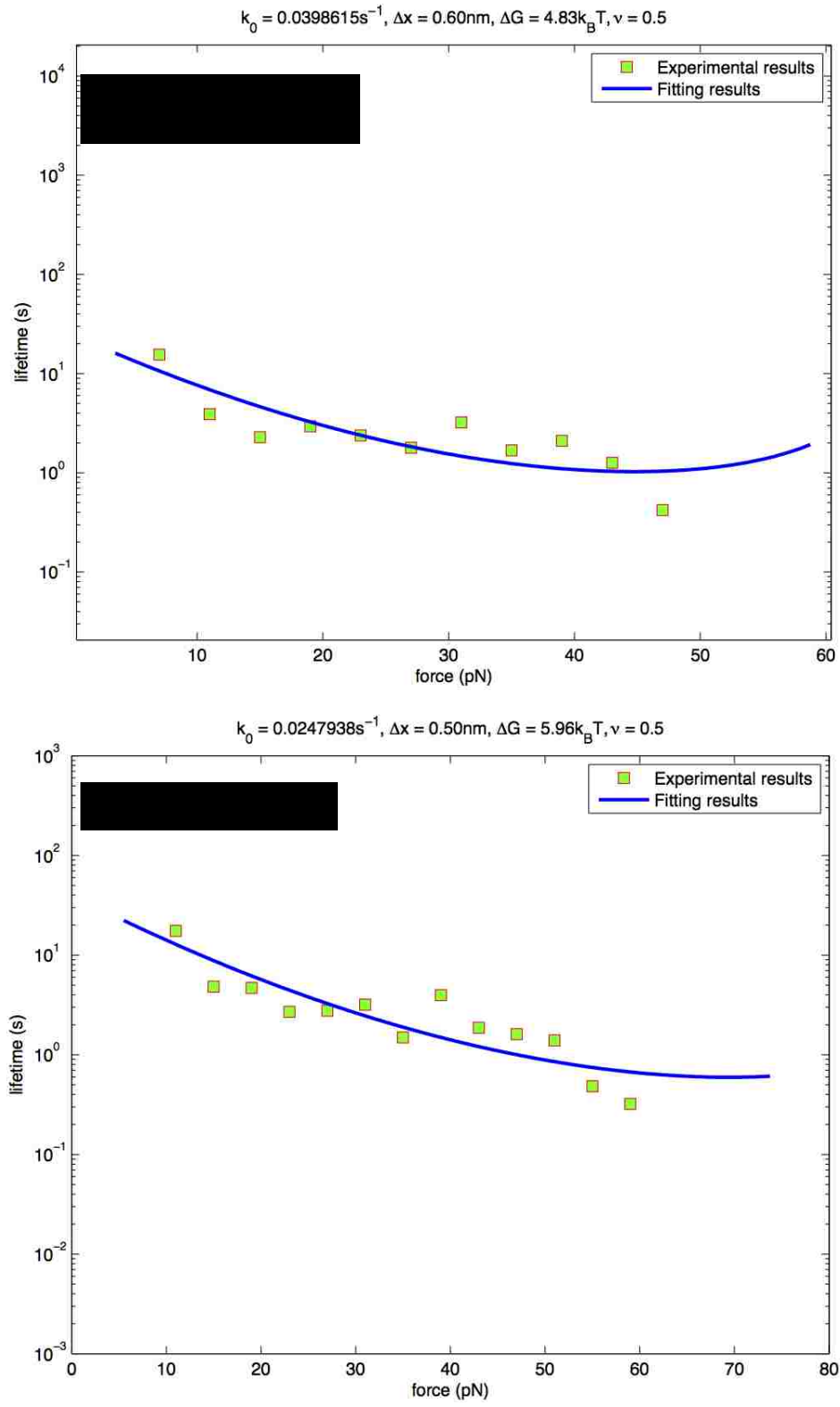


Figure 30. Lifetime (s) versus Rupture force (pN) of VWF monomer-GPIb-IX without (top) and with (bottom) botrocetin.

It is shown clearly that the most probable rupture force to unbind VWF monomer-GPIb-IX is increased after adding botrocetin into experimental buffer. With the botrocetin, the affinity was enhanced about two fold compared to without botrocetin. In the same time, based on the analysis of our data, the percentage of the unfolding of the stalk region was also improved by botrocetin from 32.05% to 65.88%. The dynamic force spectrum was applied to both cases to determine the enhancement from kinetic phase. The k_0 (disassociation rate constant) and Δx (barrier distance) were calculated by fitting the data with Dudko model [87]. The lifetime (s) versus force (pN) is then plotted as in **Figure 30**. The parameters are compared in **Table 7**.

Table 7. Comparison of the Dudko model fitted parameters before and after adding botrocetin

Sample	k_0 (s^{-1})	Δx (nm)	ΔG (k_B)	Unfolding percentage
Without Botrocetin	$0.0398615s^{-1}$	0.60nm	$4.83k_B$	32.05%
With Bothocetin	$0.0247938s^{-1}$	0.50nm	$5.96k_B$	65.88%.

4. Conclusion

In this chapter we first present evidence for a mechanosensor region in the GPIb-IX complex. By conducting force-induced pulling assay on the optical-tweezers platform, the VWF A1 domain was driven to pull the GPIb-IX complex. Additionally, two antibodies that bind onto different locations within GPIb-IX complex have been applied

to identify the position of the mechanosensor. Work here demonstrates conclusively that the mechanical sensing domain is localized to the stalk region of GPIIb/IIIa.

Meanwhile, based on the setup of this experiment, the enhancement of botrocetin on VWF-GPIIb-IX interaction has been studied. The optical-tweezers successfully mimicked the physiologic environment before and after the involvement of botrocetin. Our result indicates the botrocetin is not only promoting the adhesive affinity between VWF and GPIIb-IX, but also altering the mechanical property of VWF. This experiment has built a solid foundation for the study of hemostasis and thrombosis in the future.

CHAPTER 4

Biomechanical Properties of von Willebrand Factor (VWF)

Multimer

1. Introduction

The multimeric von Willebrand Factor is one of the largest proteins in the human body. The multimer (> 20000 KDA) can be constructed of 250 monomers at most [88]. With the help of an electron microscope, people have seen the 50-fold expansion in length between stored VWF in WPB and the stretched form after secretion from endothelial cells in vitro [89]. The VWF multimer is the final functional form of VWF, thus its properties have the most physiological and pathologic meaning. In the present study, multiple experimental methods are employed to further uncover its structural and functional characteristics. Using these experimental methods, the VWF can be studied from a domain phase to a multimer phase, in that the newly discovered properties are more universally examined. First, on the platform of atomic force microscope (AFM), both unfolding and unbinding assays have been done on plasma VWF multimer, recombinant VWF multimer and mutant VWF multimer. The result will be compared with those acquired from the VWF monomer and the single domains. Second, microfluidic devices are utilized. Since the stretched VWF multimer is of an ultra-large size, it can be observed easily under fluorescent microscope. The benefit of this method is that the experiment can be conducted in a real time and the conformational change can then be recorded in a real time. Finally, the optical-tweezers have also been employed to

probe the sophisticated intramolecular interactions within the VWF multimer. A novel assay with double antibodies has been developed for this topic.

2. Materials and Methodology

2.1. VWF multimer

The plasma VWF multimer is purchased from CALIBIOCHEM Company. The recombinant VWF monomer is processed by SINO Biotech, Inc. Dr. Thomas A. J. McKinnon supplies us with the recombinant wild type VWF multimer and the mutant VWF multimers.

The plasma VWF multimer is fluorescently labeled with Alexa 488 (Thermo Fisher Alexa Fluor® 488 Microscale Protein Labeling Kit A30006) and biotinylated with Biotin-xx Microscale Protein Labeling Kit B30010 from Thermo Fisher.

2.2. Microfluidic Flow Chamber

The PDMS chamber was made in Dr. Xuanhong Cheng's lab with Oxygen plasma treatment. Afterward, the functionalization process was performed inside the chamber by following the protocol below:

1. Use glass syringe to inject acetone into the chamber and soak it for 5 min to clean.
2. Clean by UV/plasma cleaner for 20 min.

3. Use syringe to inject 2% APTES (200ul APTES, 8.8ml isopropyl alcohol, 1ml DI water) into the chamber and incubate the device in a clean petri dish sealed with Parafilm for 15min in room temperature.
4. Wash the chamber 5 times by injecting fresh DI water into it.
5. Freshly prepare 0.1% glutaraldehyde solution (8ul 25% glutaraldehyde, 2ml PBS).
6. Inject the 0.1% glutaraldehyde solution from 5 into the chamber and then incubate for 30 min in clean petri dish sealed with Parafilm.
7. Dry by flowing nitrogen gas through the chamber.
8. Inject the protein solution, for example collagen, into the chamber and incubate for at least 1 hour in room temperature. Put it in clean petri dish and seal carefully with Parafilm.
9. Before conducting experiment, inject 50mM ethanolamine solution (in Tris buffer, pH 7.5) and incubate for 15 min to quench the free aldehyde group.
10. Wash with experimental buffer of selection.

2.3 Antibodies and DNA Handles

Two gelatin free VWF antibodies are used in this study. Both of them are purchased from Santa Cruz Biotechnology, Inc: the D'D3 monoclonal antibody (3E2D10) binds between amino acids 845 and 949 of the mature VWF and the C-terminus antibody (C-12) binds between amino acids 2779 and 2813 near the C-terminus of VWF. The antibodies are then treated with the Pierce™ Fab Preparation

Kit (Thermo Scientific 44985) to generate the fragment antigen binding (Fab fragment) to strengthen the specification of the selected binding sites.

3. Results and Discussions

3.1. Unfolding the VWF Multimer with Atomic Force Microscope (AFM)

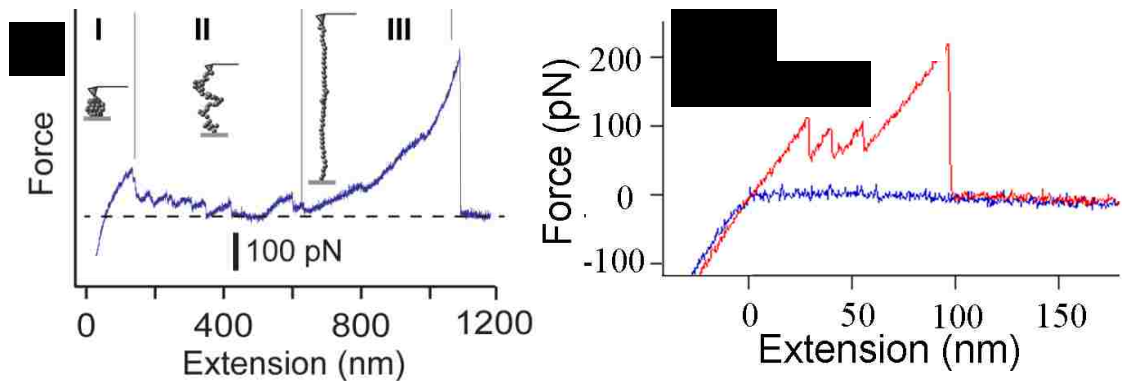


Figure 31. Unfolding the plasma AFM multimer. a. AFM Force-Extension curve of VWF multimer. b. AFM Force-Extension curve of VWF monomer.

We employed a single-molecule pulling and force-clamp measurements to better understand the details of intramolecular unfolding behavior and then relaxation of VWF multimer at a single molecule level. The plasma VWF multimer is immobilized on a gold-coated surface. On the other side, the AFM cantilever is coated with polylysine. Running the force-scanning mode with our homebuilt AMF, the individual VWF multimer has been stretched in a perpendicular direction. As shown in **Figure 31a**, force-extension curve illustrates the fully unfolding of the VWF multimer. While comparing

with the conformational change of the VWF, we can divide the entire elongation process into three stages. In stage one, the VWF multimer is in compact shape and adheres just to the cantilever tip. As shown by the dash line, in this stage the compact VWF is able to withstand a force around 100 pN. Afterwards, the process comes to the second stage. The biopolymer starts local unfolding and the contour length of VWF increases steadily. Based on previous study reported in Ref [13], A2 domain of VWF can achieve 10 to 20 pN unfolding force before it is ruptured. Thus the saw-tooth patterns in this stage indicate the unfolding of the domains. Finally, in stage three, the entire VWF is fully stretched. Force-extension curve in **Figure 31a** suggested a contour length of about 1.2 μm which agrees with the EM result of fully extended VWF [90]. Furthermore, by recalling Hook's Law, the spring constant can be estimated in the order of 1 mN/m. Comparably, as shown in **Figure 31b**, the monomeric VWF exhibits a contour length of about 75nm. But the spring constant is a little higher than multimer, about 2mN/m. The length of a fully extended VWF monomer has been reported to be around 80nm [4, 5, 91].

3.2. Characterization of the Interaction between VWF and Collagen under Shear Flow

Previous studies have shown that the shear flow can alter the conformation of VWF [17, 92, 93]. However, questions such as: what is the most essential cause of VWF's unique hydrodynamic behavior, does the conformational change depends on the adhesive affinity between VWF and collagen still remain unclear. In order to answer these questions, we employ fluorescent microscope to directly visualize the unfolding

behavior of an individual VWF multimer in a microfluidic channel under controlled hydrodynamic field. By measuring the rates of attachment to inner surface and recording the conformational changes in a real time, at the moment that VWF becomes attached on the collagen coated wall, the result may be able to answer if the adhesion is proportional to the shear rate and/or the altered conformation.

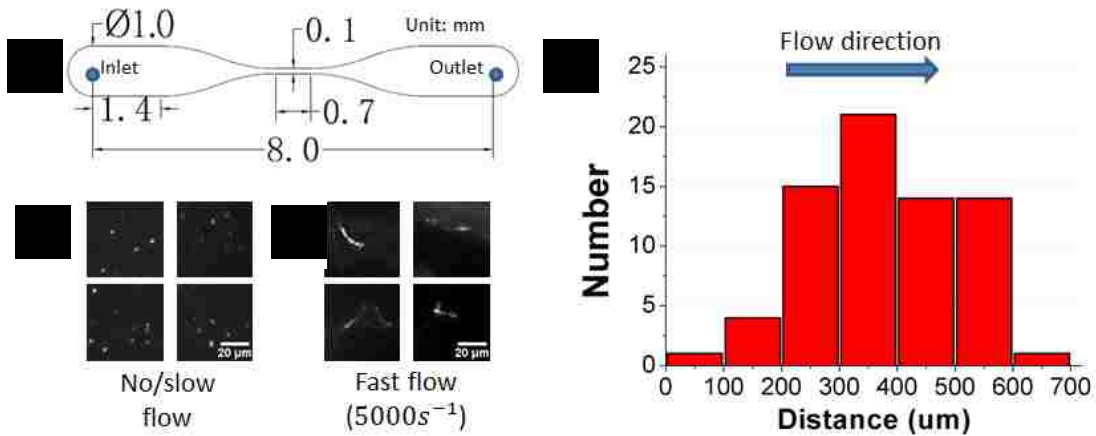


Figure 32. Microfluidic System to Achieve Controllable Flow Field. a. Schematic of microfluidic Chamber made of PDMS. b. Fluorescent VWF attached under no/slow flow. c. Fluorescent VWF attached under high shear flow. d. Attachment of VWF vs. displacement distance in chamber (5000 s^{-1}).

As shown in **Figure 32a**, we applied a homebuilt microfluidic channel into the force-induced flow experiment to study the flow-dependent interaction between VWF multimer and collagen. A Harvard Apparatus Syringe pump was utilized to precisely adjust the shear rate [94]. The inner chamber was salinized with APTES [95], conjugated with glutaraldehyde and then coupled with human collagen type I at last. Because of the formation of covalent bond, durability of the functional coating layer (collagen type I) is strengthened significantly. The VWF multimer used in this experiment is from human

plasma and labeled with Alexa 488 fluorescence dye, and then diluted into PBS to the concentration of 5 μ m/ml for experiment.

From the observation via fluorescent microscope, as shown in **Figure 32b** and **c**, it was revealed that the VWF exhibited a compact globular conformation. The VWF could still adhere onto the collagen coated surface when there is little or no-shearing applied. While applying high shearing in the flow channel (5,000 s⁻¹), The VWF stretched to an elongated shape by the hydrodynamic force and attached onto the collagen-coated surface. By comparing **Figure 32b** and **c**, it is obvious that the attached VWF multimer changed size from about 2 μ m compact shape to over 10 μ m in length. After carefully checking the entire high shear flow test section (the narrow part in the middle) of the channel, we obtained the distribution of the adhered VWF vs. the displacement of particles along the shear flow direction of our microfluidic chamber, as shown in **Figure 32d**. From the histogram it is estimated that the attachment rate of VWF multimers under applied high shear flow. At the early stage when the coiled VWF molecules just go into high shear rate flow, they need time to react. Because the globular shaped partials tend to concentrate in the middle of the flow. Shortly, they elongate after experiencing high shearing for a little while, and migrate to the wall. This is the moment when the attachment increases sharply. Another important reason is that the exposure of the A3 domain has a strong interaction with collagen type I. The attachment decreases because the shear rate becomes lower so that it cannot maintain the extension of the stretched VWF multimers. The implementation of this flow experiment established a very good observation method for large molecules. Even though the conformational change of VWF multimer could not be observed in a real time in the present study, this system is still very

applicable for further study when the mechanical properties of VWF is better understood from the study of intramolecular interaction.

3.3. Characterization of the Domain-Domain Interactions within the VWF Multimer

Recalling the result from the VWF multimer unfolding experiment, as shown in **Figure 31a**, there are several unknown force resistances during the second stage of VWF multimer stretching. Zhang et al. [13] characterized the unfolding of A2 domain as saw-tooth patterns in a force-extension curve. Another interesting phenomenon has been reported in References [92, 93] that when the VWF is not immobilized, the D'D3 domains are shielding the A1 domain in a way in which the adhesion between the VWF and the platelet is inhibited, as illustrated in **Figure 33** with a schematic. The recent study [94] indicated that this inhibition could also be due to the interaction between A1 and A2 domains. Thus the intramolecular interaction of VWF is very important to understand the dynamic mechanism of the VWF multimer. The intramolecular interaction is a very sophisticated mixture of both structural and functional sub-problems. Consequently, the best way to conduct the study on it is starting with the simplest structure and then adding more and more puzzle pieces until the entire multimeric structure is constructed.

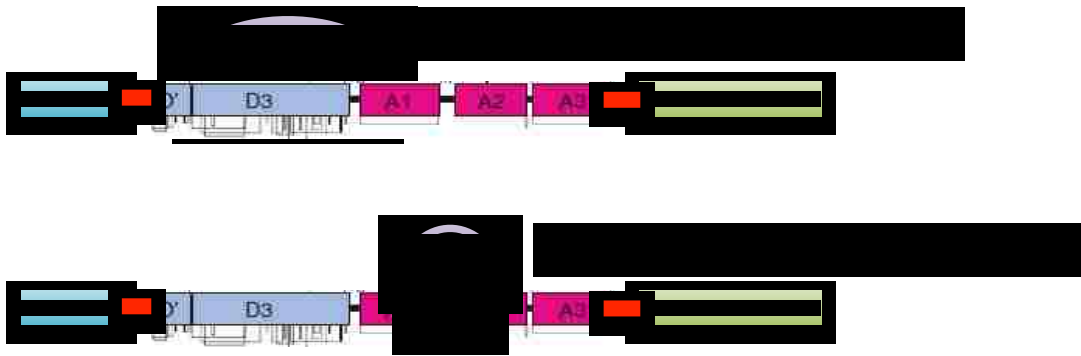


Figure 33. Schematic of domain-domain interactions.

Here a unique assay method was developed to unfold the VWF-the antibody-based pulling assay. This experimental method is designed for the VWF specifically, because two VWF antibodies are employed here to locate the selected portion that will be unfolded in later steps. The schematic depicted in **Figure 34** helps revealing the basic setup of this method. The D domain antibody and C-terminus antibody are truncated by the papain column and then purified to obtain the Fab fragments. By utilizing the same method as described in Chapter 3, the C-terminus antibody is coupled on the surface of the polystyrene 2.0 μm beads that will be immobilized on the micropipette of the optical tweezers later. On the other side, the same beads are first coated with streptavidin and then coupled with the biotinylated DNA handle (following the protocol in Chapter 3). The D domain antibody Fab is linked with the DNA handle by Traut's reagent (Life Technologies).

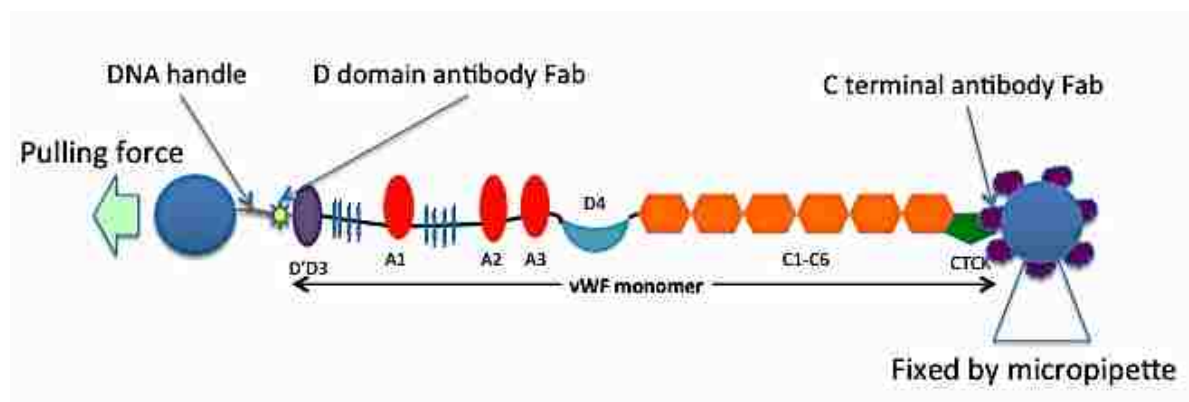
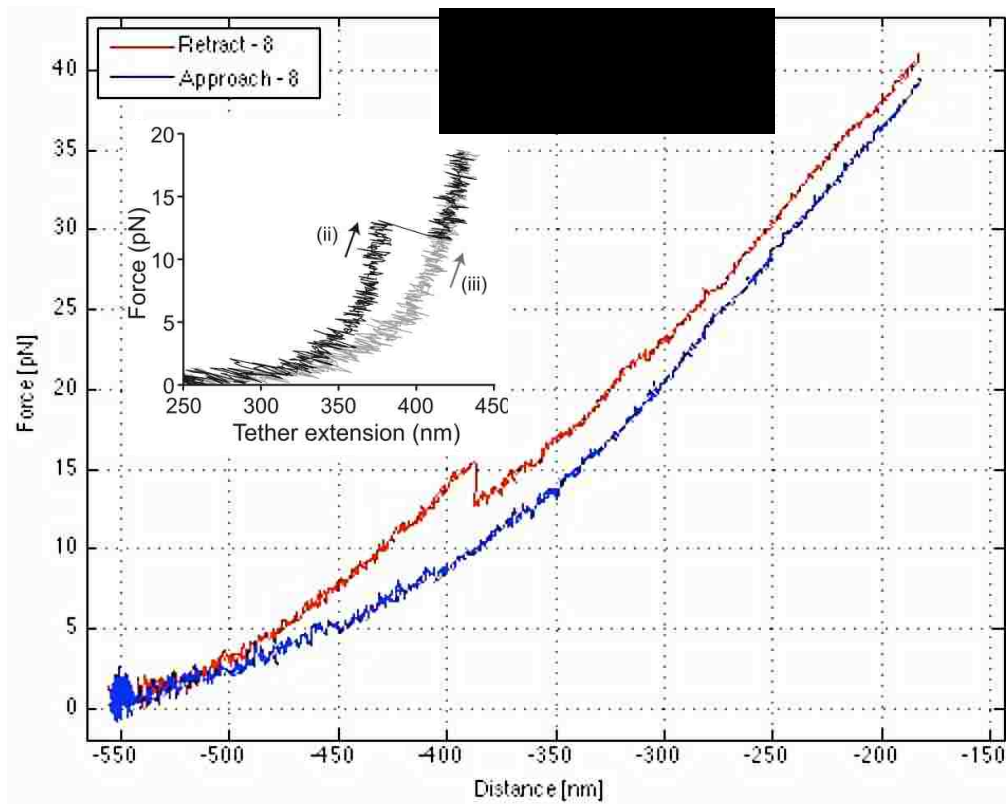
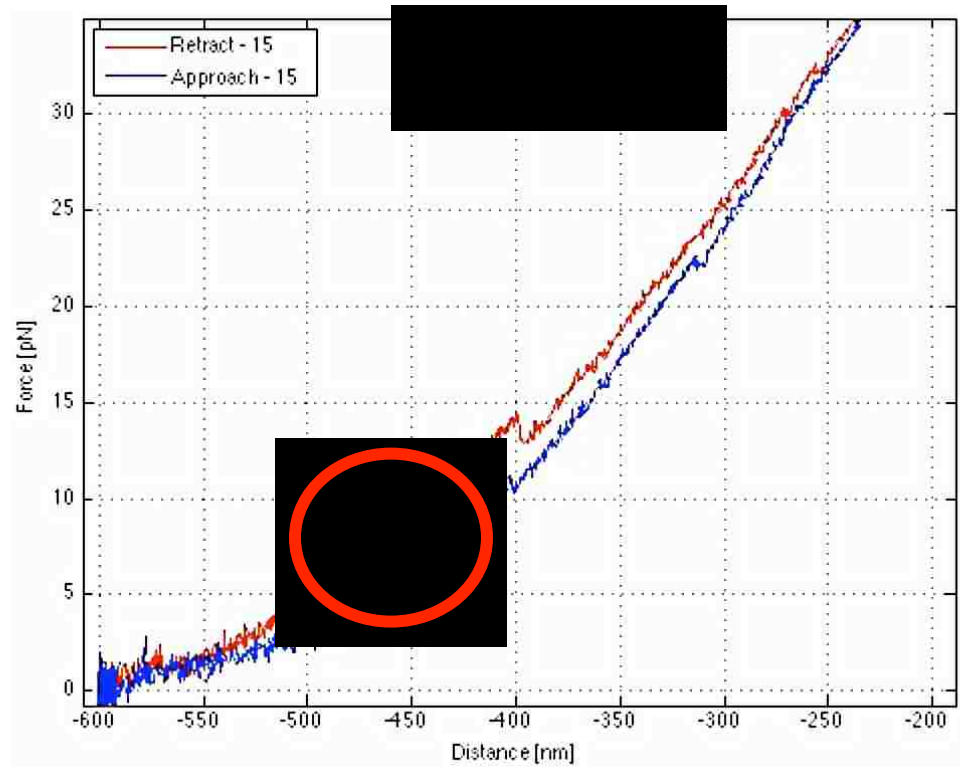
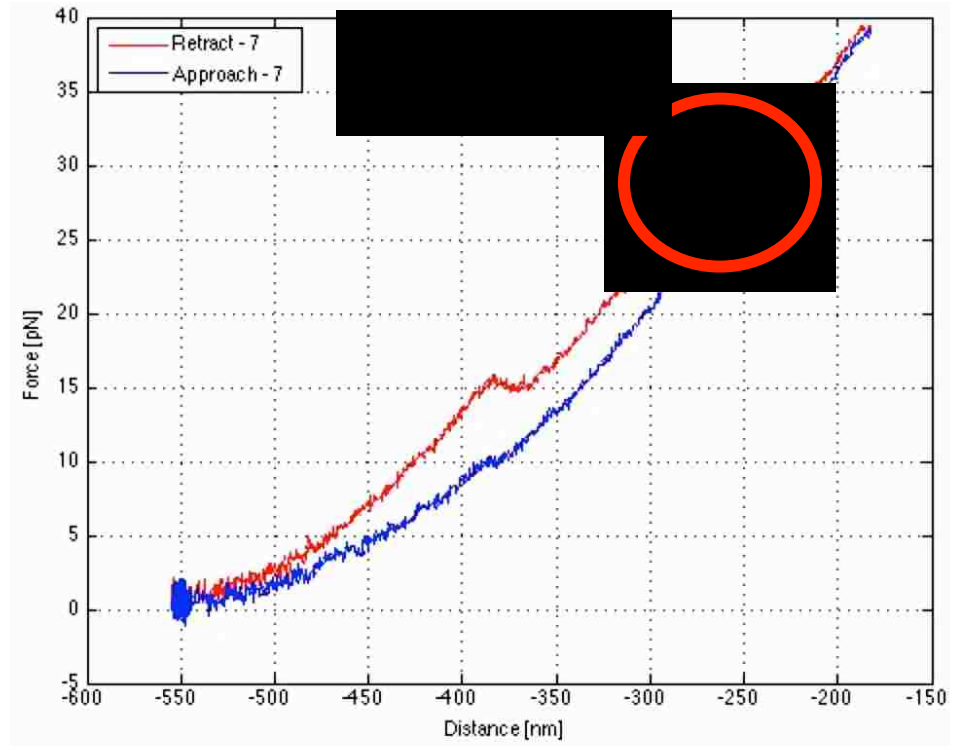


Figure 34. Schematic of the antibody-based pulling assay.

Based on the work done by Zhang, et al. [13], the mechanical properties of A2 domain within the VWF has been fully characterized. Thus the unfolding of A2 domain

can be distinguished easily on the pulling curve by the antibody-based pulling assay. With this approach, the domain-domain interactions can be filtered out from the pulling curve and will be analyzed separately. This method was first applied to unfold the VWF monomer. The resultant pulling curves are shown in **Figure 35**. In panel **a** of the figure, the pulling curve with only A2 unfolding is compared against the pulling curve reported in Ref [13]. Both of the extension and the unfolding force are very similar. At this point, the A2 unfolding in the resultant pulling curves can be determined. In panel **b** and **c**, besides the A2 unfolding, another unfolding dips are shown either above the A2 unfolding or below it. In panel **d** all three kinds of unfolding appear together.





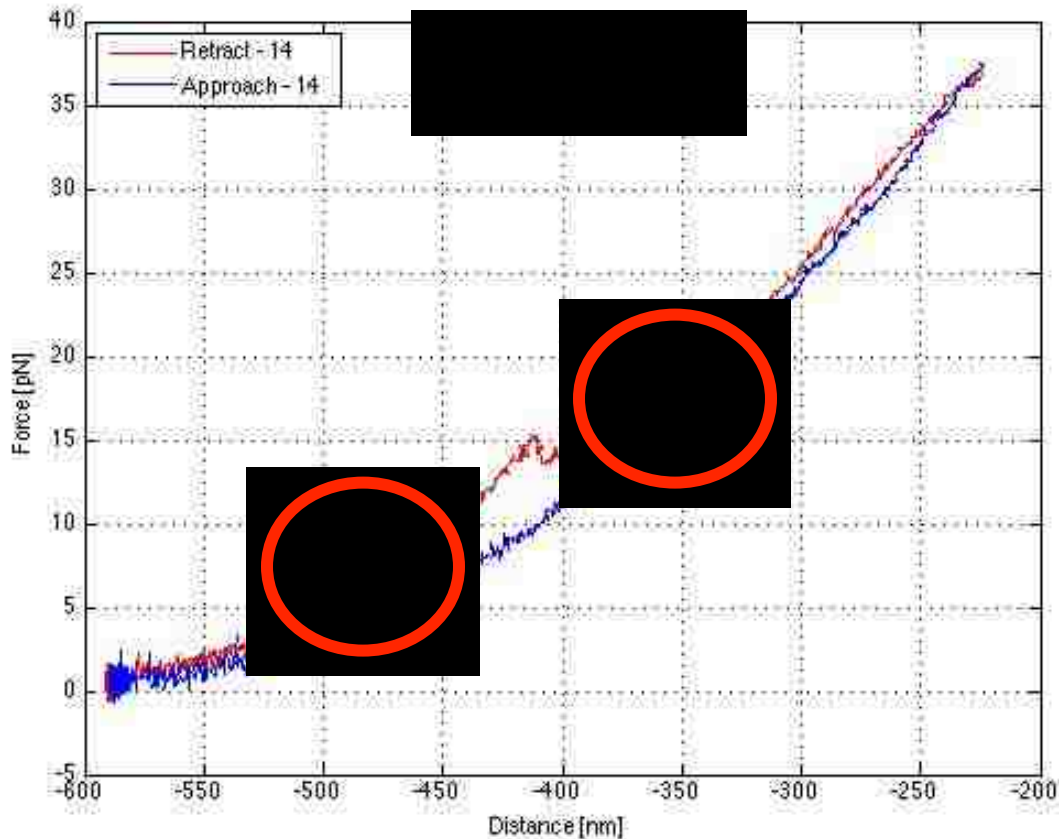


Figure 35. Pulling VWF monomer with the antibody-based pulling assay. a. A2 domain unfolding only, comparing with literature. b. Domain-domain interaction above A2 unfolding. c. Domain-domain interaction below A2 unfolding. d. Domain-domain interactions show both above and below the A2 unfolding.

Pulling VWF with the antibody-based method is the first experiment in the field that is examining the domain-domain interactions on a single-molecule level. When the result of literature [92, 93] in a dynamic way is considered, the shielding effect between D'D3 domain and A1 domain doesn't influence the unfolding of A2 domain. Thus the D'D3-A1 interaction can appear either before the A2 unfolding or after. Meanwhile, the A1-A2 interaction reported in Ref [94] does involve the A2 domain. Consequently, the unfolding of A1-A2 interaction has to be before the A2 unfolding. This leads to the conclusion that

the antibody-based pulling assay is capable to capture the domain-domain interactions. However, to identify and characterize each interaction, a greater number of experiments are needed. Also, pulling the entire monomer is preliminary and quantitative. The similar assays can be conducted on shorter fragments of the VWF to precisely locate and characterize the domain-domain interaction.

4. Conclusion

Within this chapter, our research target has been scaled up from domain interactions to the multimeric structure. The unfolding assay on plasma VWF multimer suggested extremely complicated intramolecular structure of the VWF multimer. Different stages of the VWF conformational change have been categorized and the required force level was finally related to each stage. The result drew a big map of VWF multimer, which successfully oriented the following experiments. Next, another map was brought to us by the microfluidic flow experiment. The fluorescently labeled VWF multimer showed that the rough relationship between the structure and adhesive function exist. Afterward, the AFM unbinding assay was conducted on VWF mutations and the force spectrum of each sample pair was put together showing up a good comparison and summary. From the results, the mechanical properties of each mutation are quantified. The pathologic observations were then connected firmly with physical indicators. This established methodology has tremendous potential to study biological systems, because it initialized a standard to normalize the bio-affinities. Compared with the traditional biology analysis that has been used for many years, the single molecule measurement is much more accurate. The multidisciplinary study on biological objectives will be increasingly

beneficial on the development of biotechnology in the future. Last but not the least, the antibody-based method on the optical tweezers platform delivered very good results that agreed with previous study. However, it is difficult to find proper antibodies that are able to pull any designated fragments from within the VWF multimer. Therefore, in its current stage, it is challenging to precisely locate the intramolecular interactions.

CONCLUDING REMARKS AND OUTLOOK

The research work discussed in this dissertation has systematically studied the structure and function of von Willebrand factor (VWF) from domain level to multimer level. With multiple single molecule methods, we study the conformational change intermolecular interaction and intramolecular interactions. The result helps us understand the mechanical properties of VWF as an adhesion mediator. Consequently, we treat VWF as a mechanical system, and utilize the resultant information to simulate it artificially. On the other hand, with the presence of external ligands such as Collagen, platelets GpIb and Factor VIII, we study the interactions from the pathologic and biological perspectives. In this way, we understand the function of this unique human protein better and use our result to solve clinical problems. At last, with the presence of both force and ligands, the research will be increasingly close to what is actually happening in human body.

Firstly, we started with the VWF A3 domain- collagen interaction. By applying AFM unbinding assay, we successfully measured the strength of the bond in between. The force spectrum gave us the ability to quantify the energetic properties of the VWF monomer-collagen bond and the VWF A3 domain-collagen bond. From the comparison, it was convincing that the A3 domain is the dominant binding site of collagen within VWF and the A1 domain didn't contribute to binding with collagen. The Arrhenius Plot was a novel method to study the bioaffinities. At this point, we calculated the activation energy of the VWF A3 domain-collagen bond. These parameters are extremely desirable for researchers conducting simulation study on biological objectives.

Secondly, as the other end of the VWF “bridge”, the interaction with GPIb-IX complex has been examined from mechanical perspective. By smartly introducing the definition of mechanosensor into the biological structure, we were able to predict, describe and manipulate the biological behaviors of the GPIb-IX complex. The signal transmission and processing functions of the mechanosensitive domain in GPIb-IX were determined by the unfolding assay. Based on that, using two antibodies with different binding locations, the mechanosensitive domain has been located in the stalk region. The result uncovers the dynamic mechanism of the platelet activation procedure, which is very helpful to the future studies on hemostasis and thrombosis. Additionally, the enhancing effect of botrocetin has been quantified and compared with normal condition. The influence is very obvious, showing the enhancement promotes the VWF A1 domain-GPIb-IX interaction with two folds.

Finally, our research was given clinical background by involving with pathological mutations. Within this part of the reach work, 3 mutant VWF multimers and the Nem treated VWF multimer have been measured with single molecule studies. The adhesive function between VWF and collagen was kept the same from domain phase to multimer phase. The mechanical properties of the VWF mutations are consistent with the clinical observations of these VWD mutations. The result provides very important information to developing therapeutic treatment and devices of VWD and thrombosis.

There is no doubt that a lot of outstanding research work has been done in this dissertation on domain phase and monomer phase. However, at multimer lever, the intramolecular mechanism still remains mysterious. To continue with what have been

done here, the future work can be focused on the domain-domain interaction of VWF multimer. The Howarth Group at Oxford University has found a very interesting covalent binding pair [94], which is named SpyTag-SpyCatcher complex. By employing this technique, it is possible to truncate different fragments from VWF structure [95]. AFM or optical tweezers will be the preferred tools to conduct measurement on the truncations. Moreover, the established antibody-based pulling assay can be utilized as a diagnostic method to characterize the plasma VWF sample directly from patients, especially for those with deficient A2 domain. Lastly, the intramolecular study can supply local information to modeling and simulation work. The mechanical properties of domain-domain, monomer-monomer and dimer-dimer interactions can be converted into the parameters of the intra-potentials, which will be very helpful to simulating the dynamic behaviors of VWF as a biopolymer.

BIBLIOGRAPHY

1. *Molecular basis of von Willebrand disease and its clinical implications.* Haematologica, 2004. **89**(9): p. 1036-1036.
2. Nishino, M. and A. Yoshioka, "*The revised classification of von Willebrand disease including the previously masqueraded female hemophilia A (type 2N) (vol 66, pg 22, 1997).*" International Journal of Hematology, 1997. **66**(4): p. 531-531.
3. Sadler, J.E., *A Revised Classification of Von-Willebrand Disease.* Thrombosis and Haemostasis, 1994. **71**(4): p. 520-525.
4. Sadler, J.E., *New concepts in von Willebrand disease.* Annu Rev Med, 2005. **56**: p. 173-91.
5. Springer, T.A., *Biology and physics of von Willebrand factor concatamers.* J Thromb Haemost, 2011. **9 Suppl 1**: p. 130-43.
6. Wagner, D.D., *Cell biology of von Willebrand factor.* Annu Rev Cell Biol, 1990. **6**: p. 217-46.
7. Zenner, H.L., et al., *High-pressure freezing provides insights into Weibel-Palade body biogenesis.* Journal of Cell Science, 2007. **120**(12): p. 2117-2125.
8. Berriman, J.A., et al., *Structural organization of Weibel-Palade bodies revealed by cryo-EM of vitrified endothelial cells.* Proc Natl Acad Sci U S A, 2009. **106**(41): p. 17407-12.
9. Truett, M.A., et al., *Characterization of the Polypeptide Composition of Human Factor-Viii-C and the Nucleotide-Sequence and Expression of the Human-Kidney Cdna.* DNA-a Journal of Molecular & Cellular Biology, 1985. **4**(5): p. 333-349.
10. Everse, S.J., et al., *Crystal structure of fragment double-D from human fibrin with two different bound ligands (vol 37, pg 8637, 1998).* Biochemistry, 1998. **37**(51): p. 18128-18128.
11. Vickers, J.D., *Binding of polymerizing fibrin to integrin alpha(IIb)beta(3) on chymotrypsin-treated rabbit platelets decreases phosphatidylinositol 4,5-bisphosphate and increases cytoskeletal actin.* Platelets, 1999. **10**(4): p. 228-237.
12. Morales, L.D., C. Martin, and M.A. Cruz, *The interaction of von Willebrand factor-A1 domain with collagen: mutation G1324S (type 2M von Willebrand disease) impairs the conformational change in A1 domain induced by collagen.* Journal of Thrombosis and Haemostasis, 2006. **4**(2): p. 417-425.

13. Zhang, X.H., et al., *Mechanoenzymatic Cleavage of the Ultralarge Vascular Protein von Willebrand Factor*. Science, 2009. **324**(5932): p. 1330-1334.
14. Springer, T.A., *von Willebrand factor, Jedi knight of the bloodstream*. Blood, 2014.
15. Huang, R.H., et al., *Assembly of Weibel-Palade body-like tubules from N-terminal domains of von Willebrand factor*. Proc Natl Acad Sci U S A, 2008. **105**(2): p. 482-7.
16. Lankhof, H., et al., *A3 domain is essential for interaction of von Willebrand factor with collagen type III*. Thrombosis and Haemostasis, 1996. **75**(6): p. 950-958.
17. Schneider, S.W., et al., *Shear-induced unfolding triggers adhesion of von Willebrand factor fibers*. Proc Natl Acad Sci U S A, 2007. **104**(19): p. 7899-903.
18. Battle, J., et al., *Proteolytic degradation of von Willebrand factor after DDAVP administration in normal individuals*. Blood, 1987. **70**(1): p. 173-6.
19. Barg, A., et al., *Soluble plasma-derived von Willebrand factor assembles to a haemostatically active filamentous network*. Thrombosis and Haemostasis, 2007. **97**(4): p. 514-526.
20. Savage, B., J.J. Sixma, and Z.M. Ruggeri, *Functional self-association of von Willebrand factor during platelet adhesion under flow*. Proc Natl Acad Sci U S A, 2002. **99**(1): p. 425-430.
21. Ulrichs, H., et al., *The von Willebrand factor self-association is modulated by a multiple domain interaction*. Journal of Thrombosis and Haemostasis, 2005. **3**(3): p. 552-561.
22. Riddell, A.F., et al., *Characterization of W1745C and S1783A: 2 novel mutations causing defective collagen binding in the A3 domain of von Willebrand factor*. Blood, 2009. **114**(16): p. 3489-3496.
23. McKinnon, T.A., et al., *Specific N-linked glycosylation sites modulate synthesis and secretion of von Willebrand factor*. Blood, 2010. **116**(4): p. 640-8.
24. Tischer, A., et al., *Misfolding Induced By the Mutations V1314D and F1369I Affects the Function and the Structure of the Von Willebrand A1-Domain*. Blood, 2014. **124**(21).
25. Binnig, G., C.F. Quate, and C. Gerber, *Atomic Force Microscope*. Physical Review Letters, 1986. **56**(9): p. 930-933.

26. Gautschi, G., *Piezoelectric sensorics : force, strain, pressure, acceleration and acoustic emission sensors, materials and amplifiers*. 2002, Berlin ; New York: Springer. xiii, 264 p.
27. Florin, E.L., V.T. Moy, and H.E. Gaub, *Adhesion Forces between Individual Ligand-Receptor Pairs*. *Science*, 1994. **264**(5157): p. 415-417.
28. Oberhauser, A.F., et al., *Stepwise unfolding of titin under force-clamp atomic force microscopy*. *Proc. Natl. Acad. Sci. U. S. A.*, 2001. **98**: p. 468-472.
29. Fernandez, J.M. and H. Li, *Force-clamp spectroscopy monitors the folding trajectory of a single protein*. *Science*, 2004. **303**(5664): p. 1674-8.
30. Ashkin, A., et al., *OBSERVATION OF A SINGLE-BEAM GRADIENT FORCE OPTICAL TRAP FOR DIELECTRIC PARTICLES*. *Optics Letters*, 1986. **11**(5): p. 288-290.
31. Binnig, G., C.F. Quate, and C. Gerber, *Atomic force microscope*. *Phys. Rev. Lett.*, 1986. **56**: p. 930-933.
32. Evans, E., *Probing the relation between force--lifetime--and chemistry in single molecular bonds*. *Annu Rev Biophys Biomol Struct*, 2001. **30**: p. 105-28.
33. Alon, R., D.A. Hammer, and T.A. Springer, *Lifetime of the P-selectin-carbohydrate bond and its response to tensile force in hydrodynamic flow.[erratum appears in Nature 1995 Sep 7;376(6544):86]*. *Nature*, 1995. **374**(6522): p. 539-42.
34. Smith, S.B., Y.J. Cui, and C. Bustamante, *Optical-trap force transducer that operates by direct measurement of light momentum*. *Biophotonics, Pt B*, 2003. **361**: p. 134-162.
35. Wootton, R.C.R., R. Fortt, and A.J. de Mello, *A microfabricated nanoreactor for safe, continuous generation and use of singlet oxygen*. *Organic Process Research & Development*, 2002. **6**(2): p. 187-189.
36. Vilkner, T., D. Janasek, and A. Manz, *Micro total analysis systems. Recent developments*. *Analytical Chemistry*, 2004. **76**(12): p. 3373-3385.
37. Sia, S.K. and G.M. Whitesides, *Microfluidic devices fabricated in poly(dimethylsiloxane) for biological studies*. *Electrophoresis*, 2003. **24**(21): p. 3563-3576.
38. Jahnisch, K., et al., *Chemistry in microstructured reactors*. *Angewandte Chemie-International Edition*, 2004. **43**(4): p. 406-446.

39. Sunkara, V., et al., *Simple room temperature bonding of thermoplastics and poly(dimethylsiloxane)*. Lab Chip, 2011. **11**(5): p. 962-965.
40. Huizinga, E.G., et al., *Crystal structure of the A3 domain of human von Willebrand factor: implications for collagen binding*. Structure, 1997. **5**(9): p. 1147-1156.
41. Ruggeri, Z.M., *von Willebrand factor and fibrinogen*. Current Opinion in Cell Biology, 1993. **5**(5): p. 898-906.
42. Sixma, J.J. and A. van den Berg, *The haemostatic plug in haemophilia A: a morphological study of haemostatic plug formation in bleeding time skin wounds of patients with severe haemophilia A*. Br J Haematol, 1984. **58**(4): p. 741-53.
43. Rand, J.H., et al., *Co-localization of von Willebrand factor and type VI collagen in human vascular subendothelium*. Am J Pathol, 1993. **142**(3): p. 843-50.
44. Traub, W., A. Yonath, and D.M. Segal, *On the molecular structure of collagen*. Nature, 1969. **221**(5184): p. 914-7.
45. Cruz, M.A., et al., *Interaction of the Von-Willebrand-Factor (Vwf) with Collagen - Localization of the Primary Collagen-Binding Site by Analysis of Recombinant Vwf α -Domain Polypeptides (Vol 270, Pg 10822, 1995)*. Journal of Biological Chemistry, 1995. **270**(33): p. 19668-19668.
46. Hoylaerts, M.F., et al., *von Willebrand factor binds to native collagen VI primarily via its A1 domain*. Biochemical Journal, 1997. **324**: p. 185-191.
47. Denis, C., et al., *Localization of von Willebrand factor binding domains to endothelial extracellular matrix and to type VI collagen*. Arterioscler Thromb, 1993. **13**(3): p. 398-406.
48. Sing, C.E., J.G. Selvidge, and A. Alexander-Katz, *Von Willebrand Adhesion to Surfaces at High Shear Rates Is Controlled by Long-Lived Bonds*. Biophysical Journal, 2013. **105**(6): p. 1475-1481.
49. Wienken, C.J., et al., *Protein-binding assays in biological liquids using microscale thermophoresis*. Nature Communications, 2010. **1**.
50. Evans, E. and K. Ritchie, *Dynamic strength of molecular adhesion bonds*. Biophysical Journal, 1997. **72**(4): p. 1541-1555.
51. Bell, G.I., *Theoretical-Models for the Specific Adhesion of Cells to Cells or to Surfaces*. Advances in Applied Probability, 1980. **12**(3): p. 566-567.
52. Bell, G.I., *Models for the specific adhesion of cells to cells*. Science, 1978. **200**(4342): p. 618-27.

53. Sing, C.E. and A. Alexander-Katz, *Force Spectroscopy of Self-Associating Homopolymers*. *Macromolecules*, 2012. **45**(16): p. 6704-6718.
54. Neuman, K.C. and A. Nagy, *Single-molecule force spectroscopy: optical tweezers, magnetic tweezers and atomic force microscopy*. *Nature Methods*, 2008. **5**(6): p. 491-505.
55. Hoffmann, T. and L. Dougan, *Single molecule force spectroscopy using polyproteins*. *Chemical Society Reviews*, 2012. **41**(14): p. 4781-4796.
56. Riener, C.K., et al., *Simple test system for single molecule recognition force microscopy (vol 479, pg 59, 2003)*. *Analytica Chimica Acta*, 2004. **506**(1): p. 115-115.
57. Ebner, A., P. Hinterdorfer, and H.J. Gruber, *Comparison of different aminofunctionalization strategies for attachment of single antibodies to AFM cantilevers*. *Ultramicroscopy*, 2007. **107**(10-11): p. 922-927.
58. Hermanson, G.T., *Bioconjugate techniques*. 1996, San Diego: Academic Press. xxv, 785 p.
59. Rankl, C., et al., *Multiple receptors involved in human rhinovirus attachment to live cells*. *Proceedings of the National Academy of Sciences of the United States of America*, 2008. **105**(46): p. 17778-17783.
60. Mendolicchio, G.L. and Z.M. Ruggeri, *New perspectives on von Willebrand factor functions in hemostasis and thrombosis*. *Semin Hematol*, 2005. **42**(1): p. 5-14.
61. Flood, V.H., et al., *VWF Interaction With Type IV Collagen Is Mediated Through Critical VWF A1 Domain Residues*. *Blood*, 2013. **122**(21).
62. Flood, V.H., et al., *Crucial role for the VWF A1 domain in binding to type IV collagen*. *Blood*, 2015. **125**(14): p. 2297-304.
63. Morales, L.D., C. Martin, and M.A. Cruz, *The interaction of von Willebrand factor-A1 domain with collagen: mutation G1324S (type 2M von Willebrand disease) impairs the conformational change in A1 domain induced by collagen*. *J Thromb Haemost*, 2006. **4**(2): p. 417-25.
64. Schwesinger, F., et al., *Unbinding forces of single antibody-antigen complexes correlate with their thermal dissociation rates*. *Proceedings of the National Academy of Sciences of the United States of America*, 2000. **97**(18): p. 9972-9977.
65. Smith, D.E., H.P. Babcock, and S. Chu, *Single-polymer dynamics in steady shear flow*. *Science*, 1999. **283**(5408): p. 1724-1727.

66. Degennes, P.G., *Coil-Stretch Transition of Dilute Flexible Polymers under Ultrahigh Velocity-Gradients*. Journal of Chemical Physics, 1974. **60**(12): p. 5030-5042.
67. Brown, C.H., et al., *Morphological, Biochemical, and Functional Changes in Human Platelets Subjected to Shear-Stress*. Journal of Laboratory and Clinical Medicine, 1975. **86**(3): p. 462-471.
68. Moake, J.L., et al., *Involvement of large plasma von Willebrand factor (vWF) multimers and unusually large vWF forms derived from endothelial cells in shear stress-induced platelet aggregation*. J Clin Invest, 1986. **78**(6): p. 1456-61.
69. Peterson, D.M., et al., *Shear-induced platelet aggregation requires von Willebrand factor and platelet membrane glycoproteins Ib and IIb-IIIa*. Blood, 1987. **69**(2): p. 625-8.
70. Auton, M., et al., *N-terminal Flanking Region of A1 Domain in von Willebrand Factor Stabilizes Structure of A1A2A3 Complex and Modulates Platelet Activation under Shear Stress*. Journal of Biological Chemistry, 2012. **287**(18): p. 14579-14585.
71. Tischer, A., et al., *A molten globule intermediate of the Von Willebrand factor A1 domain firmly tethers platelets under shear flow*. Proteins-Structure Function and Bioinformatics, 2014. **82**(5): p. 867-878.
72. Pula, G., et al., *PKCdelta regulates collagen-induced platelet aggregation through inhibition of VASP-mediated filopodia formation*. Blood, 2006. **108**(13): p. 4035-44.
73. De Marco, L., et al., *Interaction of purified type IIB von Willebrand factor with the platelet membrane glycoprotein Ib induces fibrinogen binding to the glycoprotein IIb/IIIa complex and initiates aggregation*. Proc Natl Acad Sci U S A, 1985. **82**(21): p. 7424-8.
74. Savage, B., F. Almus-Jacobs, and Z.M. Ruggeri, *Specific synergy of multiple substrate-receptor interactions in platelet thrombus formation under flow*. Cell, 1998. **94**(5): p. 657-66.
75. Zhang, W., et al., *Identification of a juxtamembrane mechanosensitive domain in the platelet mechanosensor glycoprotein Ib-IX complex*. Blood, 2015. **125**(3): p. 562-9.
76. Du, X.P., et al., *Glycoprotein-Ib and Glycoprotein-Ix Are Fully Complexed in the Intact Platelet Membrane*. Blood, 1987. **69**(5): p. 1524-1527.
77. Huizinga, E.G., et al., *Structures of glycoprotein Ibalpha and its complex with von Willebrand factor A1 domain*. Science, 2002. **297**(5584): p. 1176-9.

78. Ju, L., et al., *The N-terminal flanking region of the A1 domain regulates the force-dependent binding of von Willebrand factor to platelet glycoprotein Ibalpha*. J Biol Chem, 2013. **288**(45): p. 32289-301.
79. Kim, J., et al., *A mechanically stabilized receptor-ligand flex-bond important in the vasculature*. Nature, 2010. **466**(7309): p. 992-5.
80. Fukuda, K., et al., *The snake venom protein botrocetin acts as a biological brace to promote dysfunctional platelet aggregation*. Nat Struct Mol Biol, 2005. **12**(2): p. 152-9.
81. Read, M.S., R.W. Shermer, and K.M. Brinkhous, *Venom coagglutinin: an activator of platelet aggregation dependent on von Willebrand factor*. Proc Natl Acad Sci U S A, 1978. **75**(9): p. 4514-8.
82. Sanders, W.E., et al., *Thrombotic thrombocytopenia with von Willebrand factor deficiency induced by botrocetin. An animal model*. Lab Invest, 1988. **59**(4): p. 443-52.
83. Andrews, R.K., et al., *Purification of Botrocetin from Bothrops-Jararaca Venom - Analysis of the Botrocetin-Mediated Interaction between Vonwillebrand-Factor and the Human-Platelet Membrane Glycoprotein-Ib-Ix Complex*. Biochemistry, 1989. **28**(21): p. 8317-8326.
84. Fukuda, K., et al., *Structural basis of von Willebrand factor activation by the snake toxin botrocetin*. Structure, 2002. **10**(7): p. 943-50.
85. Kim, J., et al., *A mechanically stabilized receptor-ligand flex-bond important in the vasculature*. Nature, 2010. **466**(7309): p. 992-U123.
86. Dudko, O.K., G. Hummer, and A. Szabo, *Intrinsic rates and activation free energies from single-molecule pulling experiments*. Physical Review Letters, 2006. **96**(10).
87. Sadler, J.E., *Biochemistry and genetics of von Willebrand factor*. Annual Review of Biochemistry, 1998. **67**: p. 395-424.
88. Dong, J.F., et al., *ADAMTS-13 rapidly cleaves newly secreted ultralarge von Willebrand factor multimers on the endothelial surface under flowing conditions*. Blood, 2002. **100**(12): p. 4033-4039.
89. De Ceunynck, K., S.F. De Meyer, and K. Vanhoorelbeke, *Unwinding the von Willebrand factor strings puzzle*. Blood, 2013. **121**(2): p. 270-277.
90. Widmaier, E.P., et al., *Vander's human physiology : the mechanisms of body function*. 12th ed. 2011, New York: McGraw-Hill.

91. Ulrichs, H., et al., *Shielding of the A1 domain by the D'D3 domains of von Willebrand factor modulates its interaction with platelet glycoprotein Ib-IX-V*. J Biol Chem, 2006. **281**(8): p. 4699-707.
92. Lenting, P.J., et al., *Regulation of von Willebrand factor-platelet interactions*. Thromb Haemost, 2010. **104**(3): p. 449-55.
93. Karoulia, Z., et al., *Studies on the Essential Intramolecular Interaction Between the A1 and A2 Domains of von Willebrand Factor*. Protein and Peptide Letters, 2013. **20**(2): p. 231-240.
94. Zakeri, B., et al., *Peptide tag forming a rapid covalent bond to a protein, through engineering a bacterial adhesin*. Proc Natl Acad Sci U S A, 2012. **109**(12): p. E690-E697.
95. Voorberg, J., et al., *Domains Involved in Multimer Assembly of Vonwillebrand-Factor (Vwf) - Multimerization Is Independent of Dimerization*. Embo Journal, 1990. **9**(3): p. 797-803.

VITA

Yan Xu

8 Duh Dr APT 224, Bethlehem, PA 18015 | +1-610-739-9813 | styxyuan@gmail.com

Research Interest

1. Single-molecule study on characterizing biomechanical properties of biomolecules.
2. Microfluidic system design, fabrication and application (bioaffinity assays, FACS, cell rolling assays, surface functionalization).
3. Diagnostic and therapeutic solutions for von Willebarnd Disease (VWD), Ebola and HIV.
4. Medical devices design, prototyping and commercialization.

Education

PhD in Mechanical Engineering, Lehigh University, Bethlehem, PA, USA

MS in Mechanical Engineering, Lehigh University, Bethlehem, PA, USA

Bachelor in Mechanical Engineering, Beijing University of Technology

Publications

Yan Xu, Anne Golding, Thomas A. J. McKinnon, Chenyu Wu, Xuanhong Cheng, Alparslan Oztekin, Edmund B. Webb III and X. Frank Zhang, Biomechanical Characterization of VWF-collagen Interaction (In preparation).

Xu, Y., Schutt, K., Dragovich, M.A., Maury, W., and Zhang. X. (2015): Biophysical mechanisms of Ebola virus-host cell interaction (In preparation).

Fu, X. **Xu, Y.**, Wu, C., Moy, V.T., and Zhang, X. (2015): Anchorage-dependent binding of integrin I-domain to adhesion ligands. *Journal of Molecular Recognition*, 28:385-92.

W. Zhang, W. Deng, L. Zhou, **Y. Xu**, W. Yang, X. Liang, Y. Wang, J. D. Kulman, X. F. Zhang*, R. Li*, Identification of a juxtamembrane mechano-sensitive domain in the platelet mechanosensor glycoprotein Ib-IX-V complex. *Blood*. 2014 Oct 30. pii: blood-2014-07-589507.

Yan Xu, Wojciech Z. Misiolek, Numerical Modeling of Extrusion Welding in Magnesium Alloys, *Key Engineering Materials* Vol. 491 (2012) pp 159-171.

Awards/Recognitions

Engineer in Training (EIT).

RCEAS Fellowship from ME&M Department, Lehigh University.

Loewy Fellowship For Graduate Student from Loewy Family Foundation.

Outstanding student leader, Scholarship for outstanding performance by Beijing University of Technology.